Chem Soc Rev

REVIEW ARTICLE

View Article Online
View Journal

Recent advances in heterogeneous selective oxidation catalysis for sustainable chemistry

Cite this: DOI: 10.1039/c3cs60282f

Zhen Guo,[a] Bin Liu,[a] Qinghong Zhang,[b] Weiping Deng,[b] Ye Wang*[b] and Yanhui Yang*[ab]

Oxidation catalysis not only plays a crucial role in the current chemical industry for the production of key intermediates such as alcohols, epoxides, aldehydes, ketones and organic acids, but also will contribute to the establishment of novel green and sustainable chemical processes. This review is devoted to dealing with selective oxidation reactions, which are important from the viewpoint of green and sustainable chemistry and still remain challenging. Actually, some well-known highly challenging chemical reactions involve selective oxidation reactions, such as the selective oxidation of methane by oxygen. On the other hand some important oxidation reactions, such as the aerobic oxidation of alcohols in the liquid phase and the preferential oxidation of carbon monoxide in hydrogen, have attracted much attention in recent years because of their high significance in green or energy chemistry. This article summarizes recent advances in the development of new catalytic materials or novel catalytic systems for these challenging oxidation reactions. A deep scientific understanding of the mechanisms, active species and active structures for these systems are also discussed. Furthermore, connections among these distinct catalytic oxidation systems are highlighted, to gain insight for the breakthrough in rational design of efficient catalytic systems for challenging oxidation reactions.

Received 31st July 2013

DOI: 10.1039/c3cs60282f

www.rsc.org/csr

[a] School of Chemical and Biomedical Engineering, Nanyang Technological University, Singapore 637459, Singapore. E-mail: yhyang@ntu.edu.sg; Fax: +65-67947553; Tel: +65-63168940

[b] State Key Laboratory of Physical Chemistry of Solid Surfaces, Collaborative Innovation Center of Chemistry for Energy Materials, National Engineering Laboratory for Green Chemical Productions of Alcohols, Ethers and Esters, College of Chemistry and Chemical Engineering, Xiamen University, Xiamen 361005, China. E-mail: wangye@xmu.edu.cn; Fax: +86-592-2183047; Tel: +86-592-2186156

1. Introduction and scope of this review

Selective oxidation reactions play a pivotal role in the current chemical industry. Oxidation is the second largest process after polymerization and contributes ~30% of total production in the chemical industry.[1] Many key chemicals and intermediates such as alcohols, epoxides, aldehydes, ketones and organic

Zhen Guo

*Zhen Guo received his BS and MSc degrees in chemistry from Wuhan University in China, and PhD degree in chemical engineering from Nanyang Technological University in 2011. His doctoral advisor is Prof. Yanhui Yang. He is currently working in the Agency for Science, Technology and Research (A*STAR) of Singapore as a scientist. His research interest is the development of efficient catalysts on the basis of understanding the catalytic mechanism and rational design methodology.*

Bin Liu

Bin Liu received his BE and ME degrees in Chemical Engineering from the National University of Singapore, and obtained his PhD degree from the University of Minnesota in 2011. He worked as a postdoctoral researcher at the University of California, Berkeley during 2011–2012 and then joined School of Chemical and Biomedical Engineering at Nanyang Technological University as an Assistant Professor in 2012. His main research interests are nanomaterial architectures for energy conversion and energy storage.

acids are produced *via* selective oxidation catalysis. Among the selective oxidation processes in the current chemical industry, the selective oxidation of propene to acrolein, the ammoxidation of propene to acrylonitrile, the selective oxidation of butane to maleic anhydride, the epoxidation of ethylene to propylene and the selective oxidation of methanol to formaldehyde are the best known examples. The success in performing these reactions has shed light on our scientific understanding of selective oxidation catalysis. Some concepts have been proposed based on the phenomenological or intuitive knowledge obtained particularly from the selective oxidation of olefins, such as the Mars–van Krevelen (M–v K) mechanism or the lattice oxygen-based redox mechanism, phase cooperation and site isolation.[2–7]

Selective oxidation catalysis is also the key to establishing green and sustainable chemical processes. Take selective oxidation of hydrocarbons as an example. On one hand, the selectivity in the current chemical industry has to be further raised to decrease the formation of non-selective products, particularly CO_2. This requires further optimization of the catalyst and the process employed in the current chemical industry. On the other hand, there is a strong incentive to develop new oxidation processes that satisfy the principles of green chemistry.[8,9] In particular, it is highly desirable to develop new catalytic oxidation processes to replace the current energetically inefficient and/or environmentally unfriendly multi-step reactions.

The catalytic oxidation of alcohols to aldehydes or ketones, which is widely recognized as one of the most fundamental transformations in organic chemistry, represents an example of green oxidation. Oxidizing reagents including permanganate and dichromate have traditionally been employed for the oxidation of alcohols, but these stoichiometric oxidants are expensive and/or toxic, and more seriously, produce a large amount of heavy-metal wastes. The development of heterogeneous catalytic systems using O_2 or air as an oxidant, which is cheap and safe, and produces water as the sole by-product, would contribute to establishing green and sustainable chemical processes.[10–13]

In addition, the utilization of versatile resources, particularly abundant, cheap and renewable resources to replace the diminishing petroleum is also an attractive research target.

Qinghong Zhang

Qinghong Zhang received her BS and MSc degrees from Nanjing University of China in 1989 and 1992, and obtained her PhD degree from Hiroshima University of Japan in 2002. She joined Xiamen University in October of 2002, and was promoted to a full professor in 2010. Her research interests include the synthesis and characterization of novel materials with advanced catalytic properties.

Weiping Deng

Weiping Deng received his BS degree in chemistry from Hubei University of China in 2003, and obtained his PhD degree from Xiamen University in 2009 under the guidance of Professor Ye Wang. He is currently an engineer in the National Engineering Laboratory for Green Chemical Productions of Alcohols, Ethers and Esters. He focuses on selective oxidation and biomass conversion.

Ye Wang

Ye Wang received his BS and MSc degrees from Nanjing University of China, and obtained his PhD degree in 1996 from Tokyo Institute of Technology of Japan. He worked as research associate at Tokyo Institute of Technology, Tohoku University and Hiroshima University during 1996–2000 and was promoted to associate professor at Hiroshima University in 2001. He became a full professor of Xiamen University in the August of 2001. He is currently the director of Institute of Catalysis Science and Technology of Xiamen University. His main research interests are heterogeneous catalysis for selective oxidation and for energy-related transformations.

Yanhui Yang

Yanhui Yang received his BS degree in chemical engineering from Tsinghua University and PhD degree in chemical engineering from Yale University in 1998 and 2005, respectively. Dr Yang joined School of Chemical and Biomedical Engineering, Nanyang Technological University, Singapore as an assistant professor in August 2005 right after he graduated from Yale. Dr Yang's primary research area is heterogeneous catalysis over metals and metal oxides, in particular the fundamental catalytic concepts and phenomena using well-defined model catalysts and chemically probed reactions. Dr Yang was promoted to associate professor with tenure in chemical engineering in 2010.

In this context, methane, which is available not only as a fossil resource, a major component of natural gas, coal-bed gas and shale gas, but also from a variety of renewable sources as biogas,[14] could provide an economical and sustainable alternative to petroleum. Furthermore, methane is one of the most destructive greenhouse gas. Thus, the transformation of methane to liquid fuels or building-block chemicals has received much renewed interest in recent years.[15–18] Currently, the relatively mature technology for chemical utilization of methane involves high-temperature steam reforming to produce synthesis gas and the subsequent synthesis of methanol from synthesis gas or the Fischer–Tropsch synthesis to provide hydrocarbon fuels or chemicals. However, the steam reforming of methane is an energy- and cost-intensive process. The high-capital investment and the large-scale requirements of the reforming process hinder the utilization of remote and scattered natural gas or shell gas resources or small-scale biogas resources. There is a strong incentive to develop new routes for the transformation of methane to valuable chemicals. However, the direct transformation of methane to building-block chemicals such as olefins and oxygenates is a very difficult challenge. Generally, the difficulty arises from two aspects. First, methane only possesses saturated C–H bonds with a high bond dissociation energy (434.7 kJ mol^{-1}), and thus, the conversion of methane usually needs to overcome a high energy barrier and stringent conditions. Second, more seriously, the reactivity of the target products (*e.g.*, olefins and oxygenates) is typically much higher than that of the methane molecule, and thus, these products may easily undergo consecutive conversion such as deep oxidation to CO and CO_2 under the reaction conditions. The activation and selective transformation of alkanes including methane represents a ''Holy Grail'' in the chemical community.[19]

Hydrogen as the cleanest energy source for fuel cells is primarily produced by reforming of hydrocarbons or methanol followed by the water–gas shift reaction. A small amount of CO (0.5–2.0 wt%) contained in so-produced H_2 can poison the Pt-based anode in the polymer electrolyte membrane (PEM) fuel cell. The preferential oxidation (PROX) of CO in H_2-rich stream is regarded as one of the simplest and most cost-effective routes for the removal of CO in H_2. The most important requirement for a PROX catalyst is a high CO oxidation activity at mild temperature while prohibiting undesirable H_2 oxidation in a wide temperature region. Various noble and non-noble catalysts have been reported as candidates for PROX catalysts. These have resulted in an interesting direction in ''selective oxidation'' (preferential oxidation) catalysis. Here, the control of selectivity means how we can accelerate the oxidation of CO while avoiding the oxidation of H_2. This requires the design of new oxidation catalyst concepts.

In this review article, we focus our attention on three important and challenging reactions in the field of selective oxidation for a sustainable future: the oxidation of methane to organic oxygenates or olefins; the aerobic oxidation of alcohols; and the preferential oxidation of CO. These three catalytic systems are chosen, not only because of their importance for a sustainable future, but also due to their diverse reaction natures, namely the high stability of methane, oxygen transfer from the gas phase to the liquid phase *via* the surface of solid catalysts, and selective oxidation of CO in an H_2-rich stream. Comparisons among these three systems may shed light on the general features shared by good catalysts. By summarizing the classical pioneering work and novel catalytic systems developed in the recent 5–10 years, we try to figure out the connections among these three important catalytic reactions, in terms of active sites, active structures and advanced strategies for the rational design of efficient catalysts or catalytic systems.

2. Selective transformation of methane

Many potential routes have been reported for the selective transformation of CH_4 into valuable chemicals *via* synthesis gas. Fig. 1 shows the typical products that can be formed from CH_4 transformation *via* oxidative or non-oxidative routes. In addition, the production of HCN from the reaction of CH_4 with NH_3 in the presence of O_2 (known as the Andrussow process, eqn (1)) or in the absence of O_2 (known as the Degussa or BMA process, eqn (2)) catalyzed by Pt at temperatures up to 1573 K has been commercialized for several decades.[20]

$$CH_4 + NH_3 + 1.5O_2 \rightarrow HCN + 3H_2O \qquad \Delta H = -483 \text{ kJ mol}^{-1} \quad (1)$$

$$CH_4 + NH_3 \rightarrow HCN + 3H_2 \qquad \Delta H = 251 \text{ kJ mol}^{-1} \quad (2)$$

2.1 General mechanism for activation of CH_4

The selective partial oxidation of methane starts by activation of C–H bond or the oxidant. In a heterogeneous process, the cleavage of C–H bond undergoes either a heterolytic dissociation or a homolytic dissociation, which was proposed as follows:[21]

Heterolytic dissociation:

$$[O^{2-}] + CH_4 \rightarrow [O^{2-}\cdots H^{+}] + {}^{-}CH_3 \quad (3)$$

Homolytic dissociation:

$$[O] + CH_4 \rightarrow [OH] + {}^{\bullet}CH_3 \quad (4)$$

where [O] denotes the oxidizing surface center, with a high affinity to hydrogen atom. Further transformations of carbanion or methyl radicals, such as the addition of oxygen, combination with a CO or NH group or coupling with a methyl radical and

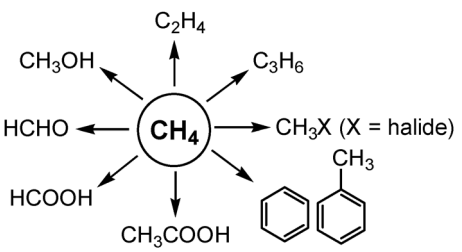

Fig. 1 Potential routes for selective transformation of CH_4 to valuable chemicals.

subsequent dehydrogenation, lead to the formation of oxygenates, nitriles, ethane and ethene, *etc.*[22]

Much of the debate centers on the manner of the breaking of these two C–H bonds. For the oxidation of methane to methanol catalyzed by Pt(II) or Pd(II) complexes in acid medium, the activation of the C–H bond follows the heterolytic mechanism. The methyl anion coordinates with the electrophilic noble metal cation.[23] Support for the heterolytic mechanism on heterogeneous catalysts was presented by Choudhary and Rane who studied the oxidation of methane on a series of rare earth metal oxides.[24] Conversion of methane is related to both the catalyst acidity and basicity, therefore activation of the C–H bond by a surface acid–base pair was proposed, which can be shown as follows:

$$[M^{n+}\cdots O^{2-}] + CH_4 \rightarrow [M^{n+}\cdots {}^{-}CH_3] + [O^{2-}\cdots H^{+}] \quad (5)$$

where metal cation M^{n+} and surface O^{2-} act as the Lewis acid site and strong base site, respectively. Oxidation of fluorocarbon (CH_3F) over basic oxides (Sm_2O_3 and Li/MgO) was studied under oxidative methane coupling (OMC) conditions.[25] The conversion rate of CH_3F is an order of magnitude larger than that of methane, which was explained by a more stabilized transition state in the form of $FH_2C^{\delta-}\cdots H^{\delta+}$(*vs.* $H_3C^{\delta-}\cdots H^{\delta+}$). These results support indirectly the heterolytic splitting of C–H on metal oxides. In the oxidative functionalization of methane with HCl, it was suggested that the C–H bond can be heterolytically broken by an OCl^- on the surface of an La-based catalyst by exchanging a proton for Cl^+, producing a CH_3Cl and a surface hydroxyl group.[26] The heterolytic mechanism was also proposed by Ito *et al.* on the basis of *ab initio* calculations and the chemisorption behaviour of CH_4 towards well-degassed MgO.[27]

However, there is also evidence supporting the homolytic dissociation of C–H bond during the oxidation of methane. By feeding a mixture of CH_4 and CD_4 in the OMC system, CH_3CD_3 was produced as the main product.[28] This result strongly supports the hypothesis that ethane is formed by the coupling of methyl radicals. Using a matrix isolation electron spin resonance (MIESR) system, Lunsford *et al.* detected surface-generated gas-phase radicals over various metal oxide based catalysts, such as Li/MgO, Li/ZnO, Na/CeO_2 and La_2O_3.[29] According to the suggestion of Lunsford, the abstraction of a hydrogen atom from CH_4 is induced by the oxygen-centered radical species on the surface of the catalyst.[29] For example, methane could react with the $[Li^+–O^{\bullet -}]$ on Li/MgO, leading to the formation of surface hydroxyl and methyl radicals. The presence of $[Li^+–O^{\bullet -}]$ center on Li/MgO was substantiated by electron paramagnetic resonance (EPR) studies.[30] The formation of methyl radicals has been further confirmed by synchrotron VUV photoionization mass spectroscopy.[31] The role of oxygen-centered radicals in the abstraction of hydrogen atom has been evidenced by gas-phase studies on mass-selected metal oxide ions.[15] The homolytic mechanism is also proposed for the partial oxidation of methane to methanol. For the iron-doped zeolite (Fe-ZSM-5) catalyzed system, it is suggested that the C–H bond is evenly cracked by two so-called "α sites" containing active radical oxygen species (Fe(III)–$O^{\bullet -}$), leading to a hydroxyl group and a methoxyl group on surface.[32] A similar theory has been developed for the partial oxidation of methane over Cu-ZSM-5, in which a hydrogen atom from methane is abstracted by the oxygen of Cu(II)–$O^{\bullet -}$–Cu(II) species.[33] In sum, there is little disagreement about the heterolytic dissociation of the C–H bond for methane oxidation catalyzed by noble metal complexes, as well as the homolytic theory for OMC. Therefore, the mechanism for activation of methane may change from one catalytic system to another. Certain notions should be elaborated before making a conclusion.

Kinetic study is a useful tool to probe the catalytic mechanism. Using a temporal product analysis (TPA) reactor, Baerns *et al.* confirmed that methyl radicals are formed over Sm_2O_3 by the direct reaction of gaseous methane with surface oxygen species in an Eley–Rideal (E–R) type of mechanism.[34] Kinetic isotope effect (KIE) studies conducted by Cant *et al.* indicate that cleavage of the C–H bond is the rate-limiting step for the OMC process with O_2 as the oxidant.[35] However, Lunsford *et al.* suggested that there is no unique rate determining step, because the KIE changed with the CH_4/O_2 ratio.[29] Re-oxidation of the catalyst reduced by CH_4 could be the rate determining step.[29,36] In this case, the rate of the steady-state reaction proceeds *via* the M–v K mechanism.[21]

The active oxygen species on the surface of a catalyst can be divided into two groups: electrophilic and nucleophilic. Electrophilic oxygen comprises electron deficient adsorbed species such as O_2^-, O_2^{2-} and O^- which are generated from activation of O_2, whereas nucleophilic oxygen includes saturated species such as the terminal oxygen group (M═O) and the bridging oxygen (M–O–M), both with the oxygen atom in a nominal O^{2-} state.[37] As discussed above, electrophilic oxygen species, generated from the activation of gas-phase oxidants, are mainly responsible for the homolytic dissociation of the C–H bond. Therefore, the reactivity of methane is generally much greater in the presence of a gas-phase oxidant.[29,38] The existence of O_2^- on LaOF during the OMC has been proved by the high-temperature *in situ* FTIR studies.[39] On the other hand, it has been proposed that nucleophilic oxygen contributes to the heterolytic dissociation of C–H bond.[25] The influence of nucleophilic oxygen on the catalytic oxidation of methane is identified. For the oxidation of methane to formaldehyde over an Mo based catalyst, a high density of Mo═O groups led to low activity but high selectivity.[40,41] Results obtained from a TPA reactor indicated that even bulk lattice oxygen may participate in the reaction, but at a slower rate.[29] Additionally, it is noteworthy to mention that one cannot rule out the equilibrium between electrophilic oxygen and nucleophilic oxygen.

Besides heterogeneous catalytic systems for the transformation of CH_4, the research on the activation of C–H bonds of CH_4 and other alkane molecules is a frontier in organometallic chemistry. Different reaction paths for the activation of CH_4 by transition metal complexes, which are typically highly reactive and coordinatively unsaturated, such as electrophilic activation, oxidative addition, σ-bond metathesis, 1,2-addition and metalloradical activation have been known for many years.[19,42–45] Recent studies disclosed some new approaches such as electrophilic carbene insertion.[17,46] Metal–oxo complexes (*e.g.*, Fe(IV)═O) are also

capable of activating the C–H bond of alkanes including CH_4.[47,48] In addition, the activation of CH_4 with small metal clusters or metal–oxo clusters in the gas phase has been studied elegantly, and the studies in this field have provided useful information on the mechanism of CH_4 activation by these small clusters on a molecular level without the interference of solid surfaces and solvent effects.[15] This article will not include this content.

2.2 Selective oxidation of methane into organic oxygenates

Here, we do not attempt to give an exhaustive review of heterogeneous catalytic conversion of CH_4. Instead, we focus on systems developed in recent years, which are conceptually attractive or have provided new clues for the rational design of efficient catalysts for selective transformation of CH_4.

2.2.1 Selective oxidation of methane with concentrated H_2SO_4. Although most of the studies on organometallic complexes for CH_4 activation could not lead to the catalytic functionalization of CH_4, a few intriguing homogeneous catalytic systems have been developed based on these studies. The best-known example was reported by Periana and co-workers.[49] The oxidation of CH_4 with sulphuric acid in the presence of a Pt(II) bipyrimidine complex could afford a high yield of methyl bisulphate (~72%), which can subsequently be hydrolyzed to methanol (eqn (6) and (7)).[49] By further combining the reoxidation of SO_2 produced from H_2SO_4 with O_2 (eqn (8)), the net reaction is the selective oxidation of CH_4 to CH_3OH with O_2 (eqn (9)).

$$CH_4 + 2H_2SO_4 \rightarrow CH_3OSO_3H + SO_2 + 2H_2O \quad (6)$$

$$CH_3OSO_3H + 2H_2O \rightarrow CH_3OH + H_2SO_4 \quad (7)$$

$$SO_2 + 1/2O_2 + H_2O \rightarrow H_2SO_4 \quad (8)$$

$$\text{Net: } CH_4 + 1/2O_2 \rightarrow CH_3OH \quad (9)$$

The oxidation of CH_4 by H_2SO_4 to methyl bisulphate is believed to proceed *via* electrophilic C–H activation by the coordinatively unsaturated (cus) Pt complex followed by oxidation and functionalization steps (Fig. 2).[49] Although many problems (*e.g.*, the difficulties in the separation of catalyst, the hydrolysis of methyl bisulphate in concentrated H_2SO_4, and the accumulation and re-oxidation of SO_2) still remain, hindering the commercialization of this process, to date this process has the highest single-pass yield for the selective transformation of CH_4. The high performance of this system is believed to result from the formation of a product, *i.e.*, methyl bisulphate, which is stable under reaction conditions. A recent theoretical study suggests that the bisulphate group protects the C–H bonds of the product by making them less nucleophilic, and thus, decreases the interaction with the electrophilic Pt complexes.[50]

To overcome the problem of catalyst separation, Palkovits *et al.* recently prepared electrophilic Pt centres attached to a polymer, which was a covalent triazine-based framework (CTF), for the oxidation of CH_4 by concentrated H_2SO_4 (Fig. 3).[51,52] Both the Pt–CTF and ($K_2[PtCl_4]$)–CTF, which were prepared by the pre-coordination of Pt in the CTF and the simple combination of CTF with $K_2[PtCl_4]$, respectively, led to efficient catalysts for

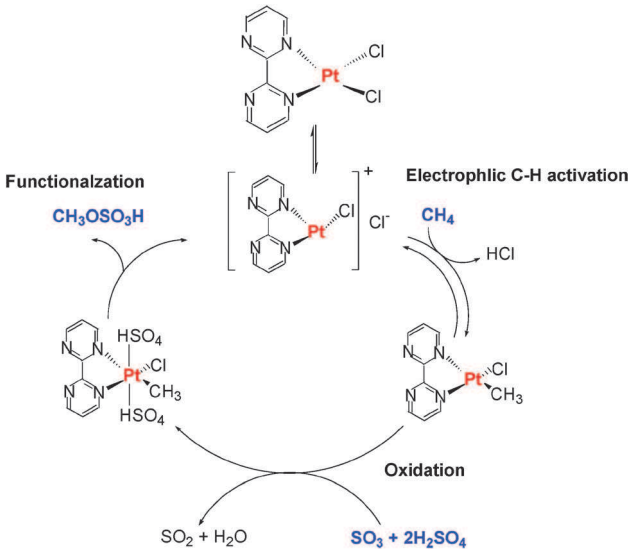

Fig. 2 Proposed reaction mechanism for electrophilic activation of CH_4 followed by oxidation with concentrated H_2SO_4 into methyl sulphate catalyzed by Pt^{II} bipyrimidine complex.[49] Adapted from ref. 49, with the permission of AAAS, copyright 2003.

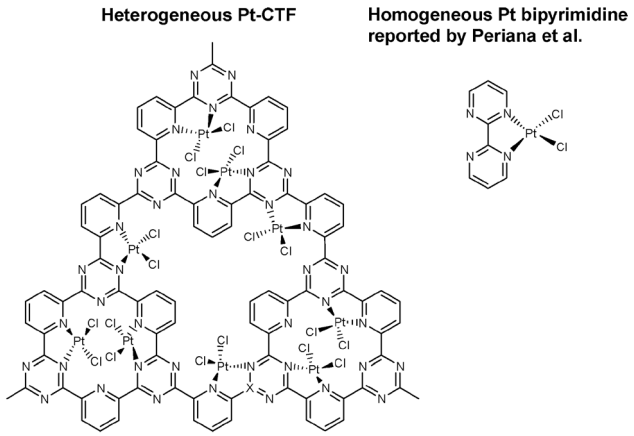

Fig. 3 Pt attached into the CTF polymer framework as a heterogeneous catalyst for the oxidation of CH_4 by concentrated H_2SO_4.[51] Reprinted from ref. 51, with the permission of the John Wiley and Sons.

the oxidation of CH_4 in oleum (H_2SO_4–30% SO_3). After 2.5 h of reaction at 488 K under 40 bar CH_4 pressure, the final concentrations of CH_3OH after hydrolysis of the reaction solution for these two heterogeneous catalysts were 1.80 and 1.54 mol L^{-1}, which were comparable to those obtained for the homogeneous catalyst of Periana *et al.*[51] The turnover numbers (TONs) for the Pt–CTF and ($K_2[PtCl_4]$)–CTF catalysts reached 246 and 201, respectively. These two catalysts were demonstrated to be stable at least after five reaction cycles.[51]

2.2.2 Selective oxidation of methane with H_2O_2. As compared with concentrated H_2SO_4, H_2O_2 is a greener oxidant. Although H_2O_2 is currently more expensive than C_1 oxygenates derived from CH_4 (*e.g.*, CH_3OH), the selective oxidation of CH_4 by H_2O_2 is of fundamental significance. Some studies have been devoted to oxidising CH_4 with H_2O_2 in organic solvents such as

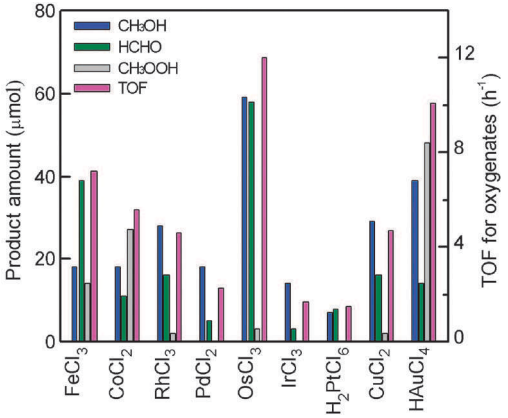

Fig. 4 Selective oxidation of methane with H_2O_2 into oxygenates in water medium catalyzed by various metal chlorides.[53] Adapted from ref. 53, with the permission of the John Wiley and Sons. The relative errors for product amount and turnover frequency number (TOF) were within ±10%. Reaction conditions: metal chlorides, 1.0 mmol dm^{-3}; CH_4, 3 MPa; H_2O_2, 0.5 mol dm^{-3}; H_2O 10 mL; temperature, 363 K; reaction time, 1 h.

acetonitrile catalyzed by vanadium or iron complexes.[54,55] Yuan *et al.* investigated the catalytic behaviour of a series of transition metal chlorides for the oxidation of CH_4 with H_2O_2 in water medium and found that $OsCl_3$ exhibited the highest activity for the selective oxidation of CH_4 to methanol, formaldehyde and methyl hydroperoxide (Fig. 4).[53] The TOF for the formation of these C_1 oxygenates (CH_3OH, HCHO and CH_3OOH) was 12 h^{-1} at 363 K. CO_2 was formed as a main by-product, and the selectivity to C_1 oxygenates was 61%. $HAuCl_4$ also showed a better catalytic performance for the selective oxidation of CH_4 with H_2O_2 in water. A TOF of ~10 h^{-1} and a selectivity of 57% were obtained for the formation of C_1 oxygenates catalysed by $AuCl_3$ at 363 K. However, precipitation was observed after the reaction, possibly due to the formation of Au^0 powder. This indicates that Au(III) is unstable under the reaction conditions in Fig. 4. Since the addition of a radical scavenger, hydroquinone, could quench the reaction, the oxidation of CH_4 with H_2O_2 catalyzed by $OsCl_3$ was proposed to proceed *via* a radical mechanism.[53] Os(IV) was observed by UV-vis spectroscopic measurements in the solution of Os(III)–H_2O_2. The redox between Os(IV) and Os(III) was proposed to account for the activation of H_2O_2, likely forming OH radicals for CH_4 activation.

Inspired by the results achieved in the homogeneous systems, recently, Hutchings and co-workers paid attention to the development of heterogeneous catalysts for the selective oxidation of CH_4 by H_2O_2 in aqueous solution.[56–59] They found that Au–Pd alloy nanoparticles supported on TiO_2 could catalyze the selective oxidation of CH_4 by H_2O_2 in aqueous solution, providing CH_3OH and CH_3OOH as the main partial oxidation products.[59] Over a 0.5 wt% Au–0.5 wt% Pd/TiO_2 catalyst, the TOF for the formation of all the products was 6.85 h^{-1}, and the selectivities to CH_3OH and C_1 oxygenates were 12.1% and 85.4%, respectively, at 323 K and CH_4 pressure of 30.5 bar. The increase in the reaction temperature to 363 K increased the TOF to 25.7 h^{-1}. The selectivities to CH_3OH and C_1 oxygenates changed to 19.8% and 88.4%, respectively, at the same time. The increase in the loadings of Au and Pd both to 2.5 wt% increased the selectivity to CH_3OH to 49.3% while almost retaining the selectivity to total C_1 oxygenates. CH_4 could also be transformed selectively into CH_3OH and CH_3OOH by H_2O_2 in the presence of a 2.5 wt% Au–2.5 wt% Pd/TiO_2 catalyst at a low temperature (275 K). Since Au–Pd/TiO_2 is an efficient catalyst for the direct synthesis of H_2O_2 from H_2 and O_2,[60] CH_4 can be selectively oxidized using an H_2–O_2 gas mixture. This confirms that Au–Pd/TiO_2 is an efficient catalyst for the selective oxidation of CH_4 to C_1 oxygenates in an H_2–O_2 gas mixture. As compared to the case of using H_2O_2, the selectivity to CH_3OH became higher by using an H_2–O_2 gas mixture, and a value of 68% was obtained at 323 K over the 2.5 wt% Au–2.5 wt% Pd/TiO_2 catalyst. Furthermore, the use of reduced NADH (nicotinamide adenine dinucleotide), which is a reductant usually existing in enzyme systems, in combination with O_2 can also replace H_2O_2 to oxidize CH_4 selectively.[59] The selectivity of CH_3OH when using NADH/O_2 could further be increased to 89%. Both OH and CH_3 radicals have been detected by ESR under reaction conditions. Thus, the reaction is proposed to proceed *via* a radical mechanism.

Hutchings and co-workers found that Fe-containing ZSM-5 (or silicalite-1) also catalyzed the selective oxidation of CH_4 with H_2O_2 to C_1 oxygenates, including CH_3OH, HCOOH and CH_3OOH in aqueous medium.[56–58] Although homogeneous Fe^{3+} could also work for the oxidation of CH_4 with H_2O_2 possibly *via* the Fenton-type radial reactions, the heterogeneous Fe-ZSM-5 or Fe-silicalite-1 exhibited significantly higher selectivities to oxygenates (>80% *versus* ~50% in the case of homogeneous catalysis).[57] The catalyst could be used repeatedly without significant deactivation at least for 5 cycles, and no leaching of iron species was detected during repeated use.[58] This demonstrated the heterogeneous feature of this system.

Only a very small amount of Fe (Fe content, 0.014 wt%) existing in the zeolites was already efficient for the selective oxidation of CH_4 by H_2O_2. Through UV-vis and X-ray absorption near edge structure (XANES) spectroscopic studies, the extra-framework oligonuclear Fe species (*e.g.*, the binuclear iron species) worked as the active species.[56,58] Fig. 5 displays the proposed reaction mechanism for this system with binuclear iron as the active site. The addition of a radical scavenger into the system catalyzed by Fe-ZSM-5 did not affect significantly the total amount of oxygenates formed, whereas the radical scavenger remarkably suppressed the oxygenate formation in the Fenton system with $Fe(NO_3)_3$ as the homogeneous catalyst.[57] This suggests that the Fe-containing zeolite-catalyzed reaction is not based upon the homolytic decomposition of H_2O_2 and a subsequent free-radical chain reaction. Through DFT calculations, the Fe(IV)=O species, which is a high-valent iron–oxo species and is usually supposed to be the active species for selective oxidation in enzymatic systems such as cytochrome P450,[61] has been proposed to be responsible for the activation of CH_4, forming a CH_3OOH adsorbed species with the help of the adjacent Fe–OOH site (Fig. 5).[56] The kinetic studies further confirmed that CH_3OOH was the primary product and that CH_3OH was formed from CH_3OOH.[57] Over the Fe-ZSM-5 or Fe-silicalite-1, HCOOH was the

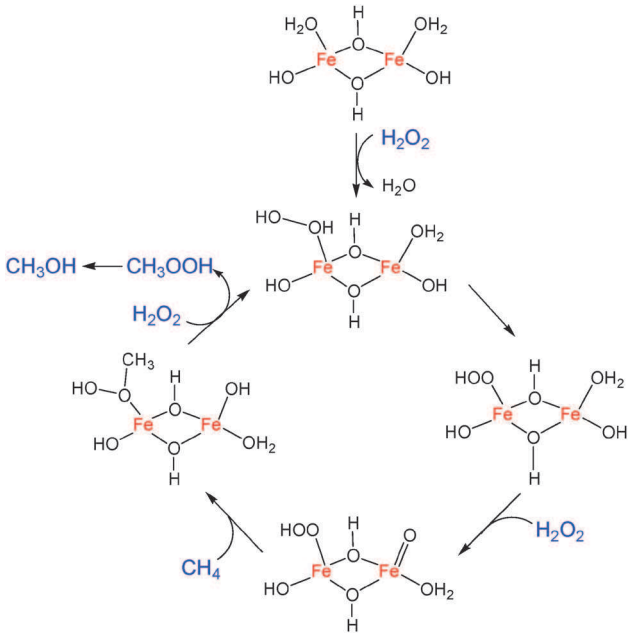

Fig. 5 Proposed reaction mechanism for selective oxidation of CH_4 with H_2O_2 catalyzed by Fe-ZSM-5 or Fe-silicalite-1 in water.[56] Reprinted from ref. 56, with the permission of the John Wiley and Sons.

main product, which was likely formed from CH_3OH due to the presence of OH radicals.

The presence of Cu species either as a homogeneous additive (*e.g.*, $Cu(NO_3)_2$) or as a heterogeneous component (*e.g.*, Cu/silicalite-1) in Fe-containing ZSM-5 or Fe-silicalite-1 can increase significantly the selectivity of CH_3OH while almost retaining CH_4 conversion.[56,57] In the presence of Fe-silicalite-1 and Cu/silicalite-1, a CH_4 conversion of 10% and a CH_3OH selectivity of 93% could be obtained. On the other hand, a Cu-containing catalyst alone such as Cu/silicalite-1 was inactive for the oxidation of CH_4 by H_2O_2. The role of the Cu-containing component was proposed to decrease the concentration of the OH radicals. Thus, Fe is the key active species for CH_4 oxidation in this system. The TOF based on Fe was evaluated to be $>2200\ h^{-1}$, demonstrating that this Cu- and Fe-containing zeolite is an excellent system for the selective oxidation of CH_4 with H_2O_2.

2.2.3 Selective oxidation of methane with N_2O. Fe-containing heterogeneous catalysts, in particular Fe-ZSM-5, are known to be unique for selective oxidations using N_2O as an oxidant.[62] A unique active oxygen species designated as α-oxygen (O_α) can be formed on the catalyst surface, and this oxygen species can oxidize benzene to phenol. The Fe^{II} site, which could be formed by high-temperature (870–1270 K) treatment of Fe-ZSM-5 in steam, vacuum or an inert atmosphere, was believed to be the active site for N_2O activation. Panov and co-workers also demonstrated that this α-oxygen could oxidize CH_4 to CH_3OH at room temperatures.[63,64] The CH_3OH formed on catalyst surfaces could be obtained by extraction with a suitable solvent such as water or a water–acetonitrile mixture, whereas the desorption of CH_3OH by heating only led to the formation of CO and CO_2. This means that this system is not a catalytic cycle but a stoichiometric reaction between CH_4 and the α-oxygen.

In situ Fourier transform infrared (FTIR) spectroscopic studies revealed that the exposure of Fe-ZSM-5 to CH_4 and N_2O at >448 K resulted in the formation of methoxy groups.[65] The active sites for the oxidation of CH_4 to methoxy species by N_2O were demonstrated to be extra-framework Fe sites associated with framework Al. The methoxy groups decomposed to CO_x when the temperature was raised to >523 K but they could be rapidly hydrolyzed to CH_3OH when reacted with H_2O at 523 K. The steady-state oxidation of CH_4 with N_2O at 523 K produced primarily CO_x only with a very small amount of CH_3OH (selectivity $<2\%$).[65]

A recent study using the N_2O/Fe-ZSM-5 system with a high concentration of α-oxygen (100 μmol g^{-1}) revealed that dimethyl ether (DME) could also be formed on the catalyst surface in addition to CH_3OH, and DME corresponded to 6–7% of the CH_4 reacted.[66] The use of acetonitrile or tetrahydrofuran in combination with 10 vol% H_2O as a solvent was quite efficient for the extraction of products formed on the catalyst surface, and the total amount of the extracted methanol and DME comprises 75% of the CH_4 reacted. The missing product remained on the catalyst surface. Further studies on the simultaneous exposure of Fe-ZSM-5 to CH_4 and N_2O at 433 K, at which the α-oxygen could be generated but the product still remained on catalyst surface without formation of CO_x, showed that the stoichiometric ratio of reacted CH_4/N_2O was 1 : 1.[67] Furthermore, a larger amount of N_2O or CH_4 than the amount of the active iron sites, known as the α-sites, was consumed. The TON could reach about 3.6 after an adequate longer reaction time. The extracted products contained 76% CH_3OH and 23% DME together with a small fraction of acetaldehyde. The yield of product extracted (fraction of the extracted products in CH_4 converted) was $\sim$70%. The TON higher than 1 was believed to arise from the spillover of the formed CH_3OH from the α-sites, which liberated the α-sites for further deposition of α-oxygen species and subsequent reaction. This was regarded as a "quasi-catalytic" oxidation of CH_4 by N_2O to CH_3OH and DME.[67]

Only a few studies have so far demonstrated the true catalytic oxidation of CH_4 by N_2O to oxygenates.[68–71] In particular, $FePO_4$ or supported $FePO_4$ exhibited unique catalytic performances. CH_3OH, HCHO and CH_3OCH_3 were formed over these catalysts, and the selectivity to these oxygenates could be higher than 90% at 673 K.[69] For example, over a 40 wt% $FePO_4$/MCM-41 catalyst, the selectivities to CH_3OH, HCHO and CH_3OCH_3 were 23.7%, 48.2% and 24.7%, respectively, with a CH_4 conversion of 0.98% at 673 K. The increase in the temperature to 723 K increased the CH_4 conversion to 3.0% but decreased the selectivity of oxygenates from 96.6% to 82.1%.[69] Although the single-pass conversion was not high ($<3.0\%$), the selectivity to oxygenates was particularly excellent (up to 96.6%). X-Ray photoelectron spectroscopy (XPS) revealed that a part of Fe(III) on the catalyst surface could be reduced to Fe(II) by CH_4 or the reductive products (*e.g.*, CH_3OH) at ≥ 673 K, since N_2O was a weak oxidant.[68] The Fe(II) site with a certain steady-state concentration on catalyst surfaces during the reaction was proposed

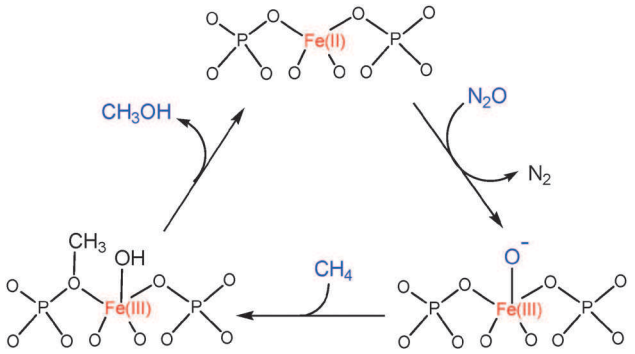

Fig. 6 Proposed reaction mechanism for selective oxidation of CH_4 with N_2O to CH_3OH catalysed by $FePO_4$ or supported $FePO_4$.[68–70] Adapted from ref. 68, with the permission of the Royal Society of Chemistry.

cause the activation of N_2O, generating an active oxygen species, likely, Fe(III)–O^-, for the activation of CH_4 (Fig. 6).[68] The presence of phosphorus was demonstrated to be essential for obtaining a high selectivity to organic oxygenates since the FeO_x/SBA-15 displayed only a low oxygenate selectivity (32.0%) and, in particular, no CH_3OH formation.[70] Thus, the phosphate groups surrounding the Fe site contributed significantly to the selective formation of CH_3OH as the primary product.

2.2.4 Selective oxidation of methane with O_2. Fe(III) is known to be the active centre for the soluble methane monooxygenase (sMMO) in methanotrophic bacteria, which can catalyse the selective oxidation of CH_4 to CH_3OH by O_2 in the presence of a biological reductant (eqn (7)).[72,73]

$$CH_4 + O_2 + 2H^+ + 2e^- \rightarrow CH_3OH + H_2O \qquad (10)$$

In this context, some heterogeneous Fe-based systems including the H_2O_2/Fe-ferrisilicalite-1,[56–58] the N_2O/Fe-ZSM-5[63–67] and the N_2O/$FePO_4$[68,69] can work for the selective oxidation of CH_4 to oxygenates. However, these Fe-based systems generally could not work well for the formation of CH_3OH when O_2 was used as an oxidant instead of H_2O_2 or N_2O.

Copper is the active centre of the particulate methane monooxygenase (pMMO), which is known to be the most efficient catalytic system for the selective oxidation of CH_4 to CH_3OH, with a TOF approaching 1 s^{-1}.[74–77] The chemistry of Cu-based selective oxidation of CH_4 by O_2 has attracted much attention in recent years. For example, Yoshizawa and Shiota performed a detailed DFT calculation for the activation of O_2 and the conversion of CH_4 over the mononuclear and dinuclear copper sites, which may exist in pMMO.[78] Their results suggest that O_2 can be activated by the mononuclear Cu(I) species to give a Cu(II)–superoxo (Cu(II)–OO^-) species in the first step. Then, the Cu(II)–superoxo species accepts an H-atom transferred from a tyrosine residue near the mononuclear Cu site to produce a Cu(II)–hydroperoxo species (Cu(II)–OOH). The Cu(II)–OOH species is then transformed into a Cu(III)–oxo (Cu(III)=O) species by the abstraction of an H atom from another tyrosine residue. The Cu(III)=O is proposed to be responsible for the activation of CH_4. In the case of dinuclear Cu sites, O_2 is first incorporated into the dicopper site to form a (μ-η^2:η^2-peroxo)dicopper species, which is then transformed into a bis(μ-oxo)dicopper species. This species can activate CH_4 with an activation energy of 17.6 kcal mol^{-1}, which is similar to that with the Cu(III)=O species. However, the formation of the bis(μ-oxo)dicopper species from dicopper site is more favorable than the formation of the Cu(III)=O species from the monocopper species. On the other hand, Chan and co-workers have strengthened the importance of the trinuclear copper cluster in pMMO for the activation of O_2 and the activation of C–H bonds.[76,79–81] Recently, Chan and co-workers have further demonstrated that a trinuclear copper complex, $[Cu^ICu^ICu^I(7\text{-}N\text{-Etppz})]^{1+}$ (Etppz = 3,3′-(1,4-diazepane-1,4-diyl)bis[1-(4-ethylpiperazine-1-yl)propan-2-ol]), can work for the oxidation of CH_4 to CH_3OH in acetonitrile by O_2.[80] A TON of 0.92 was obtained in 10 min. To be catalytic, this complex requires regeneration by H_2O_2. Furthermore, a tricopper peptide complex was synthesized and was demonstrated to be capable of working for the selective oxidation of CH_4 to CH_3OH.[80]

Schoonheydt and co-workers reported that Cu-loaded zeolites could be exploited for the oxidation of CH_4 to CH_3OH after pretreatment by O_2.[33,82–85] Cu-ZSM-5 pretreated at 723 K in O_2 flow, which was followed by an He purge to remove the gaseous O_2, could convert CH_4 into CH_3OH at 398–498 K.[82] However, CH_3OH remained on the catalyst surface and could only be obtained by extraction with a solvent. After reaction with CH_4 at 448 K, an amount of 8.2 μmol $g(cat)^{-1}$ CH_3OH was extracted from a Cu-ZSM-5 (Si/Al = 12, Cu/Al = 0.58) using a 1 : 1 water–acetonitrile solvent.[82] The reaction correlated to an absorption at 22 700 cm^{-1} in the UV-vis spectrum; the generation of this absorption was observed after O_2 treatment and it disappeared after the reaction with CH_4. Further studies showed that Cu-ZSM-5 with a Cu/Al ratio larger than 0.2 was required for the generation of the absorption band at 22 700 cm^{-1} ($\sim$440 nm), and the intensity of this absorption band increased with the Cu/Al ratio. Correspondingly, CH_3OH could only be obtained from the Cu-ZSM-5 with a Cu/Al ratio >0.2.[33] These observations clearly demonstrate that the species possessing an absorption band at 22 700 cm^{-1} is the active species for the conversion of CH_4 to CH_3OH. Detained spectroscopic studies combined with DFT calculations suggest that the active species is a bent mono(μ-oxo)dicopper(II) species ($[Cu_2O]^{2+}$) located in ZSM-5, whose structure is displayed in Fig. 7A. An absorption band at 29 000 cm^{-1} ($\sim$345 nm) was observed when the pre-reduced Cu-ZSM-5 (in He at 723 K, Cu/Al = 0.5) was exposed to O_2 at room temperature.[84] Interestingly, this band also could not be observed at lower Cu content (Cu/Al <0.2). The increase in temperature to $\geq\sim$448 K led to the appearance of the band at 22 700 cm^{-1} and the parallel disappearance of the band at 29 000 cm^{-1}. Further resonance Raman spectroscopic measurements using laser excitation at 363.8 nm led to Raman bands at 269 and 736 cm^{-1}, which could be ascribed to the O–O and the Cu–Cu stretch of the μ-(η^2-η^2)peroxo dicopper(II) ($[Cu_2(O_2)]^{2+}$) moiety, respectively.[84] Thus, the absorption band at 29 000 cm^{-1} could be assigned to be a peroxo π^*_σ into Cu(II) charge transfer transition. These results all suggest that the active species (*i.e.*, $[Cu_2O]^{2+}$) is formed *via* the $[Cu_2(O_2)]^{2+}$ precursor. Fig. 7B shows the possible reaction mechanism proposed for the

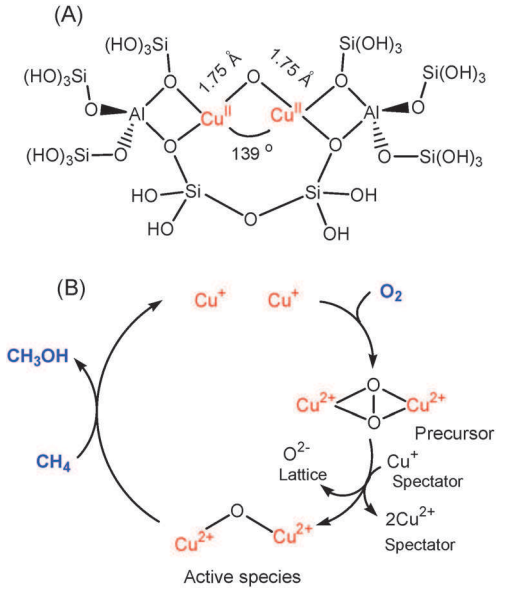

Fig. 7 (A) Possible structure of active species. (B) Proposed mechanism for the formation of active oxygen species from O_2 over Cu-ZSM-5 for the selective oxidation of CH_4 to CH_3OH.[83,84] (A) and (B) reprinted from ref. 83 and 84, with the permission of PNAS and the American Chemical Society (copyright 2010), respectively.

generation of active species in Cu-ZSM-5 from O_2, which can work for the selective oxidation of CH_4 to CH_3OH. Concerning the activation of CH_4 by the $[Cu_2O]^{2+}$ species, DFT calculation suggests that this species can abstract H from CH_4, producing CH_3OH *via* a Cu^{II}–$O^{\bullet -}$–Cu^{I} and an attached CH_3 radial (eqn (11)).[83,85]

$$[Cu^{II}\text{–}O\text{–}Cu^{II}]^{2+} + CH_4 \rightarrow [Cu^{II}\text{–}{}^{\bullet}OH\text{–}Cu^{I}]^{2+}\cdots{}^{\bullet}CH_3 \rightarrow 2Cu^{I} + CH_3OH \quad (11)$$

The calculated energy barrier for the H abstraction is 18.5 kcal mol^{-1}, which is close to that obtained from experimental studies (15.7 kcal mol^{-1}). This reaction has a KIE of 3.1 at 448 K,[83] indicating that the cleavage of C–H bond is the rate-determining step for the oxidation of CH_4.

In addition to Cu-ZSM-5, Co-ZSM-5 also showed such an ability to perform the selective oxidation of CH_4 after pretreatment in O_2.[86–88] Similar to the Cu-ZSM-5 system, the products had to be extracted from Co-ZSM-5 using a suitable solvent and the extracted products were also only a few percent of the total moles of Co. Thus, the reaction is not catalytic but stoichiometric. The Co-ZSM-5 (Si/Al = 17.5) with a lower Co content (0.9 wt%), which contained 80% isolated Co(II), provided CH_3OH and HCHO with selectivities of 25% and 75%, respectively, after exposure to CH_4 at 423 K (the products were extracted by ethanol).[86] The increase in Co content in Co-ZSM-5 led to the generation of more cobalt oxide species at the expense of isolated Co(II). The selectivity of CH_3OH increased to 45% and that of HCHO decreased to 55% at the same time. A subsequent study confirmed that the higher fraction of isolated Co(II) in the Co-ZSM-5 resulted in higher selectivity to HCHO.[87] Furthermore, the formation of formate was observed by a detailed FTIR study.[88] The following Cannizzaro reaction (eqn (12)) was proposed to take place on the surface of Co-ZSM-5.[88]

$$2HCHO + H_2O \rightarrow CH_3OH + HCOOH \quad (12)$$

Through comprehensive NMR studies, Deng and co-workers found that the Zn-modified H-ZSM-5 (Zn loading, 3.8 wt%), which was prepared by the reaction of metallic Zn vapour with H-ZSM-5 (Si/Al = 21), could activate CH_4 at room temperature. Besides zinc methyl ($Zn–CH_3$) species, surface methoxy species attached to zeolite framework were also detected at room temperature by *in situ* solid-state NMR spectroscopy.[89] The methoxy species can be readily transformed to CH_3OH by hydrolysis with H_2O or be converted into hydrocarbons at higher temperatures ($\geq$523 K). Three types of Zn species (including isolated Zn^{II}, isolated Zn^{I} and binuclear Zn^{I}–O–Zn^{II}) have been identified on the ZnZSM-5, and it is proposed that the binuclear Zn^{I}–O–Zn^{II} is responsible for the activation of CH_4, forming methoxy species possibly through the following reactions (eqn (13) and (14)).[89]

$$Z\text{–}Zn\text{–}O\text{–}Zn\text{–}Z + CH_4 \rightarrow Z\text{–}Zn(OH)\text{–}Zn\text{–}Z + {}^{\bullet}CH_3 \quad (13)$$

$$Z\text{–}O + {}^{\bullet}CH_3 \rightarrow Z\text{–}OCH_3 \quad (14)$$

where Z denotes the zeolite framework.

Although the results obtained from these zeolite-based systems are of high fundamental significance, the problem is that the products have to be extracted by a solvent and the reaction is not catalytic. Bokhoven and co-workers recently developed a multi-step route for performing the oxidation of CH_4 to CH_3OH using O_2-pretreated Cu-mordenite.[90] In the first step, the Cu-mordenite was treated by O_2 at 723 K to generate the active species, followed by cooling down to room temperature in He. The generation of the $[Cu_2O]^{2+}$ species was confirmed by the appearance of the absorption band at 22 700 cm^{-1}. Then, the temperature was raised to 473 K and the sample was exposure to CH_4. Subsequently, a gas flow of H_2O/He was introduced, and CH_3OH was observed in the outlet of the stream. After the first cycle, the Cu-mordenite was treated by O_2 again to regenerate the active species. In the second cycle, the amount of CH_3OH was found to be close to that in the first cycle, showing that the Cu-mordenite could be used for the formation of CH_3OH by repeating the reaction cycle.

On the other hand, there are also many studies devoted to the selective oxidation of CH_4 to oxygenates by O_2 at relatively higher temperatures using heterogeneous catalysts, although the advances in this direction have not been very significant in recent years. Conventionally, MoO_3/SiO_2 and V_2O_5/SiO_2 were extensively studied for the selective oxidation of CH_4 by O_2. In most cases, HCHO could be obtained with yields of $<$5%.[93–98] The reaction proceeds *via* the Mars–van Krevelen mechanism, which has been proposed for the selective oxidation of olefins to oxygenates.[2–7] The lattice oxygen, in particular, the terminal oxygen species, *e.g.*, Mo(VI)=O, might work for the activation of CH_4 (eqn (15)), and the reduced site (Mo(IV)) could be recovered by O_2 (eqn (16)).

$$CH_4 + 2Mo^{VI}{=}O \rightarrow HCHO + H_2O + 2Mo^{IV} \quad (15)$$

$$2Mo^{IV} + O_2 \rightarrow 2Mo^{VI}{=}O \quad (16)$$

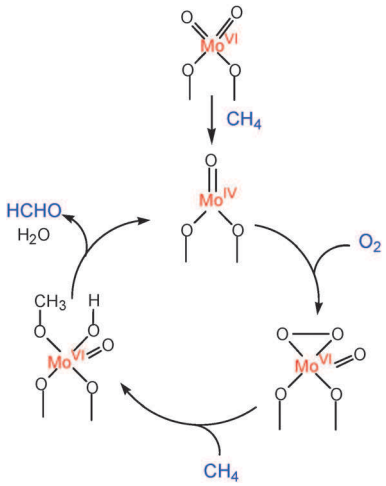

Fig. 8 Proposed reaction mechanism for the selective oxidation of CH_4 by O_2 over MoO_x/SiO_2.[91,92] Reprinted from ref. 91, with the permission of the American Chemical Society, copyright 2006.

A DFT calculation revealed that the terminal oxygen species of Mo(VI)=O in a model Mo_3O_9 cluster could abstract the hydrogen atom from CH_4.[99] However, recent studies for the MoO_x/SiO_2 catalyst with isolated MoO_x species suggested that the active oxygen species for CH_4 activation was not the lattice oxygen but might be a peroxide species generated by the activation of O_2 on the isolated reduced Mo(IV) site (Fig. 8).[91,92] This mechanism might also be applicable to the supported VO_x catalysts, for which the isolation of VO_x species is required for the selective oxidation of CH_4 to HCHO. The VO_x/SBA-15 and VO_x/MCM-41 catalysts, which contained a high dispersion of VO_x species (0.08 V atom per nm^2), could provide high TOF (0.48) for HCHO formation.[100,101] For example, a TOF of 0.48 s^{-1} could be achieved over the VO_x/SBA-15 at 898 K.[100,101]

Various transition metal cations or metal oxide nanoclusters highly dispersed on SBA-15 have recently been examined for the selective oxidation of CH_4 by O_2 at 898 K.[102] The content of the transition metal was controlled at <0.01 wt% to obtain a high dispersion. On this occasion, the MoO_x/SBA-15 and VO_x/SBA-15 showed only very low activity. Unexpectedly, the CuO_x/SBA-15 exhibited the highest HCHO formation activity, followed by FeO_x/SBA-15 and MnO_x/SBA-15.[102] This result is unique because copper is usually a good component employed in methane combustion catalyst. However, if one considers that Cu and Fe are the active centres of the methane monooxygenases (pMMO and sMMO), this observation is understandable and is certainly of interest.

Iron-based heterogeneous catalysts with Fe(III) sites highly dispersed in amorphous silica or mesoporous silica have already been known to catalyse the selective oxidation of CH_4 by O_2.[70,95,103–107] However, few studies have been devoted to the copper-based catalytic oxidation of CH_4 by O_2, although the O_2-pretreated Cu-containing zeolites could oxidize CH_4 to CH_3OH in a non-catalytic manner (Fig. 7).[33,82–86] Studies by Wang and co-workers for the CuO_x/SBA-15-catalyzed CH_4 selective oxidation clarified that a small amount of copper (0.008 wt%) existing in SBA-15 could enhance significantly the selective formation of HCHO.[108] ESR characterization indicated that this catalyst contained primarily isolated Cu(II) ions. The TOF calculated based on the moles of HCHO formed per mole of Cu^{II} sites per unit time reached 5.6 s^{-1} at 898 K for this catalyst.[108] This value is several orders of magnitude higher than those reported for other catalysts and is even higher than that for pMMO ($\sim$1 s^{-1}).[81] In addition, a 0.6 wt% CuO_x/SBA-15 catalyst prepared by the grafting approach, which contained a higher fraction of isolated Cu(II) attached on the framework of SBA-15, was found to be significantly more selective for HCHO formation than the catalyst with a similar Cu content but prepared by the impregnation method.[109] The latter catalyst possessed a larger fraction of Cu_mO_n clusters. This suggests that the isolated Cu(II) site is responsible for the selective oxidation, while the Cu_mO_n cluster catalysed the complete oxidation of CH_4 to CO_2.

Further studies using the pulse reaction technique in combination with ESR spectroscopic measurements revealed that the lattice oxygen or the oxygen species associated with Cu sites in the CuO_x/SBA-15 oxidised CH_4 to CO and CO_2 but not HCHO. The presence of gaseous O_2 was indispensable for the formation of HCHO. Part of the Cu(II) sites could be reduced to Cu(I) by CH_4 molecules under the reaction conditions. The increase in the concentration of Cu(I) at the initial reaction stage increased both the CH_4 conversion and the HCHO selectivity. Thus, the Cu(I) site generated under reaction conditions accounts for the activation of O_2 to provide an active oxygen species for the selective oxidation of CH_4 to HCHO (Fig. 9).[108,109] This mechanism is different from the conventional M–v K mechanism proposed for the supported MoO_x and VO_x oxide catalysts. The lattice oxygen in the CuO_x clusters instead oxidizes CH_4 to CO_x, and this is believed to be the main reason why the isolated Cu(II) site is required for the selective formation of HCHO. Concerning the nature of the active oxygen species, the DFT calculations by Yoshizawa and Shiota suggest that the Cu(II)–superoxo (Cu^{II}–OO^-) species, which can be easily formed by the activation of O_2 on the mononuclear Cu(I) species, can activate the C–H bond of CH_4 with an activation energy of 155 kJ mol^{-1}.[78] The reaction with such an activation energy is difficult under physiological temperatures but may be possible at relatively higher temperatures ($\geq$773 K). In the solid state, the oxygen species generated from O_2 on a single Cu(I) site with organic complexes has also been

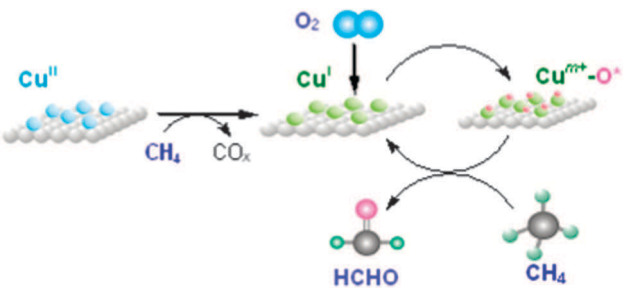

Fig. 9 Proposed reaction mechanism for the selective oxidation of CH_4 by O_2 over CuO_x/SBA-15 with isolated Cu(II) dispersed on SBA-15.[108,109] Reprinted from ref. 108, with the permission of the Elsevier, copyright 2010.

demonstrated to be capable of breaking the C–H bond.[110] Further studies are needed to elucidate the nature of the active oxygen species in the current isolated Cu(II)-based catalytic system for the selective oxidation of CH_4 to HCHO by O_2.

2.2.5 Oxidative conversion of methane into acetic acid or its derivatives. In addition to C_1 oxygenates such as CH_3OH and HCHO, the direct oxidative functionalization of CH_4 to acetic acid has also attracted research attention, particularly in homogeneous systems using transition metal salt or metal complex catalysts.[49,111–114] A few early studies also pointed out that CH_4 could be carbonylated to acetic acid in the presence of CO and a superacid such as HF–SbF_5 or FSO_3H–SbF_5.[115,116] The conversion of CH_4 in the presence of strong acid might form a methyl cation, followed by carbonylation with CO to give the acetyl cation ($[CH_3C{=}O]^+$), which undergoes hydrolysis to acetic acid (eqn (17)–(19)).[115,116]

$$CH_4 + HF\text{–}SbF_5 \rightarrow CH_3^+ + H_2 + SbF_6^- \quad (17)$$

$$CH_3^+ + CO \rightarrow [CH_3C{=}O]^+ \quad (18)$$

$$[CH_3C{=}O]^+ + H_2O \rightarrow CH_3COOH + H^+ \quad (19)$$

Based on solid-state ^{13}C magic-angle spinning (MAS) NMR studies, Stepanov *et al.* demonstrated that the carbonylation of isobutane by CO could proceed over a solid superacid, *i.e.*, sulphated zirconia, at 343 K, providing methyl isopropyl ketone [$(CH_3)_2CH(CO)CH_3$] and pivalic acid [$(CH_3)_3CCOOH$] as the main product in the absence and the presence of H_2O, respectively.[117] Similarly, propane could be carbonylated with CO on sulphated zirconia to form isobutyraldehyde and isobutyric acid at 373–423 K.[118] Isobutyraldehyde was the intermediate product and was almost completely converted into the acid at 423 K. The sulphate groups of sulphated zirconia were responsible for the oxidation of aldehyde to acid, and the sulphate group itself was likely reduced into a dithionate species. A subsequent study by the same research group using MAS NMR further showed that CH_4 could also be converted into CH_3COOH at 473–523 K in the presence of CO on the surface of sulphated zirconia.[119] The reaction was performed in a sealed glass tube designed for NMR spectroscopic measurements. The amount of Brønsted acid sites was about 500 μmol g^{-1}, and the conversions of CH_4 (*ca.* 300 μmol g^{-1}) with CO (*ca.* 300 μmol g^{-1}) in the absence and the presence of O_2 (*ca.* 150 μmol g^{-1}) at 523 K were 18% and 24%, respectively. The products extracted from the sample after the reaction with diethyl ether confirmed the formation of CH_3COOH. Two possible routes have been proposed for the formation of CH_3COOH. In one route, the activation of CO by the strong Brønsted acid sites occurs first, giving formate species, which may be transformed into a formyl cation $[HC{=}O]^+$. The interaction of CH_4 with the formyl cation may offer acetaldehyde, and acetaldehyde was further oxidized into acetic acid by the sulphate group or by O_2. In the other route, the activation of CH_4 by the superacid site occurs first, forming CH_3^+ cation. Then the reaction of CH_3^+ with CO produces $[CH_3C{=}O]^+$, which is subsequently transformed into CH_3CHO and finally into CH_3COOH.

Recently, the reaction of CH_4 with heteropolyacids such as $H_4SiW_{12}O_{40}$ and $H_3PW_{12}O_{40}$, which are known to possess very strong acidity,[120,121] attached on a partially dehydroxylated SiO_2 surface *via* surface organometallic chemistry method was investigated by solid-state NMR.[122] The formation of adsorbed CH_3COOH at 298–393 K was evidenced by NMR spectra. Although the detailed mechanism for CH_3COOH formation is still unclear, the following reaction was proposed to occur on the surface of heteropoly acids (eqn (20)).[122]

$$2CH_4 + [H_2SiW_{12}O_{40}]^{2-}[{\equiv}Si\text{–}O(H)_2]^+_2 \rightarrow CH_3COOH + [H_2SiW_{12}O_{36}]^{2-}[H_3O]^+_2[{\equiv}Si\text{–}OH]_2 \quad (20)$$

The activation of propane and isobutane in the presence of CO and H_2O over acidic H-ZSM-5 was also investigated by *in situ* solid-state NMR and GC analysis.[123] Isobutyric acid was formed on the surface from propane at 373–473 K, while isobutane was transformed into pivalic acid [$(CH_3)_3CCOOH$] with simultaneous production of H_2. Thus, the protons in H-ZSM-5 can also be exploited for the activation of CO or lower alkanes. Wu *et al.* performed a detailed MAS NMR study on possible C_1 surface species from CH_4 activation on Zn/H-ZSM-5, and they identified zinc methyl species, formate species and methoxy species at $\leq$573 K.[124] They further clarified that these C_1 species could undergo different reactions in the presence of different probe molecules such as water, methanol, hydrochloride, oxygen and carbon dioxide. Recently, through *in situ* ^{13}C MAS NMR studies, Deng and co-workers reported the formation of acetic acid in the presence of CH_4 and CO at 623 K on the surface of a ZnZSM-5, which was prepared by the reaction of metallic Zn vapor with H-ZSM-5.[125] Zinc methyl species (Zn–CH_3) and zinc methoxy species (Zn–OCH_3) were both observed and may function as reaction intermediates. The presence of a small amount of O_2 enhanced the formation of the Zn–CH_3 species but disfavored the formation of Zn–OCH_3 species, while the presence of H_2 favored the formation of Zn–OCH_3. Two parallel pathways have been proposed for CH_3COOH formation.[125] One pathway is the reaction of Zn–CH_3 with CO_2, and the methyl and carbonyl groups of acetic acid stem from CH_4 and CO, respectively. The other pathway is the carbonylation of Zn–OCH_3 with CO through the Koch-type mechanism. The presence of O_2 favors the former pathway, while the presence of H_2 favors the latter.

Although fundamentally interesting, the reactions in the above systems are stoichiometric but not catalytic. The formed acetic acid could only be observed by solid-state MAS NMR or be extracted by a solvent. Few studies have succeeded in performing catalytic conversion of methane to acetic acid or its derivatives using a heterogeneous catalyst. Wang *et al.* found that the introduction of CO into the gas mixture of CH_4 and N_2O resulted in the direct formation of methyl acetate over a rhodium-doped iron phosphate catalyst (eqn (21)).[126]

$$2CH_4 + N_2O + CO \rightarrow CH_3COOCH_3 + N_2 + H_2O \quad (21)$$

Further studies revealed that the preparation of Rh–$FePO_4$ catalyst with Rh(III) incorporated into the lattice of $FePO_4$ to

form a $Rh_xFe_{1-x}PO_4$ solid solution led to a significantly higher rate for CH_3COOCH_3 formation than the $Rh/FePO_4$ catalyst prepared by conventional impregnation, which contained RhO_x clusters on the surface of $FePO_4$.[127] The analysis of the structure–performance relationship suggests that the dual sites containing both Rh(III) and Fe(III) connected by phosphate groups (–Fe^{III}–O–P–O–Rh^{III}–O–P–O–) are responsible for CH_3COOCH_3 formation. Based on this structural model of active sites, a catalyst containing $Rh_xFe_{1-x}PO_4$ nanoclusters dispersed in mesoporous channels of MCM-41 was successfully prepared, and this catalyst possessed a higher concentration of the surface dual site. A methyl acetate formation rate of *ca.* 0.7 mmol $g(cat)^{-1}$ h^{-1} was achieved at 723 K over a 0.11 wt% Rh–9.1 wt% $FePO_4$/MCM-41 catalyst. The TOF for CH_3COOCH_3 formation was *ca.* 65 h^{-1} over this catalyst.

Further mechanistic studies using CO temperature-programmed reduction (CO-TPR), XPS and FTIR of adsorbed CO for the oxidative carbonylation of CH_4 in the presence of CO and N_2O suggest that simultaneous reductions of Rh(III) and Fe(III) to Rh(I) and Fe(II) occur in CO, and a Rh(I) geminal dicarbonyl species, $Rh^I(CO)_2$, has been observed in the CO adsorbed FTIR spectra.[128] The Fe(II) site generated after the reduction of the dual site by CO could activate N_2O, generating the active oxygen species for CH_4 activation (Fig. 10).[127,128] The formed CH_3 species would migrate to the neighbouring Rh(I) site coordinated by CO, and the insertion of CO into the Rh–C bond could result in the formation of an acetyl-rhodium intermediate. CH_3COOCH_3 should be formed *via* the reaction of the acetyl-rhodium species with the CH_3O species on the surface. Because the activation of CH_4 and the carbonylation of CH_3 by CO occur on iron and rhodium, respectively, it is understandable that the dual site containing Rh(III) and Fe(III) in close proximity is crucial for the formation of CH_3COOCH_3.

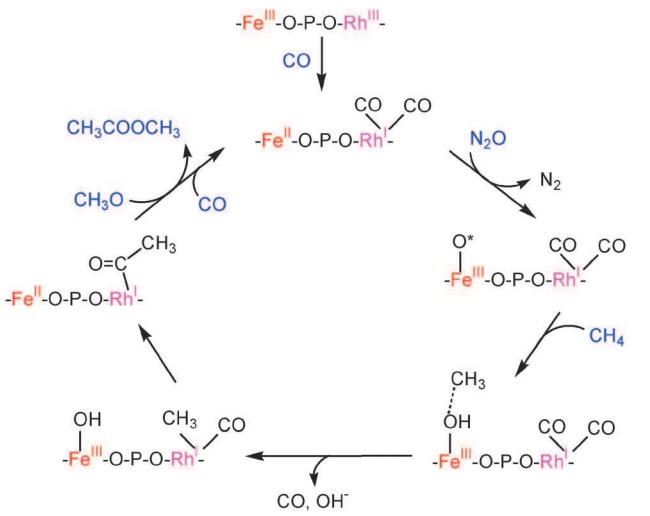

Fig. 10 Proposed reaction mechanism for the oxidative carbonylation of CH_4 in the presence of CO and N_2O over catalysts containing dual sites of Rh^{III} and Fe^{III} connected by phosphate groups.[127,128] Reprinted from ref. 128, with the permission of the American Chemical Society, copyright 2007.

2.3 Oxidative conversion of methane to higher hydrocarbons

The oxidative conversion of CH_4 to C_{2+} hydrocarbons, in particular lower olefins (ethylene and propylene), is another challenging reaction in methane chemistry. Lower olefins are very important building-block chemicals, and are primarily produced from petroleum *via* steam cracking of naphtha in the current chemical industry. The conversion of CH_4 to higher hydrocarbons requires the formation of C–C bonds. Conventionally, there are two major routes for C–C coupling. One is the Fischer–Tropsch synthesis, which involves the conversion of CO with H_2 into higher hydrocarbons with a wide distribution of products. The other route includes single-step C–C coupling, such as methanol carbonylation to acetic acid, olefin metathesis, aldol condensation and alkylation. Some catalytic systems for the oxidative carbonylation of CH_4 have been developed (Section 2.2.5), but the efficiency is still low. The oxidative methylation of aromatics with CH_4 (eqn (22)) could proceed over a suitable zeolite catalyst although the performance was limited.[129] Furthermore, CH_4 could react with ethylene to produce propylene (eqn (23)) over (LiCl + NaCl)/MgO or Ag^+-exchanged zeolite catalysts.[130,131] This article will not include these C–C couplings of CH_4 with other molecules.

$$CH_4 + C_6H_6 + 1/2O_2 \rightarrow C_6H_5CH_3 + H_2O \quad (22)$$

$$CH_4 + C_2H_4 + 1/2O_2 \rightarrow C_3H_6 + H_2O \quad (23)$$

On the other hand, direct OMC to C_2H_6 and C_2H_4 (eqn (24) and (25)) has been studied for about 30 years.

$$2CH_4 + 1/2O_2 \rightarrow C_2H_6 + H_2O \quad (24)$$

$$2CH_4 + O_2 \rightarrow C_2H_4 + 2H_2O \quad (25)$$

A large number of papers have been published in this area.[29,132–137] The reaction proceeds *via* a heterogeneous–homogeneous mechanism. In brief, the initial step is the activation of CH_4 on catalyst surface (heterogeneous), forming methyl radicals. Then, gas-phase reactions involving methyl radicals in the presence of CH_4 and O_2 (homogeneous) will proceed to a large extent.[21,36] With such a mechanism, there may exist inherent limits of product yield. An upper bound of yield to C_2 hydrocarbons has been estimated to be ~28% by kinetic modelling under conventional, packed-bed and continuous-feed operation.[138] A recent statistical analysis based on the references of the last 30 years suggests that high-performance catalysts are primarily based on Mg and La oxides.[137] The addition of alkali or alkaline earth metal ions or salts as dopants can increase the selectivity of the host oxides, while several transition metal dopants such as Mn and W have positive effects on activity. Chlorine anions existing in the catalyst may also play a positive roles in catalytic performances. The maximum C_2 yield reached 26% over optimized catalysts.[137]

Several recent papers dealt with new strategies to prepare efficient OMC catalysts. For example, a novel Cl-doped perovskite-type composite oxide catalyst, $Ba_{0.5}Sr_{0.5}Fe_{0.2}Co_{0.8}O_{3-\delta}Cl_{0.04}$, was found to be very effective for the oxidative coupling of CH_4 using N_2O as an oxidant.[139] The Cl modification significantly enhanced the selectivity, and a C_2 selectivity of ~46% could be obtained

at a CH_4 conversion of ~66%, providing a C_2 yield of ~30% at 1123 K. The ratio of C_2H_4/C_2H_6 was 2.6 at the same time. Although the loss of chlorine might occur at such a high temperature for a long time on-stream, the performance of this catalyst was stable at least for ~6 h. The use of N_2O could decrease the gas-phase radical reactions and increase the contribution of surface reactions. It remains unclear whether the surface oxygen species derived from N_2O or the lattice oxygen of the chlorinated perovskite is responsible for the activation of CH_4.

La_2O_3-based catalysts showed excellent catalytic performance for the oxidative coupling of CH_4 at relatively lower temperatures. Recently, Senkan and co-workers found that the utilisation of nanofiber-morphology La_2O_3–CeO_2 (La/Ce = 15/1) prepared by an electrospinning technique could further decrease the ignition temperature for the oxidative coupling of methane.[141] For the conventional particulate La_2O_3–CeO_2 catalyst prepared by the co-precipitation method, the conversion of CH_4 started from ~813 K, giving a C_2 yield of 5% and a C_2 selectivity of 60%. On the other hand, the La_2O_3–CeO_2 nanofibers provided a C_2 yield of 18% and a C_2 selectivity of 65% at 743 K. With increasing the temperature to 793 K, the C_2 yield and selectivity increased to 20% and 70%, respectively. It is proposed that the nanofabricated catalyst may provide better dispersion of active sites and easier access of reactants to the active sites. Furthermore, the nanofibers may expose particular facets different from those of the nanoparticles, favouring the OMC reaction. Sm_2O_3 foams fabricated by a direct foaming process have also been examined as catalysts for the OMC reaction.[142] The Sm_2O_3 catalyst prepared by the foaming technique led to unique bimodal pore-size distribution with pores of 10–100 μm and 300–400 nm. The C_2 yield and space time yield for the Sm_2O_3 foams were significantly higher than those for the Sm_2O_3 powders. These results imply that the catalyst with a more favourable mass and heat transfer is beneficial for the OMC reaction.

For the OMC catalysts developed to date, the formation of CO_x (CO and CO_2) is unavoidable, particularly at industrially relevant CH_4 conversions. How to increase the C_{2+} selectivity and to decrease the CO_x selectivity is a key issue for the OMC reaction. Recently, a new strategy has been proposed for improving product selectivity by combining the OMC reaction with the selective hydrogenation of CO_x into hydrocarbons (Fig. 11).[140] In this dual-reactor strategy, the OMC reaction was performed at a higher temperature in the first reactor containing an OMC catalyst (*e.g.*, an Mn–Na–W/SiO_2 catalyst operated at 1103 K). The outlet mixture of the reaction products and the unreacted CH_4 was mixed with a flow of pure H_2 and was directly introduced into a second reactor loaded with a CO_x hydrogenation catalyst operated at ambient pressure and a lower temperature (*e.g.*, Ru–Mn/TiO_2 operated at 473 K). The results showed that the employment of the second reactor containing the Ru–Mn/TiO_2 catalyst operated at 473 K in combination with the Mn–Na–W/SiO_2 catalyst in the first reactor did not significantly alter CH_4 conversion. The yield of CO_x decreased significantly with increasing the catalyst amount loaded in the second reactor (Fig. 11B). At the same time, the yield of C_{2+} hydrocarbons increased from ~22% to ~34%. This high C_{2+} yield confirms the usefulness of the dual-reactor strategy.

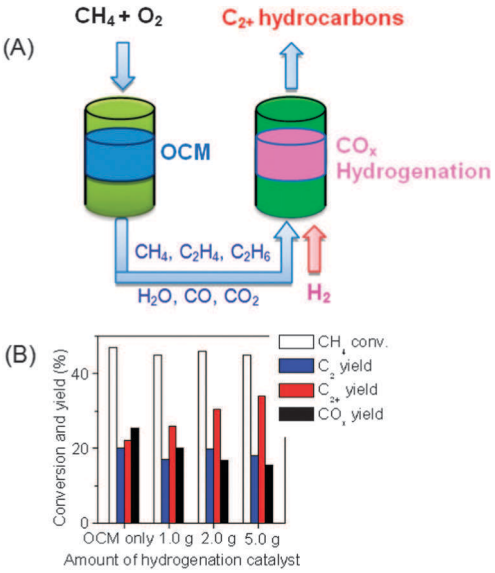

Fig. 11 (A) Dual-reactor strategy for the conversion of CH_4 to C_{2+} hydrocarbons. (B) Dependence of catalytic performance on the amount of catalyst in the second reactor. The OMC reaction was performed with Mn–Na–W/SiO_2 (250 mg) and a $CH_4/O_2/N_2$ (30/15/55) feed (flow rate: 50 mL min^{-1}). The CO_x hydrogenation was performed with Ru–Mn/TiO_2 at 473 K, and the H_2 flow rate was 20 mL min^{-1}.[140] Reprinted from ref. 140, with the permission of the John Wiley and Sons.

In addition to C_2, C_3–C_5 hydrocarbons were also obtained with a selectivity of 20–30% depending on the catalyst amount in the second reactor. CO formed in the OMC reaction in the first reactor was completely converted to hydrocarbons in the second reactor, while around 70% of CO_2 still remained unconverted at 533 K. To increase further the efficiency of the whole process, the development of OMC catalysts without CO_2 formation or hydrogenation catalysts with higher CO_2 hydrogenation abilities is required. To avoid the hydrogenation of olefins, in particular ethylene, in the second reactor is also highly desirable. Furthermore, the practical realization of this dual-reactor strategy will require an inexpensive H_2 source. Solar-driven water splitting can be attractive if efficient photocatalysts can be developed in the near future.

In addition to O_2, other oxidants have also been examined for the oxidative coupling of CH_4 to higher hydrocarbons. The use of other oxidants may decrease the gas-phase radial reactions, providing an opportunity to improve the product selectivity by controlling the reactions on catalyst surfaces. As described above, the use of N_2O as an oxidant for the OMC reaction over a Cl-doped perovskite-type composite oxide catalyst ($Ba_{0.5}Sr_{0.5}Fe_{0.2}Co_{0.8}O_{3-\delta}Cl_{0.04}$) led to high C_2 selectivity and yield (~30%).[139] CO_2 was also employed as the oxidant for the OMC reaction. The C_2 yield is, however, less than 10% at temperatures ≤1173 K, because the oxidation ability of CO_2 is too weak.[143–146]

Recently, S_2 has been exploited as a "soft" oxidant for the OMC reaction.[147] The oxidative coupling of CH_4 by S_2 to form C_2H_4 (eqn (26)) at 1073 K is thermodynamically viable, while that to form C_2H_6 (eqn (27)) is a thermodynamically uphill reaction. Although the deep oxidation to form CS_2 is thermodynamically more favourable (eqn (28)), the driving force for this over-oxidation

is less as compared that to form CO_2 in the presence of O_2 (ΔG = −792 kJ mol^{-1} at 1073 K) due to the weaker C–S and H–S bonds as compared to the C–O and H–O bonds.

$$2CH_4 + S_2 \rightarrow C_2H_4 + 2H_2S \qquad \Delta G_{1073K} = -4.9 \text{ kJ mol}^{-1} \quad (26)$$

$$2CH_4 + 1/2S_2 \rightarrow C_2H_6 + H_2S \qquad \Delta G_{1073K} = 33.9 \text{ kJ mol}^{-1} \quad (27)$$

$$CH_4 + 2S_2 \rightarrow CS_2 + 2H_2S \qquad \Delta G_{1073K} = -124 \text{ kJ mol}^{-1} \quad (28)$$

A series of transition metal sulphide catalysts have been investigated for the OMC by S_2.[147] The activation of CH_4 and the selectivity of C_2H_4 can be correlated linearly with the metal–sulphur bond strength and that the two relationships are inversely related to each other. In other words: the sites that are more active for CH_4 activation involve more weakly bound surface S atoms, which promote H abstraction from CH_4; whereas those that are more selective involve more strongly bound surface S atoms, which favour C–C coupling. PdS showed the highest C_2H_4 selectivity among the transition metal sulphide catalysts examined. The higher temperature and higher CH_4 : S_2 ratio led to a significant increase in C_2H_4 selectivity and the reduction of PdS to $Pd_{16}S_7$. The more reduced $Pd_{16}S_7$ state is more selective for C_2H_4 formation. Furthermore, the loading of $Pd_{16}S_7$ onto ZrO_2 could increase both CH_4 conversion and C_2H_4 selectivity. DFT computational studies suggest that the formation of C_2H_4 proceeds *via* the coupling of CH_2 species formed on metal sulphide surfaces *via* the activation of CH_4. However, catalytic performances obtained at the moment are still quite low; the maximum C_2H_4 selectivity of ~20% was obtained with a CH_4 conversion of ~16% at 1323 K over the ZrO_2-supported $Pd_{16}S_7$ catalyst. Moreover, the Claus process (eqn (29)) for the regeneration of sulphur from the H_2S produced has to be incorporated in the catalytic cycle.

$$2H_2S + O_2 \rightarrow S_2 + 2H_2O \quad (29)$$

2.4 Transformation of methane *via* methyl halides

The chlorination of CH_4 by Cl_2 is a well-known reaction in organic chemistry. At higher temperatures, this reaction proceeds *via* a radical mechanism, producing a mixture of CH_3Cl, CH_2Cl_2, $CHCl_3$ and CCl_4 and lacking selectivity to a particular compound. However, by controlling the reaction conditions and utilising a suitable catalyst, a high selectivity to methyl halide (CH_3Cl or CH_3Br) could be achieved.[149,150] For example, Olah *et al.* demonstrated that supported acid (*e.g.*, $TaOF_3/Al_2O_3$) or supported noble metal (*e.g.*, Pt/Al_2O_3) could catalyse the conversion of CH_4 by Cl_2 or Br_2 at 453–523 K, producing CH_3Cl or CH_3Br with selectivities higher than 90% (eqn (30)).[150] The hydrolysis of CH_3Cl or CH_3Br could produce CH_3OH or CH_3OCH_3 depending on the catalyst used for hydrolysis (eqn (31) or (32)).

$$CH_4 + Cl_2\ (Br_2) \rightarrow CH_3Cl\ (CH_3Br) + HCl \quad (30)$$

$$CH_3Cl\ (CH_3Br) + H_2O \rightarrow CH_3OH + HCl\ (HBr) \quad (31)$$

$$2CH_3Cl\ (CH_3Br) + H_2O \rightarrow CH_3OCH_3 + 2HCl\ (HBr) \quad (32)$$

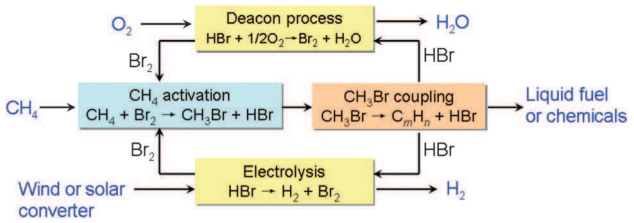

Fig. 12 Conversion of CH_4 to CH_3Br followed by subsequent coupling of CH_3Br to produce higher hydrocarbons.[18,148] Reprinted from ref. 18, with the permission of AAAS.

However, the strongly corrosive nature of Cl_2 or Br_2 is a problem. Moreover, the formed HCl or HBr has to be re-oxidised to Cl_2 or Br_2 by the Deacon process (eqn (33)), and this will further increase the cost of these procedures.

$$2HCl\ (HBr) + 1/2O_2 \rightarrow Cl_2\ (Br_2) + H_2O \quad (33)$$

Based on these early studies, the researchers at UC Santa Barbara and Gas Reaction Technologies (GRT, Inc.) have developed a process for the conversion of CH_4 to CH_3Br by Br_2 and the subsequent conversion of CH_3Br to higher hydrocarbons, in particular liquid fuels (Fig. 12).[18,148] In addition to the Deacon process (eqn (33)), the regeneration may also be carried out by the electrolysis of HBr to Br_2 and H_2.[18]

An intriguing catalytic system, MoO_2Br_2/Zn-MCM-48, which involves the activation of CH_4 by Br_2 but without adding Br_2 in the gas phase, has been reported for the direct transformation of CH_4 into CH_3OH or CH_3OCH_3 in the presence of O_2.[151] The selectivities to CH_3OH and CH_3OCH_3 reached 55% and 35%, respectively, with a CH_4 conversion of ~12% at 493 K over the 8 wt% MoO_2Br_2/Zn-MCM-48 with a Si/Zn of 20. As shown in Fig. 13, it is proposed that the MoO_2Br_2 in the catalyst can readily react with O_2, releasing Br_2 as an intermediate. Then, Br_2 can activate CH_4, forming CH_3Br and HBr. The formed MoO_3 can scavenge the Br atom from HBr and CH_3Br to provide oxidized products, *i.e.*, CH_3OH and CH_3OCH_3, and to regenerate the MoO_2Br_2 at the same time. The catalyst deactivation occurred due to the loss of Br_2 from the catalyst. The presence of Zn in MCM-48 support could enhance the catalyst stability to

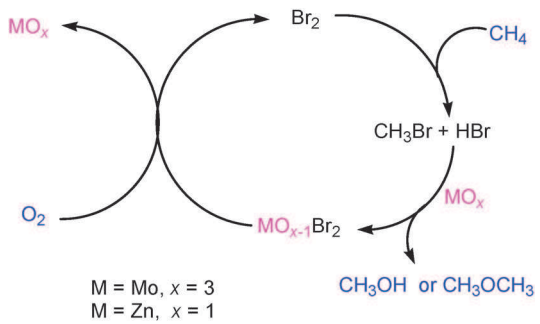

Fig. 13 Possible reaction cycle for the oxidation of CH_4 to CH_3OH and CH_3OCH_3 *via* CH_3Br over MoO_2Br_2/Zn-MCM-48 catalyst, which can uniquely release Br_2 during the reaction.[151] Reprinted from ref. 151, with the permission of the John Wiley and Sons.

some extent, likely owing to the participation of $ZnO/ZnBr_2$ in the catalyst cycle.[151]

Recently, a few groups have shown that the conversion of CH_4 by HCl or HBr in the presence of O_2 can also produce CH_3Cl or CH_3Br (eqn (34)).[152–154] There is no need for the expensive Deacon process for the regeneration of Cl_2 or Br_2. For the subsequent transformation of CH_3Cl or CH_3Br, besides oxygenates (*e.g.*, CH_3OH and CH_3OCH_3) and liquid fuel-based higher hydrocarbons, lower olefins (C_nH_{2n}), in particular C_2H_4 and C_3H_6, which are key building-block chemicals, are also attractive target products (eqn (35)). The combination of these two reactions will result in a new two-step process for the oxidative dehydrogenation of CH_4 into lower olefins (eqn (36)).

$$CH_4 + HCl\ (HBr) + 1/2O_2 \rightarrow CH_3Cl\ (CH_3Br) + H_2O \quad (34)$$

$$CH_3Cl\ (CH_3Br) \rightarrow 1/nC_nH_{2n} + HCl\ (HBr) \quad (35)$$

$$\text{Net: } CH_4 + 1/2O_2 \rightarrow 1/nC_nH_{2n} + H_2O \quad (36)$$

For the bromination of CH_4 by HBr in the presence of O_2, supported noble metal catalysts such as Ru/SiO_2 and Rh/SiO_2 have been reported to be efficient.[152,153] The high cost of the noble metal catalysts have stimulated recent studies on non-noble metal catalysts for the oxidative bromination of CH_4 to CH_3Br. $FePO_4/SiO_2$ showed a CH_4 conversion of $\sim$50% with a CH_3Br selectivity approaching 50% at 843 K.[154] One-pot hydrothermally synthesized $FePO_4$-SBA-15 also exhibited good performance for the oxidative bromination of CH_4, giving a CH_3Br selectivity of 32% at CH_4 conversion of 46% at 863 K.[155] The $FePO_4$-SBA-15 catalyst was found to be very stable, keeping its catalytic performance for 1000 h. The $FePO_4$ phase was transformed into $Fe_7(PO_4)_6$ and $Fe_2P_2O_7$ after the reaction. It was proposed that the redox of Fe^{III}/Fe^{II} may participate in the catalytic process. Although the selectivity to CH_3Br was lower than 50%, these studies suggested the production of a mixture of CH_3Br and CO with a ratio of 1 : 1, and such a product mixture could be exploited for the production of acetic acid in the subsequent step (eqn (37)).[152,154,155]

$$CH_3Br + CO + H_2O \rightarrow CH_3COOH + HBr \quad (37)$$

For the chlorination of CH_4 by HCl in the presence of O_2, Lercher and co-workers reported that $LaCl_3$-based catalysts were efficient, providing a CH_3Cl selectivity of $\sim$55% at CH_4 conversion of 12% at 748 K.[26,157,158] $LaCl_3$ was known as a catalyst promoter for the chlorination of hydrocarbons in Cu-based catalysts but was never considered as a main catalyst. This is because a reducible metal is generally believed to be indispensable. Thus, to understand the nature of the active site for the irreducible $LaCl_3$-catalysed oxidative chlorination of CH_4 is of fundamental significance. The DFT calculations suggest that the reactions in eqn (38)–(40) may proceed on La-based catalyst surfaces.[26] In brief, O_2 activates surface Cl^- species on $LaCl_3$ forming OCl^-, and the oxidation state of chlorine changes from -1 to +1. These OCl^- are capable of serving as the active species for the activation of CH_4. This catalytic cycle, which involves the redox between OCl^- and Cl^- for the activation of CH_4 without any changes in the oxidation state of underlying metal, is quite unique.

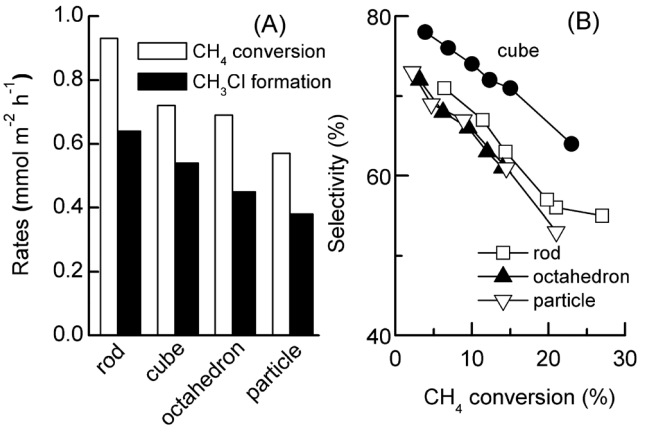

Fig. 14 Catalytic performances of CeO_2 nanocrystals with different morphologies for the oxidative chlorination of CH_4 to CH_3Cl. (A) Rates of CH_4 conversion and CH_3Cl formation. (B) CH_3Cl selectivity *versus* CH_4 conversion. Reaction conditions: T = 753 K, $CH_4/HCl/O_2/N_2/He$ = 4/2/1/1.5/1.5, total flow rate = 40 mL min^{-1}.[156] Reprinted from ref. 156, with the permission of the John Wiley and Sons.

$$Cl^-\ (surface) + 1/2O_2\ (g) \rightarrow OCl^-\ (surface) \quad (38)$$

$$OCl^-\ (surface) + CH_4\ (g) \rightarrow CH_3Cl\ (g) + OH^-\ (surface) \quad (39)$$

$$OH^-\ (surface) + HCl\ (g) \rightarrow H_2O\ (g) + Cl^-\ (surface) \quad (40)$$

Recently, various metal oxides were further examined as catalysts for the oxidative chlorination and bromination of CH_4 by HCl or HBr in the presence of O_2. CeO_2 was found to be an outstanding catalyst for both reactions.[156] The morphology of CeO_2 affected the catalytic performances. For both reactions, CeO_2 nanorods exposing (110) and (100) planes showed the highest rates of CH_4 conversion and methyl halide formation, whereas CeO_2 nano-octahedra and nanoparticles, which exposed (111) planes, were the least active (Fig. 14A).[156] CeO_2 nanocubes exposing (100) planes exhibited the highest selectivity to CH_3Cl during the oxidative chlorination of CH_4 (Fig. 14B).

In situ Raman spectroscopic studies suggest that a part of CeO_2 can be transformed into $CeCl_3$ in HCl gas flow at 723 K. No CeOCl was observed likely because of the instability of this compound at such a temperature. However, in a gas flow of CH_4–HCl–O_2 at 723 K, no $CeCl_3$ or CeOCl was observed. This indicates that CeO_2 can be sustained during the reaction without formation of $CeCl_3$ or CeOCl. The XPS studies for the catalysts after reaction showed that the Cl/Ce ratio was much lower ($<$0.05), supporting the idea that there was no formation of Cl-containing compounds on the catalyst surfaces.

The surface energy of CeO_2 increases in the order of (111) $<$ (110) $<$ (100).[159] The H_2-TPR studies suggest that the reducibility of CeO_2 catalysts with different morphologies decreases in the following sequence: nanorod $>$ nanocube $>$ nano-octahedron $\approx$ nanoparticle.[156] This sequence is similar to the activity order in Fig. 14. Thus, the reducibility of CeO_2 surfaces determines the

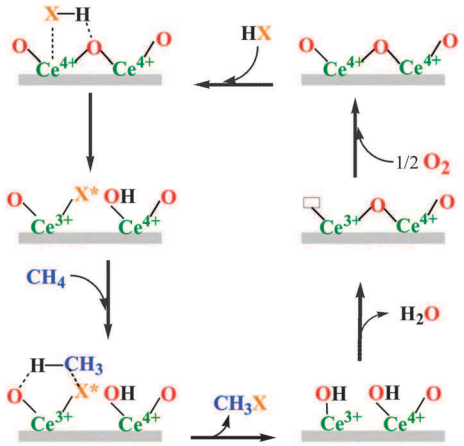

Fig. 15 Possible reaction mechanism for the oxidative chlorination or bromination of CH_4. X denotes Cl or Br. X* denotes active Cl or Br species.[156] Reprinted from ref. 156, with the permission of the John Wiley and Sons.

catalytic behaviour for the oxidative chlorination and bromination of CH_4. A plausible reaction mechanism for the oxidative halogenation of CH_4 over CeO_2 is displayed in Fig. 15. In brief, the adsorbed halide anion is oxidized by Ce^{4+} on the surface, forming active Cl or Br species, and the Ce^{4+} is reduced into Ce^{3+}. The active Cl or Br activates CH_4 to form CH_3Cl or CH_3Br. The surface undergoes dehydration and re-oxidation by O_2 to complete the catalytic cycle. The formation of active halogen species is a key step in this catalytic cycle, and the driving force for this step involves the electron transfer between Cl^- and Ce^{4+}. This is in agreement with the experimental result that the reducibility of CeO_2 surfaces determines the catalytic behaviour. This also provides further clues for improving the catalytic performance, since the modification of CeO_2 by doping other transition metal components can accelerate the redox of Ce^{4+}/Ce^{3+}. Actually, a FeO_x–CeO_2 solid-solution nanorod catalyst has been found to be more efficient for the oxidative chlorination of CH_4, providing a CH_3Cl selectivity of 74% with CH_4 conversion of 23% at 753 K. This catalyst was quite stable, and a CH_3Cl yield of $>15\%$ could be sustained for at least $\sim$100 h.

3. Aerobic oxidation of alcohols

As one of the most fundamental organic transformations, the catalytic selective oxidation of alcohols to corresponding aldehydes or ketones has attracted significant attention among engineers and scientists because aldehydes and ketones are important intermediates or precursors for making drugs, fine chemicals, vitamins and fragrances.[12,160,161] From the viewpoints of atom economy and environment, it is highly desirable to develop heterogeneous catalysts to catalyze the oxidation reaction and apply molecular oxygen as the oxidant. Over the past few years, extensive work on catalytic selective oxidation of alcohols has been carried out, including the metallic Pt catalyzed oxidation of alcohols in aqueous media,[162] the catalytic oxidation of primary and secondary alcohols over Pd,[163] the engineering aspects of noble metal catalyzed alcohol oxidation,[164] and immobilized metal complexes and particles for oxidation of alcohols.[12,13] Very recently, Davis *et al.* summarized the selective oxidation of alcohols, such as polyols and sugars, produced from biomass conversion.[165]

3.1 Mechanisms of aerobic selective oxidation of alcohols

A number of mechanisms have been proposed for the aerobic oxidation of alcohols over both noble metal and nonprecious transition metal (NTM) based catalysts. Developments of these fundamentals are the driving forces for fabricating novel and efficient catalytic processes. Therefore, it is necessary to understand some general details during the catalytic oxidations of alcohols before the discussion of recent achievements.

3.1.1 Noble metal catalysts. For oxidation of alcohols over noble metals, there are 3 essential steps (as shown in Fig. 16 with Pd catalyzed oxidation of a primary alcohol as an example): the first step is the insertion of a metal atom in between the O–H bond of an alcohol, which leads to the formation of a metal alkoxide and a metal hydride (adsorbed on a neighbouring metal atom); then, a hydrogen is removed by surface Pd atom *via* a β-hydride elimination process, yielding the desired aldehyde as a product; finally, Pd active site is regenerated *via* the oxidation of adsorbed hydrogen by molecular oxygen.

These 3 critical steps have been repeatedly verified in many reaction systems. Reaction of ligand-stabilized single Pd(0) atom with methanol led to the formation of Pd hydride in the form of CH_3O–Pd(0)H–Ln (Ln: other ligands).[166] Adding O–H bonds to the surface of a "giant" Pd nanocluster (around 2000 Pd atoms, stabilized by anion ligands) was also proposed.[167] Moreover, by purging 2-butanol vapour through the Pd(111) crystalline face, the alkoxide species were directly evidenced by *in situ* reflection infrared spectroscopy.[168] Further increase in temperature caused the desorption of 2-butanol and the production of corresponding ketones. Besides direct insertion of a metal atom into the O–H group, metal alkoxide may also be produced from ligand exchange between adsorbed OH groups (OH(ad)) and alcohols, yielding water as a co-product.[169]

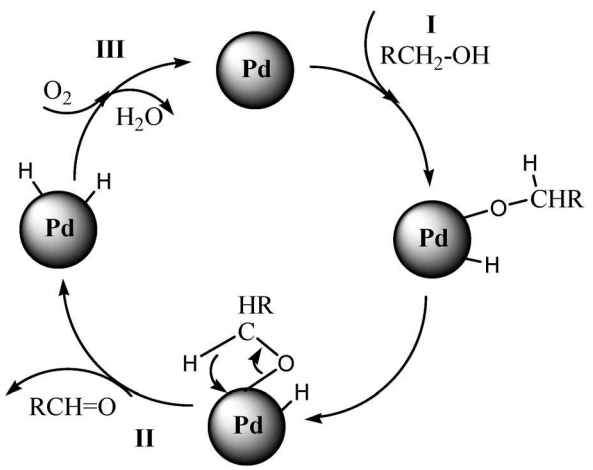

Fig. 16 Oxidation of alcohol to the corresponding aldehyde over a noble metal.

The adsorbed alkoxide species undergo β-hydride elimination, producing aldehydes or ketones (see Fig. 16, step II). The Hammett methodology was employed to verify this particular step. Formation of carbocation intermediates due to the hydride subtraction from a metal alkoxide was substantiated from the oxidation of various *p*-substituted benzyl alcohols over Ru catalysts.[169,170] The rates for decomposition of CH_3OH and CH_3OD (D = deuterium) over Pt and Ru were almost the same, suggesting that inserting a metal atom into the O–H bond is not the rate-determining step.[171] In contrast, the remarkable difference between the activation energies for the decomposition of CH_3OH and CD_3OH implies that the dissociation of a C–H bond in the adsorbed CH_3O group is the rate-determining step.[171] Similar kinetic isotope effects were also found in the liquid phase, such as the competitive oxidation of 2-propanol and 2-propanol-d7 (C_3D_7OH) over Pt (k_H/k_D = 3.2)[172] and the competitive oxidation of benzyl alcohol and benzyl-d7 alcohol ($C6D_5CD_2OH$) (k_H/k_D = 7).[173]

Finally, the metal hydrides generated from the dissociation of O–H bond of alcohol and β-hydride elimination are oxidized by molecular oxygen, leading to the regeneration of the activation sites (see Fig. 16, step III).[174] The existence of metal hydrides was evidenced by the formation of hydrogenation and hydrogenolysis products during the oxidation of cinnamyl alcohols.[175] During the oxidation of hydrides, a peroxide intermediate (metal–OOH) was postulated.[169] Dissociation of molecular oxygen over the Pt surface was proposed for the oxidation of methyl α-D-glucoside.[176] In aqueous solution, O_2 may interact with H_2O leading to the formation of OH(ad).[162] Hydrides can be oxidized by OH(ad) with H_2O as a product. The direct contact between adsorbed oxygen and hydrogen may not be necessary. Based on an electrochemical local cell mechanism, the oxidation of metal hydrides and reduction of adsorbed oxygen containing species may occur at separate sites of the metal surface, while the metal itself acts as a short circuit to transport electrons from hydrogen to oxygen.[172] A zero-order dependence on oxygen pressure was found in the oxidation of benzyl alcohol over Ru,[170] implying that re-oxidation of metal hydride is not the rate-determining step. Keresszegi *et al.* suggested that oxygen not only removes adsorbed hydrogen but also cleans the metal surface by oxidation of CO and other degradation products during the oxidation of alcohols.[175]

Besides the stepwise oxidation mechanism discussed above, a one-step oxidation of alcohols to carbonyl products by adsorbed hydroxyl groups on the metal surface was also proposed by Kluytmans *et al.*[164]

3.1.2 Nonprecious transition metal (NTM) oxide catalysts. Up to now, there has been no generally accepted mechanism for aerobic oxidation of alcohol over NTM oxides, mainly due to the multi-valency of NTM and the involvement of the lattice oxygen of NTM oxides. A highly cited theory is the M–v K mechanism.[2] As illustrated in Fig. 17 with oxidation of a primary alcohol as an example, the catalytic path includes 2 successive steps: metal oxides are reduced by alcohols, leading to the formation of aldehydes and reduced catalysts. This step includes the transfer of lattice oxygen atoms and the reduction of the NTM oxides. Subsequently, the reduced catalysts are re-oxidized by aerobic oxygen, replenishing oxygen back to the lattice. The M–v K

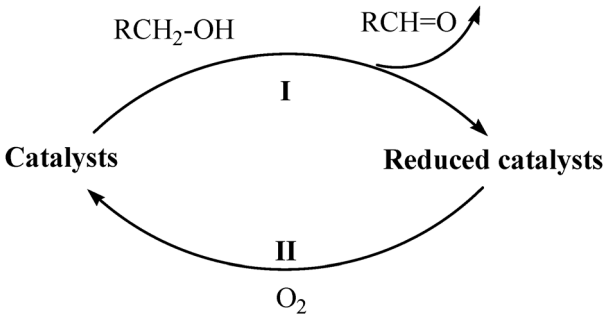

Fig. 17 Oxidation of alcohol to the corresponding aldehyde over NTM oxide based on the M–v K mechanism.

mechanism is frequently observed in gas-phase oxidation,[177,178] which is also applicable for oxidation processes in the liquid phase.[179,180] Makwana *et al.* demonstrated that the kinetic behaviour of aerobic oxidation of benzyl alcohols over manganese oxide (MnO_x) can be fitted well using the M–v K model.[180]

Just like oxidation of alcohols on noble metals, formation of alkoxides as intermediates has also been proposed for NTM oxide-catalyzed alcohol oxidations.[178,181–183] Introducing alcohols on the surface of NTM oxides gives rise to the formation of alkoxy groups which were detected by *in situ* infrared spectroscopy.[181–183] Oxygen vacancy sites (V_O) on the surface of metal oxides are employed to interpret the dissociation of alcohols.[182] There are two types of V_O: the terminal oxygen vacancy (M–□, M: metal), missing oxygen of M=O; and the bridged oxygen vacancy (M–□–M), missing oxygen of M–O–M.[182] It is possible for O–H bond to dissociate on both types of V_O, nonetheless, alkoxy groups on terminal oxygen vacancy sites favour the production of aldehydes.[182] Scission of the O–H bond of an alcohol over coupled V_O and bridging oxygen leads to a pair of alkoxy (M–OR) and hydroxyl groups (M–OH) which can re-combine together.[184] A different mechanism for the formation of alkoxide proposes the dissociation of an O–H bond by breaking a M–O–M bond, which also yields a pair of alkoxy and hydroxyl groups.[178] Kooli *et al.* proposed that alkoxy groups were generated through the condensation of surface hydroxyl groups with alcohols, as formation of water was observed in the *in situ* infrared spectroscopy study of 2-propanol adsorption on a mixed NTM oxide.[183]

β-Hydride elimination was proposed for the production of aldehydes from chemically adsorbed alkoxide intermediates.[178,182] Different from a similar elimination mechanism for noble metals, the hydrogen on the β carbon is subtracted by the terminal oxygen group (M=O) adjacent to the adsorbed alkoxy group. This step is accompanied by electron transfer from the substrates to the metal cations, namely the reduction of the NTM oxides.[178,180,182] KIE studies revealed that breaking of the β C–H bond is the slow step in the catalytic cycle. A kinetic ratio of (k_H/k_D) 4.06 was found for the competing oxidation of benzyl alcohol and its deuterium counterpart ($C_6H_6CD_2OH$).[180] For oxidation of methanol over Mo oxides, an even larger KIE was observed (k_H/k_D = 7.3).[178]

Loss of lattice oxygen during oxidation of alcohols was observed using the *in situ* infrared technique. Exposing reduced catalysts in an aerobic oxygen stream led to the recovery of

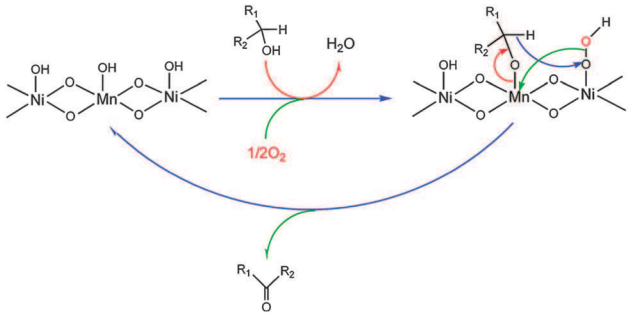

Fig. 18 Proposed mechanism for the aerobic oxidation of benzyl alcohol over Mn–Ni mixed hydroxide catalyst.[185] Reprinted from ref. 185, with the permission of the Elsevier, copyright 2011.

structural oxygen.[182] Long term exposure of catalysts in oxygen-deficient conditions resulted in the reduction of metal oxides, which decreased the selectivity to aldehyde.[182] The participation of lattice oxygen of MnO_x in alcohol oxidation was ascertained by an oxygen isotope labelling study. When $^{18}O_2$ was fed to an MnO_x catalyzed benzyl alcohol oxidation system, the initial rates of $H_2{}^{16}O$ and $H_2{}^{18}O$ generation are the same.[180] Additionally, the exchange between molecular oxygen and lattice oxygen cannot take place without the presence of benzyl alcohol.[180] These observations clearly demonstrated oxygen transfer from the lattice to the substrate as well as the replenishment of lattice oxygen from aerobic oxygen feeding. If manganese and nickel (Mn–Ni) mixed hydroxides are employed, conversion of benzyl alcohol increased with O_2 partial pressure, while benzaldehyde selectivity remained almost unchanged.[185] These results imply that the active oxygen species, generated from the activation of O_2, are responsible for oxidation of benzyl alcohol. The synergistic interactions between Mn(III) and Ni(II) cations through oxygen bonding was proposed to explain the enhanced activity of Mn–Ni mixed hydroxide. As illustrated in Fig. 18, Ni(II) cations are coordinated with Mn(III) through oxygen bonding, in which Mn(III) cations act as Lewis sites, which activate alcohols to form alkoxide anions. On the other hand, oxygen is activated on Ni(II) sites, and the activated oxygen species attack alkoxides, which are bound to Mn(III), to form carbonyl compounds by dehydrogenation.

3.2 Catalysts design for aerobic selective oxidation of alcohols

Bearing in mind the mechanisms summarized above, the design of a heterogeneous catalyst with high efficiency resembles the assembly of a nano-sized machine. Usually the performance of a heterogeneous catalyst is largely determined by three factors: active sites; promoters; and supports. In respect to these 3 aspects, recent advances in the oxidation of alcohols over heterogeneous catalysts will be discussed sequentially.

3.2.1 Active sites. Two types of metals are frequently used as active sites for selective oxidation of alcohols: noble metals including Pd, Pt, Ru and Au; and NTM, such as Mn, V, Mo and Ti, usually in the form of metal oxides. Some of the recent published results are summarized in Table 1. TOF, as a good indicator of activity, is calculated by dividing the moles of the desired carbonyl compounds produced per hour by the moles of total active metals. Metallic promoters are not counted in the TOF calculation, and Au is always regarded as an active metal due to its high value. For a convenient comparison, only oxidation of benzyl alcohol to benzyl aldehyde, which is frequently

Table 1 Summary of reaction conditions and results for oxidation of benzyl alcohol with aerobic oxygen as oxidant in liquid phase

Active sites	Support	Solvent	Temperature/K	Reaction time/h	Conversion (%)	Selectivity (%)	TOF[a]	Ref.
Pd	MnO_x-CNT	Solvent free	433	1	15.4	100.0	19 467	187
Pd	$MnCeO_x$	Solvent free	433	1	18.4	98.6	15 112	188
Pd	Modified TUD-1	Solvent free	433	1	22.3	95.2	5625	189
Pd	Silica–alumina	Solvent free	353	24	99.9	99.9	748	190
Pd	γ-Al_2O_3	Solvent free	361	8	97.0	96.0	1862	191
Pd	NaX zeolite	Solvent free	373	4	66.0	97.0	608	192
Pd[b]	MgO	Solvent free	298	7	100.0	>99.0	10	193
Pd	—	Acetic acid	333	14	95.0	92.0	2	167
Pd	Poly(ethylene glycol)	Supercritical CO_2	353	13	83.1	99.8	1	194
Pt[c]	Activated carbon	Water	333	3	50.0	80.0	66	195
Au[d]	TiO_2	Solvent free	433	6	55.0	73.7	4864	196
Au	Hydrotalcite	Toluene	313	24	85.0	91.7	7	197
Au	Polystyrene	Diglyme	298	15	—	79.0[e]	—	198
Pd–Au	Modified SBA-16	Solvent free	413	1	22.3	94.4	8483	161
Pd–Au[c]	Activated carbon	Water	333	3	96.0	94.0	150	195
Ru	Al_2O_3	Trifluorotoluene	356	1	>99.0	>99.0	39	169
RuO_2[b]	Faujasite zeolite	Toluene	353	1.5	100.0	>99.0	8	199
Ru^{3+}	Hydroxyapatite	Toluene	363	3	100.0	>99.0	2	173
MnO_x	Activated carbon	Toluene	373	6	>99.0	>99.0	2	200
MnO_2	γ-Al_2O_3	Toluene	373	3	72.9	>99.0	1	201
MnO_x	γ-Al_2O_3	Toluene	373	4	90.9	>99.0	0.8	202
MnO_x	γ-Al_2O_3	Toluene	373	4	93.0	99.0	0.4	203
V_2O_5	Activated carbon	Toluene	373	3	>99.0	>99.0	7.5	204
$Mo_xV_yO_z$	—	Toluene	353	24	22.0	>99.0	—	205
$Mn_xNi_yO_z$	—	Toluene	373	1	89.0	99.0	—	185
TiO_2[f]	—	Benzotrifluoride	298	4	91.0	100.0	0.07	206

[a] Calculated based on total active metal in reaction system except promoters. [b] Air was used as oxidant. [c] Pressure of oxygen is 1.5 bar. [d] Pressure of oxygen is 10 bar. [e] Yield. [f] Photocatalytic process, the catalysts were pretreated with hydrofluoric acid before reaction.

utilized as a model reaction, is summarized. It can be seen that the activities of noble metals are generally higher than those of transition metal oxides. However, the significant lower costs of NTM make them competitive to noble metals at the economical point of view.

Among various noble metals, Pd is the most popular metal for the catalytic oxidation of alcohols. Pd exhibits the highest catalytic activity among all the metals. A TOF up to 270 000 h^{-1} was reported by Hutchings and co-workers for the oxidation of phenyl ethanol over Pd based catalysts modified with Au.[186] For oxidation of benzyl alcohol over the same catalysts, TOF of 86 500 h^{-1} was obtained. By using monometallic Pd catalysts, a high TOF (19 000 h^{-1}) for oxidation of benzyl alcohol was achieved in our group.[187] Additionally, Pd based catalysts are efficient to catalyze a wide range of alcohols, including phenyl alcohols, allylic alcohols, aliphatic alcohols and alcohols containing heteroatoms (such as S, O and N).[161,174,186,187,190,193]

It has been shown that the active Pd species are metallic Pd(0) rather than monomeric Pd(II).[174] An induction period was observed when unreduced Pd(II) catalysts (or catalysts with large portion of Pd(II)) were directly used in oxidation reactions.[174,187,191] During the induction period, Pd(II) are reduced by alcohols, forming metallic Pd(0) nanoparticles, which act as the catalytically active species. On the other hand, supported Pd(II) cations that are strongly coordinated with ligands cannot be reduced by substrates, and thus no reaction took place bearing only Pd(II) species.[174] It was found that the initial reaction rate of benzyl alcohol oxidation increased with the Pd(0)/Pd(II) ratio.[188] Results were also reported on the high catalytic efficiency for selective oxidation of phenyl alcohols due to the cooperative effect of specific ensemble sites consisting of Pd(0), Pd(I) and Pd(II) on Pd nanoclusters.[167] The π-bond between the phenyl group of the substrate and the Pd(II) species enhanced the interaction of Pd clusters with alcohols. Pd(I) in the form of Pd_2O can transfer oxygen readily to neighbouring Pd hydrides (Pd–H) that are formed during the catalytic cycle to produce H_2O and regenerate Pd(0).

Catalytic oxidation of alcohols over Pd is ''structure sensitive''.[174,190,192] By assuming the cubooctahedral shape of Pd nanoparticles, Kaneda *et al.* calculated the number of Pd atoms at edges and corners based on the mean diameters of Pd nanoparticles.[174] TOFs of alcohol oxidation normalized to the low coordination number atoms were found to be independent of Pd particle size. Therefore, the cus Pd atoms may act as the key active sites on the surfaces of Pd nanoclusters. However, for oxidation of benzyl alcohol, a volcano profile was obtained by plotting TOFs against Pd particle sizes, as shown in Fig. 19.[190] The highest TOF was obtained over Pd particles with a mean size of *ca.* 4 nm. It was speculated that benzyl alcohol may adsorb on Pd nanoparticles *via* the interaction of the π-bond of the benzene ring with terrace Pd atoms. Subsequently, the transformation of benzyl alcohol to benzaldehyde was catalyzed by cus Pd atoms at edges or corners. If the adsorption step is crucial, a balance between Pd atoms at edges or corners should be necessary to achieve a high activity.[190] A similar trend was also observed on zeolite-supported Pd nanoparticles in the oxidation of benzyl alcohol.[192] In this case, the optimal mean size of Pd was 2.8 nm. On the other hand, the

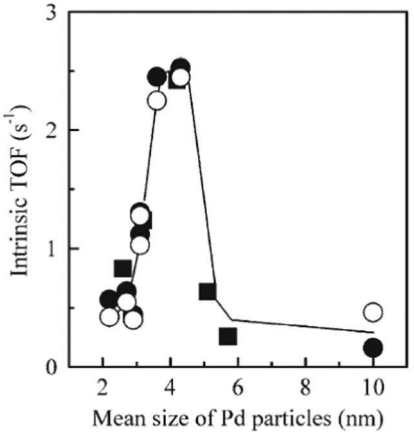

Fig. 19 Dependence of intrinsic TOFs on the mean size of Pd particles. ■: Catalysts reduced with hexanol; ●: catalysts reduced with H_2; TOFs were estimated by mean size of Pd; ○: catalysts reduced with H_2, and TOFs estimated by CO chemisorptions results of Pd.[190] Reprinted from ref. 190, with the permission of the John Wiley and Sons.

oxidization of geraniol or 2-octanol without a delocalized π-ring turned out to be structure-insensitive.[192] TOFs for oxidation of these substrates were almost independent of the mean particle size of Pd nanoparticles.

Pt-based catalysts for aerobic oxidation of alcohols in aqueous solution was thoroughly reviewed by Mallat and Baiker, in 1994.[162] Similar to Pd, alcohol oxidation reactions take place on a metallic Pt(0) surface. Pre-reduction of air-stored Pt catalyst with H_2 promoted initial reaction rates.[162] Due to the stronger oxidizing ability of Pt as compared to Pd(Pt(0)/Pt(II): E_{ox} = +1.12 V *versus* Pd(0)/Pd(II): E_{ox} = +0.95 V, E_{ox}: activation energy for oxidation),[207] Pt can be over oxidized by oxygen leading to deactivation of catalysts.[208] Oxidation of alcohols, especially primary alcohols, over Pt is prone to produce carboxylic compounds which can strongly adsorb on the Pt surface, breaking the catalytic cycle.[162] In many Pt catalyzed oxidation reactions, base (*e.g.*, K_2CO_3 or NaOH) must be added to ensure that the reaction can go smoothly.[162] Another disadvantage of using Pt as an oxidation catalyst is its latent tendency of explosion under oxidative conditions in organic solvents.[207] Regardless of these disadvantages of Pt, stabilized Pt nanoparticles in the matrix of a polymer (PEG: polyethylene glycol) were applied in oxidation of alcohols in aqueous media under mild conditions (333 K).[207] High yields towards ketones (80–90%) were obtained when secondary alcohols were used as substrates. In this catalytic system, Pt exhibited higher activity than Pd for oxidation of cyclic aliphatic alcohols.[207] Nonetheless, oxidation of primary alcohol on Pt only yielded carboxylic acids as products. 100% selectivity of aldehyde for selective oxidation of cinnamyl alcohol was obtained over activated carbon (AC) supported Pt nanoparticles. However, selectivity towards aldehydes was low for oxidation of benzyl alcohol (80%) and 1-octanol (30%).[195] For 1-octanol, a significant amount of octanoic acid was produced as a by-product. In our group, Fe modified Pt nanoparticles supported by carbon nanotubes (CNT) were synthesized, which showed high activity towards the oxidation of benzyl alcohol (initial TOF up to 2200 h^{-1}).[209]

Compared to Pd and Pt, Au is relatively more inert for oxidation of alcohol. Under mild conditions (333 K), no reaction occurred when AC-supported Au was used as a catalyst.[195] However, Kobayashi and co-workers demonstrated that polystyrene-stabilized Au nanoclusters were able to oxidize various alcohols under room temperature.[198] Nonetheless, the mole ratio of substrates/Au in Kobayashi's system was low (around 100) and base (K_2CO_3) has to be added because it facilitated the abstraction of H from the hydroxyl group of alcohol that Au itself is unable to perform.[12,195] Due to the basic nature of hydrotalcite, oxidation of alcohols can be smoothly carried out over Au/hydrotalcite under mild conditions (313 K, in air) in the absence of bases.[197] Very high TOF (8300 h^{-1}) and selectivity (99%) were achieved for oxidation of phenyl ethanol. It has been shown that Au/hydrotalcite can catalyze a wide range of alcohols (except 1-octanol), including cyclohexanol and alcohols containing heteroatoms.

For Au-based catalysts, formation of 1 mole of the oxidation products consumes 0.5 mole of oxygen, suggesting that oxidation of hydride on Au yields water as a co-product.[198] Compared with CeO_2 supported Pd, Au/CeO_2 gives a higher chemo-selectivity for oxidation of allylic alcohol because Au–H hydride can be more easily oxidized by O_2, preventing the hydrogenation of the C=C bond.[12] Under relatively harsh conditions (433 K, 10 bar of O_2), high activity was obtained over TiO_2 supported Au without adding bases (see Table 1),[196] while a significant amount of benzoic acid (15.1% in selectivity) was generated.

Supported Ru was also studied for the selective oxidation of alcohols. Different from the above mentioned noble metals, Ru(III) cation is active for oxidation of various alcohols to the corresponding carbonyl products.[173] On hydroxyapatite supported Ru catalysts, the monomeric Ru(III) cation coordinated with 4 oxygens and 1 chlorine was the active site.[173] It is notable to mention that oxidation of 1-octanol gave rise to 1-octanal with 94% yield without the formation of carboxylic acid and ester. Superior to Ru-based metallic complexes, Ru(III)/hydroxyapatite can catalyze actively the oxidation of alcohols containing heteroatoms, including N and S, to the corresponding aldehydes. The proposed mechanism for oxidation of alcohol over the Ru(III)-based catalysts is similar to the generally accepted catalytic cycle as depicted in Fig. 16. The isotope test (competitive oxidation of benzyl alcohol and benzyl-d7 alcohol) showed that β-elimination was the rate-limiting step.[173] Good catalytic performance was found on the zeolite supported nano-sized RuO_2.[199] The activity of zeolite confined nano-RuO_2 was about 6 times higher than that of bulk RuO_2, which was attributed to the much higher density of active sites in nano-RuO_2. Besides phenyl, allylic and cyclic alcohols, nano-RuO_2 in zeolite was also active for primary aliphatic alcohols.[199] Oxidation of *n*-heptanol led to the formation of *n*-heptaldehyde with 98% yield. The zeolite confined RuO_2 species was active even at ambient temperature. 75% conversion was achieved for oxidation of benzyl alcohol in 24 h with chlorobenzene as a solvent.[199] Metallic Ru(0) also showed good catalytic activity for the oxidation of a wide range of alcohols.[169] For oxidation of aliphatic primary alcohols (1-octanol and 1-decanol), high yields towards aldehydes were obtained only with the presence of hydroquinone as an additive, implying that the hydroquinone acts as a free radical trap that prevents efficiently the further oxidation of aldehydes to carboxylic acids. Again, β-elimination was verified as the rate-limiting step based on KIE tests.[169]

Before proceeding to the discussion on bimetallic catalysts, it will be beneficial to clarify the definition of co-catalysts and promoters. In this review, two criteria will be followed to differentiate co-catalysts and promoters: (1) the content of a promoter should be much less than that of active metals; (2) the cost of a promoter should be much lower than that of active metals. Otherwise, the metal added will be regarded as a co-catalyst, *e.g.*, Au.

Compared to their monometallic counterparts, enhanced catalytic performances were achieved by chemically mixing Pd and Au to form Pd–Au bimetallic catalysts.[161,186,195,210] Take selective oxidation of benzyl alcohol as an example: Pd–Au/TiO_2 showed 3 times higher activity than that of Pd/TiO_2.[186] By using modified mesoporous silica (SBA-16) as support, the Pd–Au catalyst showed enhanced catalytic performance as compared to an Au or Pd monometallic catalyst.[161] The activity of Pd–Au bimetallic nanoparticles on SBA-15 was about 12.5 and 2 times larger than that of Au and Pd monometallic catalysts, respectively.[210] Besides, Pd–Au bimetallic catalyst exhibited long-term stability during the oxidation reaction. At low temperature (333 K), an improved activity by a factor of 5 was observed for Pd–Au bimetallic nanoparticles supported on AC as compared to Pd/AC.[195] However, under the same conditions, Au/AC is inactive. The aggregation of Pd and Au may be in the form of either an alloy[195] or a segregated core–shell structure (Pd-rich shell surrounding an Au-rich core).[186,210] In both Pd–Au arrangements, Pd was the active site and Au acted as an electronic promoter. For Pd–Au bimetallic nanoparticles with core–shell structure, the superior catalytic performance was attributed to two factors.[210] (1) changes in the interatomic distance of Pd may have both geometric and electronic effects. Au can disperse or isolate Pd sites, preventing oxygen poisoning of Pd in liquid-phase oxidation.[195] Au, with higher electronegativity, also withdraws electrons from Pd atoms, leading to an enhanced interaction of Pd atoms with the substrate, which therefore improves the activity and selectivity. It has also been reported that the presence of nano-contacts triggers electron transfer and charge redistribution in the contact region, which are highly attractive to charged organic molecules, resulting in the improvement of organic transformations.[211] (2) segregation of Pd on the Au core exposes more surface-coordination-unsaturated Pd atoms which facilitates β-hydride cleavage (the rate-limiting step in the catalytic cycle), thus leading to better activity. In contrast to Pd–Au bimetallic catalysts, Pt–Au nanoparticles in the form of alloys showed inferior catalytic performance, which was ascribed to the difference in surface interatomic distances (and thus in the electronic structure) as compared with monometallic Pt or Pd–Au nanoparticles.[195]

NTM oxides, such as MnO_x, VO_x, MoO_x and TiO_2, can serve as low cost supplements for expensive noble metals for catalytic oxidation of alcohols. As shown in Table 1, the activities of NTM-based catalysts are much lower than those of noble metals. Nonetheless, this issue can be addressed by simply decreasing the molar ratio of substrate/metal. Fairly good catalytic results

for oxidation of various substituted phenyl alcohols (conversion: 74–99%; selectivity: 99%) were obtained over potassium-promoted Mn based catalysts prepared by a facile co-impregnation method.[200,201] The TOF for oxidation of benzyl alcohol was 2 h^{-1}. By using alumina supported highly dispersed MnOOH species as catalysts, 93% of conversion for oxidation of benzyl alcohol can be reached within 4 h at 373 K with benzaldehyde as the main product (99% in selectivity).[203] Monometallic vanadium oxides were also used in the oxidation of alcohols. It seems that vanadium oxides are more active than manganese oxides. Under the same reaction conditions, 92.6% of conversion was obtained for oxidation of benzyl alcohol over VO_x/AC (4 wt%), whereas, only *ca.* 64% of conversion was reached when MnO_x/AC (5 wt%) was used as a catalyst.[212] It was found that highly dispersed vanadium species with a distorted tetrahedral coordination were active for oxidation of substituted phenyl alcohols (TOF up to 22 h^{-1}, based on the molar content of V_2O_5).[204] In addition, selectivity to carbonyl compounds was always more than 99% for all tested phenyl alcohols. Oxidation of cinnamyl alcohol to cinnamaldehyde can also be performed over VO_x/AC.[204]

High activity and selectivity have been achieved on chemically mixed transition metal oxides. For oxidation of benzyl alcohol, 90.9% of conversion and 99% of selectivity to benzaldehyde were obtained on a supported MnO_x–CuO_x microcrystalline structure under mild condition (373 K, bubbling with O_2).[202] Using supported Mn–Ni mixed hydroxides as catalysts, high specific activity of 8.9 mmol $(g\ h)^{-1}$ and high selectivity to aldehyde (99%) was achieved for the oxidation of benzyl alcohol at 373 K within 1 h.[185] Catalytic oxidation of various substituted benzyl alcohols over Mo–V–O oxides led to formation of corresponding carbonyl compounds in high selectivity (>95%), while conversions of substrates varied from 10% to 99% depending on the substituents.[205] In contrast to noble metal based catalysts, high selectivities (>90%) were achieved for the oxidation of primary aliphatic alcohols by using the crystalline Mo–V–O oxide as a catalyst, and oxidation of secondary alcohols produced olefins as the main products.[205]

Among various characterization techniques, X-ray absorption spectroscopy (XAS) with synchrotron light source has emerged as a powerful technique to probe the active site in catalysts.[203,204,212,213] X-Ray absorption near edge structure (XANES) and extended X-ray absorption fine structure (EXAFS) provide information about the local coordination and electronic properties of the catalytic active centers. For example, based on the Mn K-edge XANES spectra of manganese oxide standards with different oxidation states (MnO, Mn_3O_4, Mn_2O_3, MnO_2 and MnOOH), a linear relation was found to give a good match to the set of five experimental edge positions *versus* oxidation states (as shown in Fig. 20). The resulting linear fit was used to determine the average oxidation state of the Mn-containing samples from their Mn K-edge positions.[203] On the other hand, EXAFS spectra are used frequently to interpret the local coordination structure of metal oxides, providing information about the average coordination numbers and bond lengths.[200,201] With the help of XAS, the correlation between the intrinsic chemical nature of transition metal oxides and their catalytic performances has been studied intensively in recent years.

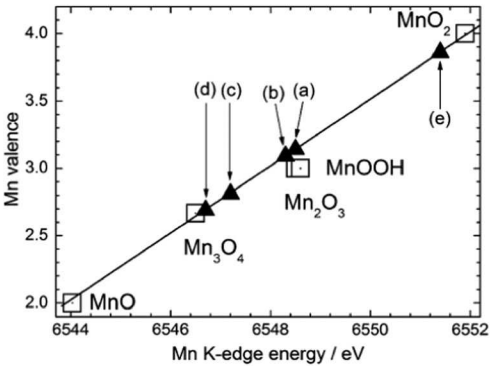

Fig. 20 Mn K-edge position of various Mn-containing catalysts along with reference compounds as a function of the Mn oxidation state: (a) 5 wt% Mn/γ-Al_2O_3-p; (b) 10 wt% Mn/γ-Al_2O_3-p; (c) 20 wt% Mn/γ-Al_2O_3-p; (d) 40 wt% Mn/γ-Al_2O_3-p and (e) 10 wt% Mn/γ-Al_2O_3-imp, where p and imp represent two preparation method of catalysts: homogeneous deposition–precipitation and impregnation, respectively.[203] Reprinted from ref. 203, with the permission of the Elsevier, copyright 2011.

Because of the participation of lattice oxygen in the oxidation process, the bond strength of M–O (M: metal) and the chemical states of metals can greatly affect the catalytic performance. Different coordination structures of transition metal oxides lead to deviations of the M–O bond strength, and subsequent different mobilities of the lattice oxygen. Based on Raman and XAS, it was shown that a large distortion of the Mn–O local coordination structure in supported manganese oxides was induced by incorporated potassium ions (K^+), which caused an increase on Mn–O bond length, leading to a dramatic improvement of the oxidation activity.[200] Similarly, introducing Cu into Mn oxide also resulted in the change of Mn–O bond strength, which was evidenced by Raman and EXAFS studies.[202] The remarkable improvement of catalytic activity was attributed to the deviation of the Mn–O bond length. The activity of MnOOH for the oxidation of benzyl alcohol was much higher than that of Mn_3O_4, due to a longer Mn–O bond length in MnOOH.[203] α-MnO_2 was found to be more active than β-MnO_2.[201] Hydrogen temperature-programmed reduction (H_2-TPR) revealed that it was easier for α-MnO_2 to be reduced than β-MnO_2, allowing a more facile supply of the oxygen species needed for the reaction. Study on the nature of VO_x on AC indicated that coordinative unsaturated vanadium species with a distorted tetrahedral symmetry outperformed the vanadium species with octahedral coordination, which was also attributed to the weakening of the V–O bond.[204]

The mobility of oxygen species was affected by the oxidation states of transition metals. The XANES spectra of potassium doped MnO_x indicated the coexistence of Mn(II) and Mn(III).[213] It was reported that the coupled Mn^{4+}/Mn^{2+} sites allowed electron exchange and, hence, oxygen migration throughout the surface and the bulk.[180] The coexistence of Mn^{2+} and Mn^{3+} may also facilitate oxygen transfer during the oxidation process, leading to improved catalytic activity.

In addition to traditional heterogeneous catalytic systems, photo-catalytic aerobic oxidation of alcohols was also performed

over silica doped TiO_2.[206] 91% conversion was obtained for oxidation of benzyl alcohol at room temperature, and benzaldehyde was the only product. The reported photocatalysts were also active for oxidation of other phenyl alcohols as well as cyclohexanol. However, photo-catalyzed oxidation of cinnamyl alcohol yielded benzaldehyde as the main products. Prior to each reaction run, the silica doped TiO_2 should be pre-treated with acid to introduce acid sites on the surface of catalyst, which is completely different from noble metal catalyzed oxidation processes in which base is frequently used as an additive.[12,162]

3.2.2 Promoters. The catalytic performance of a monometallic catalyst can be dramatically improved by introducing a second inexpensive metal as a promoter. For the oxidation of diphenylcarbinol, the yield of benzophenone was increased by a factor of 66, after the deposition of Bi species on Pt/Al_2O_3.[214] The promoting effect of Bi was ascribed to the suppressed adsorption of by-products. Recently, our group reported the remarkably improved catalytic activity of Pt/CNT for oxidation of benzyl alcohol by decorating iron oxides on Pt nanoparticles.[209] Two types of Fe promoted Pt/CNT catalysts were prepared. For PtFe/CNT, Fe is alloyed with Pt; while in FeO_x/Pt/CNT, FeO_x was preferably deposited on the surface of Pt nanoparticles. High selectivity and stability were observed when PtFe/CNT was employed as a catalyst. Compared to Pt/CNT and PtFe/CNT, FeO_x/Pt/CNT showed much higher initial activity because FeO_x on Pt surfaces enhanced the activation of both oxygen and alcohols. A plausible mechanism for the oxidation of benzyl alcohol over FeO_x/Pt/CNT was proposed. As shown in Fig. 21, FeO_x activated the molecular oxygen to form Fe–OH(ad) which reacted with Pd–H, yielding a H_2O and liberating the Pd active site.

As discussed above, a dramatic enhancement of the oxidation activity was observed when the supported MnO_x was modified by potassium dopants.[200,201] The occupation of K^+ into the interstitial sites formed during the stacking of Mn–O led to a deformed crystal structure of MnO_x, and thus weakened the Mn–O bonds and improved the oxygen mobility.

3.2.3 Support materials. Interactions between supports and active sites greatly influence the catalytic performance of a catalyst by modifying the physical and chemical status of active sites. The effects of the surface nature of supports on particle size and dispersion of metallic nanoparticles were reported. Supported Pd nanoparticles were prepared by adsorption of $PdCl_4^{2-}$ on the surface of mixed silica–alumina, followed by a thermo-reduction process.[190] Due to the stronger adsorption of $PdCl_4^{2-}$ on alumina as compared to silica, an increase in alumina content of the mixed oxide led to better distribution of Pd(II) and smaller Pd nanoparticles. By tuning the silica/alumina ratio, catalysts with different mean sizes of Pd nanoparticles were prepared. TUD-1, a kind of mesoporous molecular sieve, was functionalized with various organosilanes, and subsequent metal adsorption–reduction process produced Pd nanoparticles on modified TUD-1 (see Fig. 22).[189] The smallest mean particle size of Pd was observed on TUD-1 modified by monoamine groups (APS-TUD), which was a result of the electrostatic interaction between $-NH_3^+$ and the Pd precursor ($PdCl_2(OH_2)^{2-}$). In addition, these immobilized amino groups may also act as anchoring sites to stabilize the Pd(0) nanoparticles by binding them through covalent interactions, resulting in highly dispersed and uniformly distributed Pd nanoparticles. Likewise, a uniform dispersion of Pd nanoparticles was also achieved on SBA-16 modified with amino groups.[161] Au colloids supported by TiO_2 and AC were applied for the oxidation of benzyl alcohol.[196] High selectivity was obtained on Au/TiO_2, while AC supported Au had high activity. Since Au particle size is similar on both supports, the different catalytic behaviours were explained by changes in the shapes of Au particles induced by Au–support interactions.

A strong metal–support interaction (SMSI) benefits the stability of a catalyst. For Pd nanoparticles supported by an MnO_x/CNT hybrid support, the SMSI between Pd and support largely prevented the agglomeration of active sites during the oxidation reaction.[187] The SMSI was also found in the Pd nanoparticles on amorphous $Mn_xCe_yO_z$.[188] The enhanced catalytic stability was attributed to partial embedding of Pd nanoparticles in the mixed metal oxides. RuO_2 (*ca.* 1.3 nm) confined in the

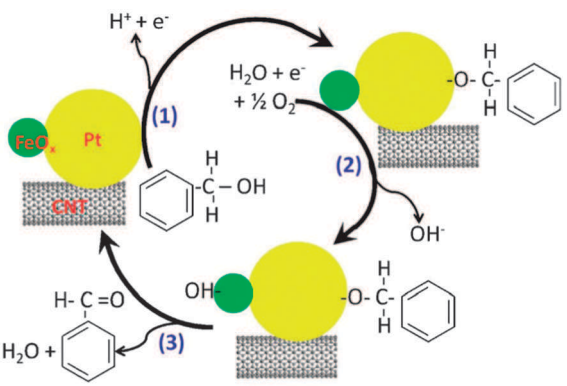

Fig. 21 Reaction scheme for the selective oxidation of benzyl alcohol to benzaldehyde over a FeO_x/Pt/CNT catalyst.[209] Reprinted from ref. 209 with the permission of the Royal Society of Chemistry.

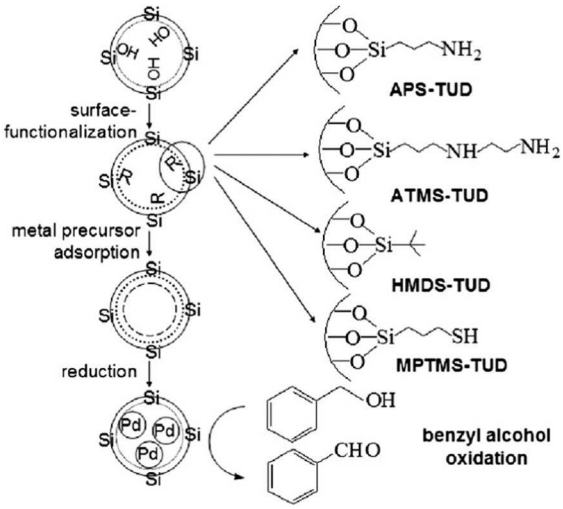

Fig. 22 Preparation procedures and catalytic evaluation of surface-functionalized TUD-1-supported Pd catalysts.[189] Reprinted from ref. 189, with the permission of the Elsevier, copyright 2010.

super-cage of faujasite zeolites were prepared by adding Ru precursors during the synthesis of zeolite.[199] EXAFS study indicated a strong interaction between RuO_2 species and the zeolitic framework in the form of "Ru–O–Si_{zeo}", where Si_{zeo} is a silicon atom in the zeolitic framework. The anchored RuO_2 nanoclusters exhibited excellent stability during the recycling tests. However, excessive SMSI is problematic, for example, by loading Pd precursors ($PdCl_2$) on the hydroxyapatites enriched with calcium-deficient sites, the strong coordination of phosphate species with Pd(II) hindered the reduction of Pd(II) to catalytic active Pd(0) by alcohols during the reaction, resulting in an inactive catalyst.[174]

Usually, supports with basicity favour high selectivity towards aldehydes and ketones. Compared to various supported materials including MgO, Al_2O_3, TiO_2, SiO_2, superior catalytic performance was achieved on hydrotalcite supported Au.[197] This observation was attributed to a concerted catalysis between the base sites of hydrotalcite and Au nanoparticles. High conversion and selectivity were obtained by using amino-group-functionalized catalysts (Pd/APS-TUD, see Fig. 22).[189] The elevated surface basicity was suggested to suppress the formation of toluene and facilitate the reactant adsorption and product desorption. Similarly, immobilizing amino groups on surface of SBA-16 led to increase of both activity and selectivity of the supported noble metals.[161] Nonetheless, for Pt-based catalysts, it was found that basic groups on AC may catalyze the aldol dimerization of carbonyl products, and the large by-products can adsorb on Pt surface, resulting in the deactivation of catalysts.[162] On the other hand, inferior selectivity to carbonyl compounds was observed in the presence of supports with acid sites. Pd supported by TUD-1 functionalized with –SH groups showed very high activity for oxidation of benzyl alcohol, but a large amount of toluene as by-product was produced due to the acidic surface of support.[189] For Au–Pd catalyzed oxidation of alcohols, the increase in selectivity to by-products was also attributed to the acidic nature of Al_2O_3 and Fe_2O_3.[186]

It is reasonable to expect a good catalytic performance by depositing highly active noble metals on NTM oxides, which may serve as an oxygen reservoir. Our recent works validate the feasibility of this idea.[187,188] High activity was achieved by loading Pd nanoparticles on NTM oxides (see Table 1). Pd nanoparticles supported by monometallic oxides (MnO_x, CeO_2) and the mixed oxide ($Mn_xCe_yO_z$) were synthesized by a facile microwave-assisted polyol reduction method.[188] Under the given reaction conditions, Pd was the single active site. The catalytic performances of these catalysts followed a sequence of: Pd on crystalline $MnCeO_x$ ($Pd/Mn_xCe_yO_z$-C, C: crystalline) > Pd on amorphous $MnCeO_x$ ($Pd/Mn_xCe_yO_z$-A, A: amorphous) > Pd/MnO_x or CeO_2 > physically mixed Pd/MnO_x and Pd/CeO_2. Pd/CeO_2 showed very high activity (TOF: 17 572 h^{-1}) for oxidation of benzyl alcohol, but the selectivity is low (88.9%), due to the formation of a large amount of toluene. X-Ray diffraction (XRD) and transmission electron microscopy (TEM) measurements suggested the formation of a solid solution of manganese and cerium oxides by incorporation of Mn cations into CeO_2 lattices. The superior catalytic activity of $Pd/Mn_xCe_yO_z$-C to that of $Pd/Mn_xCe_yO_z$-A was explained by three essential factors: more accessible Pd active sites, greater

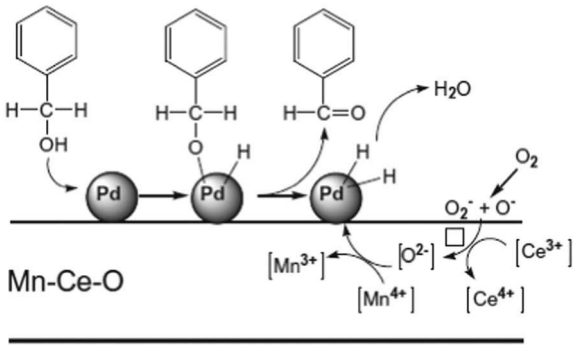

Fig. 23 Overall reaction mechanism for benzyl alcohol oxidation over Pd/$MnCeO_x$ catalysts.[188] Reprinted from ref. 188, with the permission of the Elsevier, copyright 2011.

Pd(0)/Pd(II) ratio and better porous structure. However, $Pd/Mn_xCe_yO_z$-A exhibited enhanced catalytic stability due to mutual promotion between redox properties and oxygen mobility. Based on extensive characterizations, the excellent catalytic performance of Pd on mixed Mn–Ce oxides solid-solution was ascribed to the synergistic interactions among Pd, MnO_x and CeO_2. An integrated alcohol oxidation mechanism over $Pd/Mn_xCe_yO_z$ was proposed, as shown in Fig. 23. As a supplement to the conventional dehydrogenation mechanism, the route of oxygen migration was depicted. The lattice oxygen migrates to the interface between the support and Pd active sites, where it reacts with Pd-hydride to regenerate Pd active sites. Meanwhile, lattice oxygen species are replenished by the adsorption, dissociation and migration of molecular oxygen. The dehydrogenation–oxidation of benzyl alcohol is completed *via* a synergetic redox cycle and electron transfer involving Pd, Mn and Ce: Pd ↔ Mn ↔ Ce.

The activity of Pd nanoparticles supported on CNT was significantly improved by insertion MnO_x between Pd and CNT, affording Pd supported by a hybrid support (Pt/MnO_x/CNT).[187] In this case, NTM oxide–MnO_x also acted as an oxygen reservoir. Its strong capability in activating molecular oxygen was confirmed from the rotating disk electrode (RDE) polarization voltammetry. Reducible MnO_x species at higher oxidation states can stabilize the Pd(II) cations. Thus, excess Mn loading resulted in the formation of large amounts of Pd(II) inactive species, which seriously impaired the activity of catalysts. After 1 h of reaction under either O_2 or N_2 atmosphere, the spent catalysts were investigated by XPS, Mn(IV) became the dominant species, indicating that the electrons transfer from Mn to the Pd active site making MnO_x species maintain a high-valence oxidation state. The Pd(0)/Pd(II) ratio increased due to the reduction of Pt(II) by electron transfer from Mn and alcohols. The amount of lattice oxygen showed a decreasing trend after the catalytic reaction, suggesting the migration of lattice oxygen from the MnO_x oxygen to Pd active sites participates in the oxidation reaction.

Another successful example of the combination of noble metal and NTM oxide is nano-crystalline CeO_2-supported Au nanoparticles.[215] Under mild reaction conditions (353 K), various alcohols, such as aliphatic, phenyl and allylic alcohols, can be readily converted to carbonyl products in the absence of bases.

Oxidation of phenyl ethanol in 2.5 h over Au/CeO_2 afforded 92% conversion and 97% selectivity to acetophenone. The good catalytic performance of Au/CeO_2 was attributed to the interaction between Au and Ce. Actually, the CeO_2 itself contains sites that are able to perform the oxidation of alcohols in a stoichiometric manner. But the reduced Ce is stable in the O_2 atmosphere; therefore, CeO_2 alone cannot finish the catalytic cycle. XPS spectra of Au/CeO_2 indicated the presence of positively charged Au species. It was suggested that Au nanoparticles interacted with the nanometric Ce surfaces, which stabilized the positive oxidation states of Au by creating Ce(III) and oxygen deficient sites in CeO_2. In the proposed oxidation mechanism, transformation of alcohols to corresponding carbonyl compounds was achieved by the interaction between positively charged Au, Ce(III) and the oxygen deficient sites.

Supporting materials with certain textures can exert a steric confinement on the active species, leading to enhanced or unique catalytic capability. It was demonstrated that RuO_2 trapped in a zeolite displayed a substrate-shape-selectivity imposed by the zeolitic framework.[199] Competitive oxidation of mixture of benzyl alcohol and 9-hydroxyfluorene led to complete oxidation of benzyl alcohol, and no oxidation products attributed to 9-hydroxyfluorene were detected. By using the same catalyst, the conversion of 1-heptanol was about 3 times higher than that of cyclohexanol. Benchmarked with amorphous silica, SBA-16 supported Pd catalyst showed lower activity but higher selectivity.[161] The effective confinement of mesoporous silica affords formation of metal nanoparticles with a narrow particle size distribution.[161,210] Catalytic performances of Pd nanoparticles supported by different types of modified mesoporous silica (including MCM-41, SBA-15, SBA-16, TUD-1) were examined over the oxidation of benzyl alcohol.[189] TUD-1 outperformed other porous materials, regardless of the type of surface functional groups. The advantage of TUD-1 was attributed to its unique open 3-D sponge-like mesostructure, providing strong confinement of Pd nanoparticles and suppressing the mass diffusion resistance.

The support effect can also be observed on transition metal oxide based catalysts. MnO_x was loaded on various supporting materials, such as MgO, ZrO_2, TiO_2, SiO_2 and Al_2O_3.[203] Among the supports studied, Al_2O_3 exhibited the highest conversion and selectivity for oxidation of benzyl alcohol. It was postulated that oxidation of Mn(II) by oxygen can be enhanced in the presence of Al_2O_3, facilitating the formation of MnOOH acting as the highly active site. For AC supported MnO_x species, the $MnO_x \leftrightarrow$ AC interaction was probed by the broad feature of H_2-TPR peaks.[213] It was found that AC was able to reduce Mn containing species (form Mn(III) to Mn(II)) under high temperature. The reduction of Mn species may have a negative effect on the activity of catalysts.

When supported VO_x was used as a catalyst, AC outperformed all other supporting materials, such as Al_2O_3, ZrO_2, TiO_2 and SBA-15.[204] The superior performance of AC as a support was explained by its affinity to substrates and a good mediator for electron transfer. Oxygen-containing groups were formed on the surface AC by oxidizing AC with different oxidants, such as H_2O_2, HNO_3 and O_2.[212] Improved catalytic activities were obtained on MnO_x and VO_x supported on the pre-oxidized AC. By ruling out the effects of specific surface area, active site dispersion, valence and local coordination, the elevated activity was attributed to the existence of oxygen-containing groups on AC surface. These surface oxygen groups changed the AC surface from hydrophobic to hydrophilic and from non-polar to polar, which facilitated the preferential adsorption of benzyl alcohol and the subsequent desorption of the hydrophobic product (benzaldehyde).

From a greener chemistry perspective, ionic liquids (ILs) were also utilized to modify the surface of supports. ILs containing both cations and anions can simultaneously interact with both supports and active species. Ru^{3+} was anchored on MgO nanocrystals *via* an IL–choline hydroxide mediator.[216] High yield to carbonyl products (85–99%) was achieved over this catalyst with a wide scope of alcohols as substrates, including phenyl alcohols, allylic alcohols and aliphatic alcohols. A strong synergistic effect between Ru^{3+} and the IL-modified MgO was supported by TPR and XPS measurements. The catalysts can be recycled and reused for up to seven cycles. The decrease in activity observed at the 6th and 7th cycles was attributed to the decrease of the surface area of MgO nano-crystalline. Pd nanoparticles were loaded on CNT modified by two kinds of ILs: [emin][NTf_2] and [bmin]Br.[160] Oxidation of 1-phenyl alcohols showed that introducing a small amount of [emin][NTf_2] could increase the activity sharply, while addition of another frequently used IL [bmin]Br led to very poor activity. The promoting effect of [emin][NTf_2] was explained from two aspects. Firstly, good solubility of both alcohols and O_2 in [emin][NTf_2] offered a better reactant–catalyst contact. Secondly, Pd nanoparticles surrounded by electrophilic $[NTf_2]^-$ might have low electron density, which would enhance the hydrogen abstraction ability of Pd, leading to a high activity. On the other hand, [bmin]Br with a hydrophilic property can quickly adsorb and accumulate on catalyst surfaces, resulting in the deactivation of catalysts.

Polymers, such as PEG and polystyrene, were also employed as supports. It was reported that dispersing Pd nanoparticles in PEG matrix can prevent significantly the agglomeration of active species during the oxidation reaction, which enhanced the stability of catalysts.[194] Pt nanoparticles were also introduced in PEG matrix.[207] The stabilization effect of PEG prevented the deactivation of Pt by oxygen, and thus, enabled the reuse of Pt based catalysts. Au nanoparticles were trapped in cross-linked polystyrene derivatives, due to the interaction between Au and the electrons from the benzyl ring.[198] The stabilized Au nanoparticles showed a fairly good stability.

3.2.4 Solvents. Effects of polarity of solvent on aerobic oxidation of alcohol have been studied. For Pd/hydroxyapatite catalyzed oxidation of alcohols, trifluorotoluene and water were the effective solvents, due to the high hydrophilic character of hydroxyapatite.[174] While aprotic polar solvents such as acetonitrile, dimethylformamide and dimethyl sulfoxide were not effective at all, due to the poisoning of catalysts by coordinating with Pd. In contrast, for oxidation of phenyl ethanol over Au/hydrotalcite, the highest activity was obtained in toluene rather than in high polar solvents, such as acetonitrile, ethylacetate and water.[197]

For environmental reasons, the use of water instead of organic solvents is desired. For both Pd–Au and Pt–Au bimetallic catalysts,

the enhanced catalytic activity was obtained in water instead of organic solvents[195] because water acts as a weak base to assist the abstraction of β-hydrogen from alcohol to active sites.[195,217] However, water is not applicable for primary alcohols (especially for Pt based catalysts), due to the reaction between water and carbonyl products yielding a germinal glycol, as shown below:[162]

$$RR'C{=}O + H_2O \leftrightarrow RR'C(OH) \quad (41)$$

The germinal glycol can be further oxidized to by-products, *e.g.*, carboxylic compounds.[195] Oxidation of substituted benzyl alcohols over Pt/AC was carried out in a mixture of water and dioxane.[217] Benzaldehyde was the main product in pure dioxane or low water content (10 vol%). Adding excess amounts of water dramatically accelerated the reaction. When the content of water was increased to 50 vol%, carboxylic acids with 99% yield were produced. Because the germinal glycol is a stronger acid than alcohols, the pH of the reaction solution can affect greatly the selectivity and conversion. In high pH medium, the hydration form of carbonyl products (*i.e.*, germinal glycols) are very active and trend to polymerize.[162] A high pH of reaction solution can also promote the formation of carboxylic acids which can be adsorbed on noble metal surface, leading to the deactivation of catalysts.[162,195] On the other hand, in weak alkaline solution, the competitive adsorption of OH^- and CO (a possible by-product during oxidation of alcohols) prevents the deactivation of catalysts.[162] Furthermore, the adsorbed OH(ad) on the metal surface may play a role in formation of alkoxides and also act as an oxidant to eliminate the metal hydride.[162,169] As such, for Pt-based catalysts, a pH between 7 and 9 was recommended.[162] Usually Au-catalyzed oxidation of alcohols was carried out in high pH solutions.[12]

In addition to traditional solvents, supercritical CO_2 ($scCO_2$) was also used as a reaction medium.[163,194] $scCO_2$ may provide a safe environment for oxidizing organic compounds with O_2. The pressure of $scCO_2$ can affect the catalytic reaction, due to changes in solubility of alcohols in $scCO_2$.[194] Finally, it has been repeatedly demonstrated that solvent-free catalytic oxidation of liquid alcohols is also a feasible way to produce carbonyl products with high yields.[191,192]

3.2.5 Substrate scopes. Solid metallic catalysts are able to catalyze the oxidation of a wide range of alcohols, including phenyl, allylic and aliphatic alcohols. For a given catalyst, different substrates may lead to distinct reaction results, due to the different intrinsic nature of each alcohol. Usually, phenyl and allylic alcohols are more active than aliphatic alcohols, because the π-bond interactions between noble metals and benzyl rings or double bonds of unsaturated alcohols can facilitate the rupture of O–H bonds through the neighbouring active sites, affording the formation of alkoxides.[174,218] Interestingly, the distance of Pd–Pd bond (2.76 Å) is in accordance with the distance between the center of a C=C bond and an oxygen atom for O–H group of a cinnamyl alcohol (*ca.* 2.8 Å), as depicted in Fig. 24.[174] 100% selectivity to cinnamaldehdye was obtained over Pd-based catalysts.[174] On Ru-based catalyst, the order of reactivity for substituted benzyl alcohols was $-CH_3O > -CH_3 > -H > -Cl > -NO_2$,[170] because electron-donating substituents favour the formation of carbocations as intermediates during the catalytic cycle. Similar trends were also observed in other catalytic systems with either noble metals[161,187,189] or NTM.[201] Compared to other alcohols, it is relatively more difficult to get high selectivity to aldehydes from the oxidation of primary aliphatic alcohols,[169,195,207] as aliphatic aldehydes are more active than aliphatic ketones and phenyl aldehydes.[162] They are prone to be oxidized to carboxylic acids.[195] Supported noble metal nanoparticles showed tolerance to heteroatom-containing alcohols,[173,174] however, activity of Au/hydrotalcite was hampered by O or S atoms in alcohols.[197]

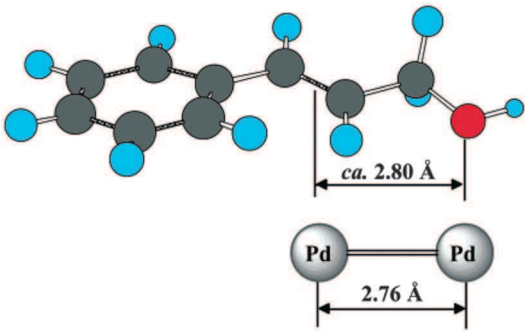

Fig. 24 Scheme for the multiple interaction between Pd–Pd paired site and cinnamyl alcohol.[174] Reprinted from ref. 174, with the permission of the American Chemical Society, copyright 2004.

4. CO oxidation

Carbon monoxide (CO) is one of the most common and widely distributed air pollutants.[219,220] Catalytic CO oxidation by molecular oxygen is of practical importance for reducing CO in the atmosphere. In addition, because of the effect of CO poisoning, PROX of CO in an H_2-rich stream is preferred.[221] Over the past decades, tremendous efforts have been devoted for the development of highly active and selective catalysts for CO PROX.[222–224] Furthermore, CO oxidation is also an ideal probing reaction to study the fundamental steps of heterogeneous catalysis. The catalytic CO oxidation on noble metals has been extensively studied and documented.[225,226] Recently, the distinct catalytic behaviors of Ru under different pressures were reviewed by Over and Muhler.[227] Besides noble metals, NTM-oxides-catalyzed CO oxidations were summarized by Duprez and Royer.[220] Wolf and co-workers reviewed the fundamental understandings of heterogeneous catalytic processes inspired by catalytic CO oxidation.[222]

4.1 Mechanisms of catalytic CO oxidation

The mechanisms for CO oxidation on noble metals and NTM oxides are different, due to the distinct adsorption manners of CO and O_2. Studies on the catalytic details of CO oxidation not only facilitate the design of efficient catalysts to fulfil the requirement of industry but also contribute to the understanding of heterogeneous catalysis processes.

4.1.1 Noble metal catalyst. Catalytic CO oxidation on noble metal catalysts seems to be a simple process. However, it is not possible to describe it using a single mechanism. The details of a CO catalytic cycle is determined by several aspects of a given

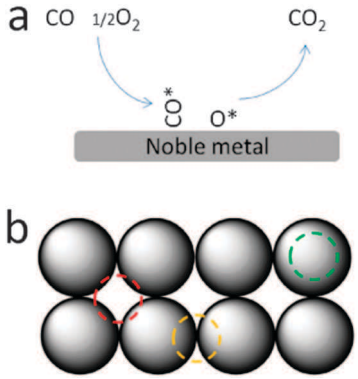

Fig. 25 (a) Oxidation of alcohol to the corresponding aldehyde over noble metals; (b) adsorption sites for oxygen and CO: 4 fold-hollow site (red-dashed circle), bridging site (yellow-dashed circle) and on-top site (green-dashed circle).

catalytic system, including the physical and chemical status of noble metals (extended metal surface *vs.* supported nanoparticles, pure metal *vs.* partially oxidized metal);[222] properties of supports and promoters; reaction parameters (temperature, pressure and CO/O_2 ratio), and *etc.* Therefore, many fundamental details associated with catalytic CO oxidation are still missing. Here, we would like to begin our discussion on catalytic CO oxidation with a simple but widely accepted Langmuir–Hinshelwood (L–H) model which was deduced from intensive CO oxidation studies over well-defined single crystalline surfaces of noble metals under ultra-high vacuum (UHV) conditions.[222]

Based on the L–H model, CO oxidation process could be divided into the following 3 steps:[220] (see Fig. 25 also)

$$CO + * \rightarrow CO(ad) \quad (42)$$

$$O_2 + * \rightarrow 2O(ad) \quad (43)$$

$$CO(ad) + O(ad) \rightarrow CO_2 + 2* \quad (44)$$

where * and (ad) denote the active sites and adsorbed species, respectively. The bonding of CO to transition-metal atom is commonly descried by the Blyholer model of M ← C σ donation and M → C π back-bonding (M: metal). The electron back-donation from metal to CO activates CO by weakening the CO bond.[222] The configurations of CO(ad) could be in the form of linear coordination with one noble metal atom (on-top), bridging between two metal atoms or simultaneously interacting with multiple metal atoms (capping) (see Fig. 25).[222] The coordination of CO(ad) depends on the types of noble metals. Based on Evans and Liu's theoretical calculations, CO(ad) prefers to reside on the bridging sites of Pd(100) and on the top sites of Rh(100).[228] On a Pt surface, O_2 dissociation occurs at temperatures above 170 K.[220] After dissociation, oxygen atoms reside on the 4 fold-hollow sites on the surface of noble metals (see Fig. 25).[228] A combination of CO(ad) and O(ad) releases CO_2, which is the rate-determining step.[222] However, if the M–O bond (M: metal) energy is low and the metal surface oxygen coverage is high, the slow step would be adsorption or dissociation of O_2 on the metal surface.[229,230]

The actual CO oxidation reaction could be far more complex than the scenario described by the L–H model, even on the surface of an extended crystalline noble metal. First, because of the stronger sticking coefficient of CO than that of O_2, the metallic surfaces could be easily poisoned by the total coverage of CO, whereas a metallic surface saturated with oxygen is still available for CO adsorption.[220] Second, CO adsorption on a metallic crystal could make the metal surface reconstruct.[231] This metal surface reconstruction could promote the adsorption of O_2, as the sticking coefficient of O_2 is structure-sensitive.[232] Third, oxides could be formed during CO oxidation on noble metal surfaces, especially at a low CO/O_2 ratio or under atmospheric pressure.[232,233] The surface oxides are very active towards CO oxidation which may undergo a M–v K type oxidation.[233] For Ru based catalysts, it has been shown that surface RuO_2 species rather than metallic Ru are the active sites for CO oxidation.[227,234] Due to the different sticking coefficients of reactants and the dynamic changes of the physical and chemical status of metallic surfaces during CO oxidation, oscillation of reaction rates has been observed under both UHV and ambient conditions.[231,233,235] At certain CO/O_2 ratios and reaction temperatures, the reaction rates fluctuated between the low value on a smooth metallic surface dominated by CO(ad) and the high value on a rough oxide-rich surface dominated by O(ad) or oxide species.[233] The periodic fluctuation along with switching of reaction mechanisms (L–H ↔ M–v K) can be completed within a few seconds at atmospheric pressure, whereas the restructuring of metallic and oxide surfaces are relatively slower, taking up to 1000 s.[233]

The catalytic cycle of CO oxidation becomes even more complicated for a real catalyst, because of the polymorphic structure of catalyst nanoparticles, the formation of oxide species on metal nanoparticle surfaces, and effects from supports and promoters. Nevertheless, improved experimental techniques have made the detailed understanding of real catalysts possible. The dynamic morphological fluctuation of a single supported Au nanoparticles in oxygen-rich conditions under room temperature was directly observed using an *in situ* environmental TEM technique.[236] By using the same technique, the reconstruction of crystalline facets of a supported Au nanoparticle induced by CO adsorption was also visualized.[237] CO oxidation over supported Pt nanoparticles was monitored by *in situ* XAS. It was found that the high reaction rates of CO oxidation were always accompanied with the formation of amorphous oxides on the Pt surface.[238] High resolution XRD study of Rh nanoparticles on magnesium oxide (MgO(001)) showed that the O–Rh–O trilayer surface oxides can be readily formed at very low oxygen pressure (2×10^{-5} mbar) above 500 K, along with a shape change of the Rh nanoparticles.[239] The surface oxides can be reduced by CO, leading to the recovery of the metallic surface and the original particle shape. CO oxidation was also carried out on Au nanoparticles with different mean sizes supported on titanium oxide (TiO_2(110)) at 300 and 400 K.[240] Two types of TOFs were calculated based on the number of exposed surface Au atoms (TOF-s) or Au atoms sitting on the periphery of Au nanoparticles (TOF-p). Interestingly, TOF-p did not change with the variation of Au nanoparticle sizes at 300 K, while TOF-s was found dependent on the mean particle sizes. These results

suggest that at low reaction temperatures, CO oxidation mainly occurs at the interface between Au and TiO_2. At high reaction temperatures (*e.g.*, 400 K), the correlation between two types of TOFs and the mean particle sizes reversed. TOF-s became independent of particle size, suggesting that surface Au atoms were active enough to catalyze the CO oxidation reaction. The catalytic active sites not only exist at the boundary between metal nanoparticles and supports but are also present at the perimeter of promoters on the surface of a metal nanoparticle. Iron oxide (FeO_x) was deposited on the surface of Pt nanoparticles supported by silica. It was suggested that O_2 dissociated mainly at the interface between the peripheries of FeO_x and Pt.[223] For CO oxidation catalyzed by nano-alloys (Pt–Ni–Co, Co: cobalt) catalyst, the active sites were proposed at the neighboring hetero-atoms, *i.e.*, M–Pt–M sites (M: Ni or Co), where CO adsorbs on Pt, concurrently Ni/Co activates O_2.[241] Oscillation of CO oxidation rates on a real catalyst (Pt on alumina (Al_2O_3)) under practical conditions was studied using *in situ* XAS and infrared spectroscopy.[242] Surface oxides with oxygen defects were speculated as the active species with the M–v K type reaction.

To understand better the catalytic CO oxidation process, many new models have been proposed by incorporating more details in the L–H or M–v K model. Based on the M–v K theory, Galwey and L'vov developed a thermochemical approach to understand the CO oxidation over Pt based catalysts.[243] In their model, the catalytic cycle is mediated by the formation of metastable gas phase Pt atoms. The modified catalytic process can be written as:

$$PtO_2(s) + 2CO(g) \leftrightarrow Pt(g) + 2CO_2(g) \quad (45)$$

$$Pt(g) + O_2 \leftrightarrow PtO_2(g) \rightarrow PtO_2(s) \quad (46)$$

where (s) and (g) denote solid and gas phase, respectively. This new model is able to explain several experimental observations, such as the inhibition of high concentration of CO_2 (eqn (42)) and the surface reconstruction during CO oxidation (formation of volatile Pt).

The formation of surface oxides during CO oxidation on Pt-group metals was simulated using the first-order phase transition theory:[244]

$$O(ad) \leftrightarrow O(s\text{-}t) \leftrightarrow O(latt) \quad (47)$$

O(latt) and O(s-t) represent the lattice oxygen and surface-termination oxygen (*i.e.*, superficial O(latt)), respectively. O(ad) and O(s-t) are removed by reacting with CO *via* the L–H or E–R mechanisms, where E–R mechanism was described as:

$$CO(g) + O(s\text{-}t) \rightarrow CO_2(g) + V_O \quad (48)$$

The simulation results suggested that small surface-oxide islands could be formed on the Pt surface at the nanometer scale. Oscillation of CO oxidation rates was simulated by a kinetic Monte Carlo scheme based on a mesoscopic skeleton model and the L–H mechanism with the consideration of surface oxides formation.[245] The simulation results showed that oscillation of CO oxidation for a given system is independent of the activity of oxide species.

The nature of the active oxygen species on Au/TiO_2 during CO oxidation was examined by multipulse measurements performed in a TPA reactor, in which the time-resolved production of CO_2 was measured when CO was admitted through the pre-oxidized catalyst.[246] An Au-assisted M–v K mechanism was proposed by Behm and Widmann to explain the CO oxidation, in which Au nanoparticles gather CO(ad) and slightly activate O(s-t) in TiO_2 at the perimeter of Au nanoparticles. Note that these activated oxygen atoms in TiO_2 are very stable even at 673 K.

4.1.2 NTM oxide catalysts. M–v K type catalytic cycle is frequently employed to describe the CO oxidation over NTM oxides.[220,247–249] The simple version of the M–v K cycle can be written as follows (see also Fig. 26):

$$CO + M^{\delta+}\text{–}O\text{–}M^{\delta+} \rightarrow OC\text{–}M^{\delta+}\text{–}O\text{–}M^{\delta+} \quad (49)$$

$$OC\text{–}M^{\delta+}\text{–}O\text{–}M^{\delta+} \rightarrow CO_2\text{–}M^{\delta+}\text{–}V_O\text{–}M^{\delta+} \quad (50)$$

$$CO_2\text{–}M^{\delta+}\text{–}V_O\text{–}M^{\delta+} \rightarrow CO_2 + M^{\delta+}\text{–}V_O\text{–}M^{\delta+} \quad (51)$$

$$O_2 + 2(M^{\delta+}\text{–}V_O\text{–}M^{\delta+}) \rightarrow 2(M^{\delta+}\text{–}O\text{–}M^{\delta+}) \quad (52)$$

It is generally accepted that CO is preferably adsorbed on metal cations,[220,247,250,251] whereas on the defected crystalline surface, CO may simultaneously bond with both a metal cation and a twofold coordinated oxygen (O^{2f}).[220] In Co_3O_4 catalyst, Broqvist *et al.* suggested that CO would be firstly adsorbed on Co(III) and then glide towards O^{2f}, leading to the formation of carbonate species (CO_2^{-2}) as intermediates.[252] CO and O_2 adsorb on different active sites on the surfaces of NTM oxides, and thus there is no competing adsorption in this catalytic system, which is different from noble metal based catalysts.

Adsorbed O_2 can transform to lattice oxygen *via* a series of steps:[253]

$$O_2(ad) \rightarrow O_2^{-}(ad) \rightarrow O_2^{2-}(ad) \rightarrow 2O^{-}(ad) \rightarrow 2O^{2-}(latt) \quad (53)$$

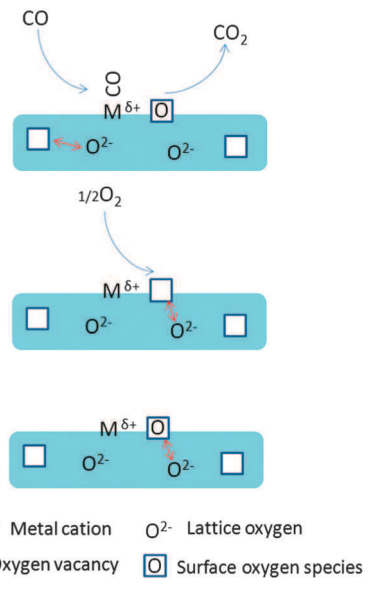

Fig. 26 Oxidation of CO over NTM oxide based on the M–v K mechanism.

where O_2^-(ad) and O_2^{2-}(ad) denote the surface superoxide and peroxide species, respectively. The formation of O_2^-(ad) and O_2^{2-}(ad) on metal oxides was proved by infrared spectroscopy.[254] All of the oxygen species may participate in the catalytic oxidation of CO. At low temperatures, adsorbed oxygen species on surfaces, such as O_2^-(ad) and O^-(ad), may act as the main oxidants.[253] For example, reaction of O_2^-(ad) and CO gives rise to CO_2 and O^-(ad); O^-(ad) can be further reduced by CO, leaving a V_O site.[255] After pre-treating a mixed oxide $Nd_{1-x}Sr_xCoO_3$ with O_2, the order of CO oxidation reaction with respect to O_2 was zero at the initial reaction stage, suggesting the existence of surface oxygen species that can easily react with CO.[256] At the steady state, the reaction order respect to O_2 became 0.5, which implied that dissociation of O_2 on the surface of oxides was the rate-determining step. The reactivity was largely affected by the density of V_O on the surface of the mixed oxide. At relatively high temperatures (*e.g.*, 573 K above), the participation of lattice oxygen was observed and the catalytic activity was dependent on the oxygen mobility of the metal oxides.[258] The involvement of oxygen from the surface and subsurface of metal oxides was also confirmed using $^{18}O_2$ as oxidant.[259]

The migration of oxygen species inside NTM was evidenced by the TPA technique.[224,257] When a CO stream was passed through the freshly oxidized Cu–Ce mixed oxide, two CO production spikes at the beginning within 50 s were observed, followed by rapid drop of CO conversion, as shown in Fig. 27.[257] The first spike of CO_2 production was assigned to the oxidation of CO by the superficial oxygen species that were readily accessible; the second increase in production rate of CO_2 was explained by the migration of bulk lattice oxygen to the surface and reaction with CO. Once all of the active oxygen species were consumed, the CO oxidation would stop. To simulate the two-step CO oxidation over a Cu–Ce binary oxide, a more detailed M–v K model containing 9 elementary steps was proposed and simulated with a Monte Carlo algorithm.[260] In this advanced model, all possible oxygen transferring processes, such as from gas phase (O_2) to solid phase and from lattice framework to surface of NTM oxides, were considered. The simulation results matched fairly well with the corresponding experimental observations, justifying the validity of these assumptions. It is noteworthy to mention that TPA measures the amount of CO_2 produced from a unit amount of an oxidized catalyst in the stream or certain amount of CO.[224,246] Therefore, the number of all of the active oxygen species (including chemisorbed or lattice oxygen) that react with CO can be deduced from the production of CO_2. This intrinsic property of a catalyst is called the "oxygen storage capacity" of a catalyst which can be used as an indicator for the activity of the catalyst.

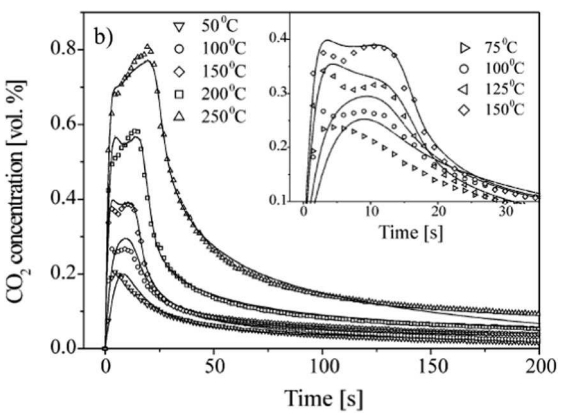

Fig. 27 Temporal CO_2 concentrations in the reactor effluent stream as a function of temperature. The markers represent experimental points. The solid lines represent the model predictions.[257] Reprinted from ref. 257, with the permission of the Elsevier, copyright 2004.

However, not all CO oxidations involve the lattice oxygen. Based on the kinetic study on CO oxidation over $LaCoO_3$, a catalytic cycle similar to the L–H mechanism was proposed. In this modified L–H model, adsorption of CO_2 was also included.[220]

4.1.3 Preferential oxidation of CO in H_2-rich stream. For preferential oxidation of CO (PROX), the selectivity to CO_2 is determined by the competitive oxidation of CO and H_2, *i.e.*, the reaction rates of CO and O_2. The L–H mechanism has been proposed for a noble metal based catalytic system (*e.g.*, noble metals on inner supports).[261] CO, H_2 and O_2 are all adsorbed on the surface of a noble metal, and thus the selective oxidation of CO depends on the surface coverage of CO, which, in turn, is largely influenced by several experimental factors, including the partial pressure of CO, the ratio of O_2/CO and temperature. Usually, high selectivity is obtained at a high partial pressure of CO, low O_2/CO ratio and low temperature.[261] On the other hand, studies on the NTM oxide catalyzed PROX process suggest the M–v K mechanism.[262,263] Transient experiments based on a TPA reactor revealed that lattice oxygen of NTM oxide could be involved in oxidation of CO even at low reaction temperatures.[262] Different from noble metal based catalysts, CO does not prohibit the adsorption of H_2; both of them can be adsorbed on the surface of NTM oxide in a non-competitive way.[262] However, oxidation of H_2 can only occur at higher temperatures than the onset temperature of CO oxidation, namely a higher activation energy for H_2 oxidation.[264] Therefore, for NTM oxide catalyzed PROX, a high selectivity up to 100% can be achieved on NTM-oxide-based catalysts at the low temperature regime, and the selectivity is not sensitive to the partial pressure of CO or the O_2/CO ratio.[262] It is interesting to see that noble metals supported on redox NTM oxide display both L–H and M–v K kinetics, for example Pt/CeO_2.[265] The selective oxidation pathway changes with CO concentration. At a relatively high CO concentration (>1%), due to the high coverage of CO on Pt, CO oxidation mainly happens at the interface between Pt and CeO_2, following the M–v K mechanism. At low temperature, the inhibited adsorption of H_2 by CO and low activity for H_2 oxidation lead to nearly 100% selectivity of CO oxidation.[265] When the CO concentration is reduced to the ppm level, CO oxidation mainly occurs on the surface of Pt, which is governed by the L–H kinetics. The low coverage of CO on Pt promotes the oxidation of H_2, resulting in a significant drop of selectivity to CO_2.[265]

4.2 Catalyst design for CO oxidation

4.2.1 Active sites. Similar to the catalytic oxidation of alcohols, both noble metals (Pt, Pd, Au, Ru, Rh *etc.*) and NTM

oxides (Co_2O_3, CuO, MnO_2, $LaCoO_3$ *etc.*) have been employed as heterogeneous catalysts for oxidation of CO. Duprez and Royer summarized the activities of different noble metals and NTM oxides for CO oxidation under the same reaction conditions (573 K, 1% CO in excess O_2).[220] The activity sequence was: Pd $\gg$ Pt $>$ Co_2O_3 $>$ CuO $>$ $LaCoO_3$ $>$ Au $>$ MnO_2 $\gg$ Fe_2O_3. It is important to note that the activity sequence listed above is just a rough guideline, as the catalytic performance of a given active catalyst depends greatly on other factors, such as reaction temperature, CO/O_2 ratio, particle size, effect of support *etc.* A typical counter example is Au, which exhibits superior activity for CO oxidation at very low temperature.[219] Because of the complexity of the CO oxidation process as well as the lack of experimental details (space time, metal loading, mass transport parameters *etc.*), it is generally difficult to compare the activity of different catalysts based on current reported data.

Despite aforementioned experimental obstacles, the activities of different noble metals in their metallic form could be estimated by theoretical calculations. The chemisorption energy of CO (kJ mol^{-1}) on different metals was calculated by DFT theory,[220] with Pt (182) $>$ Rh (173) $>$ Ru (171) $>$ Pd (168) $\gg$ Au (34). The order of chemisorption energy is consistent with the order of adsorption heat obtained by calorimetric studies. The calculated dissociative chemisorption heat of O_2 (in kJ mol^{-1}) is: Ru (446) $>$ Rh (389) $>$ Pt (209) $>$ Pd (116) $>$ Ag (63) $\gg$ Au (-52), which also agrees with the chemisorption heat of O_2 measured from the adsorption of O_2 on metal foils, except for Pd whose measured value is between that of Rh and Pd. Starting from the L–H mechanism, the upper limit of the rate of CO oxidation over different metals was evaluated by using a Sabatier analysis.[230] The Sabatier rate is the rate of reaction if the coverage of all surface species is optimized for each elementary reaction step. At high temperatures (600 K) and stoichiometric CO/O_2 ratios, the Sabatier rate of CO oxidation on close-packed surfaces of various metals follows: Pd $>$ Pt $>$ Rh $>$ Ru $>$ Ag $>$ Au. Besides the extended metal surfaces, the activities of metallic nanoclusters were also estimated using the same analysis by adding one more elementary reaction:

$$O_2^* + CO^* \leftrightarrow CO_2 + O^* + * \quad (54)$$

because the adsorption energy of O_2 or CO is much higher on cus sites of nanoclusters than that on extended metal surfaces. At low temperature (273 K) and O_2-rich conditions, the modelling results showed another sequence of the Sabatier rate: Au $>$ Pd $>$ Ag $>$ Pt. The substantial shift of adsorption energy of surface species on cus sites was the dominant reason for nanosized Au becoming the best catalyst at low temperature. Shift of Au activity towards higher value was also observed based on the DFT calculation for CO oxidation on stepped and kinked sites of Au.[266] These results suggested that the activity of Au was strongly affected by the existence of cus sites.

Both experimental and theoretical calculations indicate that Pt and Pd are very active metals for CO oxidation at high temperatures.[220,222,230] Usually, under 1 bar, the high activities of Pt or Pd based catalysts are obtained on partially oxidized metal surfaces rather than pure metallic surfaces.[231,233,238,242] For CO oxidation over extended Pt or Pd surfaces, once a thin layer of oxide was formed, the reaction rate increased linearly with CO partial pressure.[232] The rate constants for Pt(110) and Pd(100) are the same, which suggests that the reaction rate was determined by non-intrinsic properties, such as CO partial pressure. The temperature dependence of CO oxidation over supported Pt nanoparticles was examined with *in situ* XAS.[238] It was found that above the ''ignition temperature'', the catalytic activity increased sharply with the formation of Pt oxides on the Pt surface. These noble metal oxides are metastable and active. Under the ignition temperature, a trace amount of CO was sufficient to reduce the pre-oxidized catalyst. The ignition temperature increased with the CO/O_2 ratio. The surface reconstruction, lifted by CO adsorption, may facilitate the formation of metal oxides on the surface of Pt or Pd.[231] As bulk Pt oxide is nearly inactive for CO oxidation, the high activity of partially oxidized Pt catalysts was related to the cus Pt sites in oxide species.[242] A high reaction rate was observed on rough oxidized surface of Pd(001) as well.[233]

Based on the DFT calculations shown above, both CO and O_2 adsorption on Au are very weak. The negative value of dissociative chemisorption of O_2 (-52 kJ mol^{-1}) on Au suggests that the dissociation of O_2 on Au is not possible. O_2 desorbs from the crystalline Au surface below 50 K and does not dissociate over Au(110) even at 500 K and 1.8 bar.[229] Indeed, bulk Au is totally inert, only Au nanoparticles that are smaller than 5 nm are catalytically active and well-known for their high activity at low temperature (below 273 K).[219,267] The high activity of small Au nanoparticles has been explained by the following 4 aspects: quantum size effect, large amount of cus Au atoms, active sites sitting at the perimeter of supported Au nanoparticles, and the existence of positively charged Au. The relation between Au particle size and CO oxidation rate was surveyed by Bond.[268] It was suggested that the activity of Au based catalysts mainly came from Au nanoparticles whose size was less than 2.5 nm. This critical size was regarded as the transition point from a metallic to a non-metallic or ''molecular'' structure. Small Au nanoparticles have distinct properties as compared with bulk Au or Au with large particle sizes, such as very low conductivity and melting temperature. This transition may lead to the enhanced and activated chemisorptions of CO.

Adsorption of CO on cus sites of Au nanoparticles was proposed.[269] Two peaks were found in the thermodesorption spectrum of CO that was adsorbed on Au nanoparticles, which was related with the adsorption of CO on two different defect sites on Au (*e.g.*, steps and kinks). The initial adsorption probability of CO on a surface with zero coverage was used to access the adsorption capability of Au nanoparticles. It was found that the initial adsorption probability of CO reached a maximum value when the Au nanoparticle size was 3 nm.[269] Theoretical calculations showed that the bonding strengths of Au–CO and Au–O are much stronger on Au clusters that those on Au crystalline surfaces.[229] A measurable dissociation of O_2 on cus Au atoms was observed at 400 K.[229] Recently, CO adsorption on a single Au nanoparticle was studied using *in situ* environmental TEM.[237] Reconstruction of flat micro-facets of the Au nanoparticle were observed and

explained by the induction effect of adsorbed CO. This assumption was supported by *ab initio* calculations. These new findings revealed that besides the cus sites at corners and edges, a surface with a flat facet (*e.g.*, Au(100)) may undergo rearrangement that could allow CO to adsorb.

For supported Au nanoparticles, the adsorption and dissociation of O_2 mainly occurs at the perimeter of supported Au nanoparticles.[240,246] Dynamic fluctuation of facets on a gold nanoparticle supported by CeO_2 was observed at O_2-rich conditions, which was attributed to the dissociation of O_2 at the interface between Au and CeO_2.[236] It was reported that the anion cluster of Au and O_2 ($Au_3O_2^-$) cannot oxidize CO to produce CO_2, implying that dissociation of O_2 to O atoms is necessary for CO oxidation.[270] Reaction of O_2^-(ad) and O_2^{2-} (ad) with CO at Au–CeO_2 interface was confirmed by Raman spectroscopy.[271]

In the Au/MgO catalyzed CO oxidation system, it was found that the reaction rate was proportional to the ratio of Au(I)/Au(0).[272] By ruling out the size effect of Au particles, the high activity of Au/MgO was explained by the involvement of Au(I) in the catalytic cycle. In fact, it was reported that supported Au oxide was much more active than Au nanoparticles in CO oxidation.[273] However, the activity of Au oxide decayed very rapidly due to the formation of metallic Au.

Besides supported Au nanoparticles, porous gold nanostructures also exhibited high activity for CO oxidation even below 237 K.[274,275] The nanoporous bulk Au with a coral-like structure could be prepared by etching out the less noble constituent (*e.g.*, Ag or Cu) from a bulk Au alloy. As the size of ligaments (30–40 nm) in the nanoporous Au is significantly larger than the commonly agreed upper limit size (5 nm) for an active Au based catalyst, the activity of nanoporous Au was attributed to surface defects (such as steps and kinks) or residual second metal (*e.g.*, Ag or Cu) which was left on the surface during the catalyst preparation.

Under UHV conditions, metallic Ru is not catalytically active for CO oxidation, while under strongly oxidizing reaction media, formation of an epitaxially grown RuO_2(110) overlayer on metallic Ru makes it highly active towards CO oxidation.[227] RuO_2 is much more stable than Pt and Pd oxides, due to the high bonding energy of Ru–O.[276] On the RuO_2 surface, there exist two types of adsorption sites: (1) the on-top site over a cus Ru atom (Ru–□); (2) the bridging site in between two Ru atoms (Ru–□–Ru).[234] Based on the DFT calculations, the binding energies of CO and O on different adsorption sites follow: O_{br}(2.44 eV) > CO_{br}(1.64 eV) > CO_{cus}(1.31 eV) > O_{cus}(1.08 eV),[234] where cus and br denote the atop cus sites and bridging sites, respectively. The activity of RuO_2 depends on the amount of one-fold coordinately unsaturated Ru, namely the Ru–□ sites.[227] A perfect RuO_2 crystalline surface saturated with oxygen atoms is catalytically inactive.[276] CO oxidation over RuO_2 follows the M–v K mechanism.[227] Like Ru, Rh is also easily oxidized during CO oxidation, together with the formation of Rh_2O_3.[239,277] In a mixture of CO and O_2, besides metallic Rh and Rh_2O_3, formation of Rh(I)$(CO)_2$ was also detected by EXAFS. Equilibria among the three different Rh species are proposed as:

$$Rh(I)(CO)_2 \leftrightarrow Rh(0) \leftrightarrow Rh_2O_3 \qquad (55)$$

The equilibrium between Rh(I)$(CO)_2$ and Rh(0) mitigates the hindering effect of CO on the chemisorptions of O_2, resulting in improved catalytic activity. Under O_2-rich conditions, CO oxidation over Rh_2O_3 on the metallic Rh core follows the M–v K mechanism. Based on the *in situ* XPS studies, a particular type of oxide was formed during Rh-catalyzed CO oxidation, but was absent in pure O_2, suggesting the formation of CO stabilized Rh oxide as an intermediate during CO oxidation.[278]

The activity of NTM oxides for CO oxidation has long been discovered. At the beginning of the 20th century, some oxides (*e.g.*, hopcalite—a mixed Mn–Cu oxide) were discovered to oxidize CO at ambient temperature.[220] However, metal oxides may not serve as good candidates for removing CO in automotive exhaust gases, due to their high susceptibility to poisoning by sulfur and water. Compared with noble metals, NTM oxides are much cheaper, in addition, they can be used to remove volatile organic compounds (VOC) in air.[220] As a result, significant attention has been paid recently towards CO oxidation over these materials.

Cobalt oxides, especially Co_3O_4, are well-known for their catalytic activities for CO oxidation. The catalytic activities of various cobalt oxides were studied by Lin *et al.*, and the activities was found to be in the order of: CoO ≈ Co_3O_4 ≫ CoO(OH) > CoO_x (valence of Co > + 3).[279] Chen and co-workers reported a much higher activity of Co_3O_4 than that of CoO.[220] The high activity of Co_3O_4 was attributed to the coexistence of Co(II) and Co(III) ion pairs. CO oxidation studies over CoO_x with different Co(III)/Co(II) ratios further show that a balance between Co(III) and Co(II) species is important to achieve a high activity, because of the Co(II) sites and the specific Co(III)–□–Co(II) sites for CO and O_2 adsorption, respectively.[280] Adsorption of CO on Co(II) was evidenced by infrared spectroscopy.[281] However, DFT calculations suggested that CO was preferably adsorbed on the superficial Co(III) cations.[252,255] Duprez and Royer suggest that CO could be preferably adsorbed on Co(III), while Co(III) tends to be reduced to Co(II) upon the adsorption of CO.[220] Co_3O_4 nanorods with enriched Co(III) on surfaces exhibited steady catalytic activity for CO oxidation at a temperature as low as 196 K.[249] The activation energy of CO oxidation on Co_3O_4 nanorods was similar to that of Co_3O_4 nanoparticles, but the preexponential factor of Co_3O_4 nanorods was about 14 times larger than that of Co_3O_4 nanoparticles, which was attributed to high density of exposed Co(III). Two types of oxygen atoms exist on the surface of Co_3O_4: the two-fold coordinated oxygen (O^{2f}) and three-fold coordinated oxygen (O^{3f}).[220] Theoretical analysis showed that surface O^{3f} bonded with three Co(III) is slightly more active than other types of lattice oxygen.[251] Based on characterizations of infrared spectroscopy, O_2 would dissociate on Co_3O_4 and bond linearly to spinel Co_3O_4, whereas O_2 could not dissociate over CoO_x containing mainly Co(III) or Co(IV), confirming the imc of Co(III)–□–Co(II) sites.[279] Surface oxygen species including O_2^-(ad), O^-(ad) and O^{2-}(latt) were detected by oxygen temperature programmed desorption (O_2-TPD).[220] The activity of Co_3O_4 is very sensitive to SO_2. A few ppm of SO_2 can completely deactivate the catalyst.[220]

In addition to Co oxides, Cu, Mn and Zn oxides were also tested in the catalytic oxidation of CO. Study of CO oxidation

over a well-defined Cu_2O film suggested that there was an oscillation between Cu(I) and Cu(II) during the reaction.[247] The existence of Cu(I) species is important for CO oxidation over Cu oxides. Cu(I) serves as the anchoring site of CO, oxidation of CO follows the M–v K mechanism.[220] The activity of different types of MnO_2, in the order of α- ≈ δ- > γ- > β-MnO_2, is inversely proportional with the Mn–O bond strength.[248] In the M–v K type catalytic cycle, Mn(IV) was reduced to Mn(III) by the adsorbed CO, followed by oxidation of Mn(III) to Mn(IV) by molecular oxygen. The low activities of γ- and β-MnO_2 were ascribed to the strong Mn–O bonds which hindered the oscillation between Mn(III) and Mn(IV). The activity of nano-sized zinc oxide (ZnO, 2.2 nm) supported on MgO was 18 times larger than the bulk ZnO on MgO, which was attributed to the quantum confinement effect.[282] It was proposed that CO adsorption on ZnO caused the formation of carbonate species, followed by either a thermo-decomposition or an oxidative depletion of the surface carbonates, yielding CO_2 as a product.

The catalytic performance of metal oxides can be tuned finely by chemically mixing two or more types of NTM oxides together. Recently, Wang and co-workers reported the fairly good activity and stability of an $Mn_xCo_{3-x}O_4$ solid solution for PROX of CO in an H_2-rich stream.[224] Both conversion and selectivity of CO remained constant during a 100 h testing period at 373 K, while pure Co_3O_4 deactivated rapidly under the same reaction conditions. The activities of $Mn_xCo_{3-x}O_4$ and pure Co_3O_4 were also studied by using a TPA reactor conjugated with a pulse reaction technique. After each pulse of CO, the catalysts were regenerated in a stream of O_2 for 30 min. At 313 and 373 K, $Mn_xCo_{3-x}O_4$ always exhibited higher CO conversion than Co_3O_4. Furthermore, $Mn_xCo_{3-x}O_4$ could be regenerated at 313 K, but Co_3O_4 could not. The superior catalytic activity of $Mn_xCo_{3-x}O_4$ was explained by the improved oxygen mobility and oxygen storage capacity caused by the incorporation of Mn in the framework of Co oxide, which was verified by O_2-TPD measurements. CuO–CeO_2 solid solution was prepared by a sol–gel method and tested in catalytic CO oxidation.[257] A redox equilibrium for a pair of neighbouring Cu and Ce ions were postulated:

$$\text{Ce(IV)–Cu(I)} \leftrightarrow \text{Ce(III)–Cu(II)} \quad (56)$$

The synergic effect of Cu and Ce facilitated the oxygen transfer, leading to an enhanced activity. Mixed metal oxides with perovskite structure (ABO_3, usually A and B being a lanthanide cation and an NTM cation, respectively) have been extensively studied as catalysts for CO oxidation.[220] The compositions of perovskite-type mixed oxides are very flexible, both A and B cations can be partially or totally substituted by other cations. Therefore, the redox and surface properties of perovskite oxides can be easily finely tuned. The reactivity was largely affected by the density of V_O on the surface of the perovskite oxide as well as the oxygen mobility.[256,258]

Both noble metals and NTM oxide have been used as the active components for the PROX of CO, as shown in Table 2. Generally, noble metal based catalysts exhibit higher activity (high conversion at low temperature) but lower selectivity compared to NTM oxide based catalysts. The selective oxidation of CO over Pt based catalysts derives from the preferential adsorption of CO on Pt surfaces, therefore, the activation and oxidation of H_2 is subdued.[261] Under PROX conditions, formation of adsorbed water on Pt based catalysts was found by *in situ* DRIFTS.[283] It is suggested that water–gas shift (WGS) reaction may also contribute to the selective oxidation of CO.[283] Different from Pt, Pd showed very poor catalytic performance for the CO PROX process (see Table 2), although Pd is active for CO oxidation without the presence of H_2.[284] This distinct property of Pd is explained by its high affinity to hydrogen, favouring the oxidation of H_2 rather than CO.[284] Under PROX conditions at low temperature (350–380 K), H_2 can dissolve in Pd leading to the formation of Pd β-hydride, which has been confirmed by *in situ* XPS.[284] Au is a good candidate for catalytic PROX of CO, probably due to its high activity for low temperature CO oxidation, as shown in Table 2. High activation energy for H_2 oxidation has been found on Au/CeO_2, compared to that of CO oxidation.[285] When Au/MgO/Al_2O_3 was used as a catalyst, conversion of H_2 at low temperature (<323 K) decreased from 20% to zero by adding CO into the reaction system.[286] This result implied that adsorbed CO may hinder the dissociation of H_2 over Au at low temperatures, whereas at temperatures above 323 K the thermal desorption rate of CO was large enough for H_2 oxidation to commence, leading to a decrease in selectivity of CO oxidation.[286]

One important advantage of NTM oxide based catalysts is their high selectivity for CO oxidation (up to 100%).[294,296] For CO PROX over CoO_x/CeO_2, the activation energy of H_2 oxidation was always higher than that of CO oxidation, regardless of the loading of Co.[264] Moreover, the NTM oxides are less sensitive to the concentration of CO. Under similar reaction conditions, the selectivity of CO oxidation over Pt/CeO_2 dropped from almost 100% to 20% when the CO concentration decreased from 1% to

Table 2 Summary of CO PROX over variety of catalysts

Catalysts	Temperature/K	O_2/CO ratio	Conversion (%)	Selectivity[a] (%)	Ref.
1 wt% Pt/CeO_2	383	0.4	35.0	85.0	287
1 wt% Pt/CeO_2	350	0.4	60.0	80.0	283
1 wt% Pd/CeO_2	350	0.4	10.0	10.0	284
0.5 wt% Pt–Co/$YZrO_x$	350	1.0	40.0	75.0	288
1 wt% Pt–SnO_2/Al_2O_3	383	1.5	100.0	50.0	289
1 wt% Pt–Sn/Al_2O_3	393	1.0	78.0	40.0	290
5 wt% Au/MgO/Al_2O_3	313	0.5	85.0	>90.0	286
1 wt% Au/Ti-SBA-15	323	4.3	100.0	90.0	291
1.3 wt% Au/TiO_2	298	1.0	100.0	80.0	292
2 wt% Au/$MnCeO_x$	350	1.0	86.0	61.0	293
CuO–ZnO/TiO_2	393	1.0	27.0	100.0	294
Co_3O_4/ZrO_2	448	1.0	60.0	90.0	295
CoO_x/CeO_2	448	1.0	94.0	71.0	264
Au–CuO_x/CeO_2	333	1.0	57.0	84.0	296
Au/CeO_2	333	1.0	88.0	47.0	296
CuO_x/CeO_2	333	1.0	11.0	100.0	296

[a] Selectivity to CO oxidation is calculated based on the O_2 consumption for CO oxidation divided by total O_2 consumption.

the ppm level, while CuO_x/CeO_2 maintained high CO selectivity (>85%) over a wide range of low CO pressures.[265] Supported bimetallic catalysts containing both Au and CuO_x were also used in the PROX of CO.[296] As shown in Table 2 (the last three rows), Au/CeO_2 is about 9 times more active than CuO/CeO_2 but it is much less selective, while $Au–CuO_x/CeO_2$ shows mixed behavior with moderate activity and good selectivity.

4.2.2 Promoters. As discussed above, partially oxidized Pt or Pd based catalysts are more active than their metallic counterparts, due to the formation of metastable oxides on the surface of metallic nanoparticles. Deposition of NTM oxide (FeO_x) on Pa t(111) surface could also lead to a significant increase in the activity for CO oxidation.[223] Different from surface oxides of noble metals that are directly reduced by CO, the improved catalytic performance was interpreted by the preferential adsorption and activation of O_2 at the cus Fe sites located at the peripheries of FeO_x nanoislands. Adsorption of CO on the cus Fe sites was not preferable, thus preventing the poisoning effect of CO. The FeO_x promoted mechanism was further supported by the good catalytic performance of supported Pt–Fe nanoparticles in PROX of CO. Deposition of a bilayer FeO thin film on Pt(111) was also reported.[222] At O_2-rich conditions, an O–Fe–O trilayer was formed because of the dissociation of O_2 on the FeO bilayer. It was proposed that the O–Fe–O trilayer could be reduced by CO(ad) on Pt, leaving V_O sites, which, in turn, were refilled by O_2. Supported Pt nanoparticles modified by FeO_x exhibited higher activity than standard Au/TiO_2 (from World Gold Council) at low temperatures (223–273 K).[297] At 273 K, a relatively high reaction order (0.9) with respect to O_2 was obtained, which implied that CO may compete with O_2 to adsorb at the same active sites (probably the interface between FeO_x and Pt). Enhanced activity for PROX of CO was obtained by doping Co on Pt based catalysts.[298] The Co oxide nanoislands on Pt nanoparticles remained as CoO rather than Co_3O_4 which is thermodynamically preferable in air. It was suggested that the metastable CoO structure was stabilized by the strong interaction between Co oxides and Pt. By using Co as a promoter, both the activity and selectivity of Pt/ZrO_2 were greatly improved for PROX CO oxidation process.[288] The promoted activity of $Pt–Co/ZrO_2$ was attributed to the interaction between Pt–Co bimetallic nanoparticles and the reducible support containing V_O. Compared to monometallic Pt catalysts, the supported ternary nanoalloy (Pt–Ni–Co) exhibited enhanced activity and stability for CO oxidation, in which Co promoted the activity, while Ni was responsible for the improvement in stability.[241] The promoting effects of Ni and Co were ascribed to the formation of Ni–Pt–Co sites which facilitated the adsorption and activation of CO and O_2. Addition of a small amount of sodium or potassium nitrate to nitrogen free Au/TiO_2 led to an increment of conversion from 70% to 90%.[299] By ruling out all other factors (*e.g.*, Au particle size, effect of cations), it was postulated that the promoting effect should originate from NO_3^-.

For CO PROX processes, both activity and selectivity of CO oxidation can be promoted by decorating noble metal based catalysts with metal oxides. By adding K to Pt/Al_2O_3, the conversion of CO increased from 20% to 100% and the selectivity of CO oxidation elevated from 10% to 50% (temperature range: 360–400 K).[300] For the Pt/YSZ (YSZ: yttria-stabilized zirconia) catalyzed CO PROX system, addition of Co to Pt/YSZ doubled conversion and selectivity at 423 K.[288] The promoting effect of Ge on Pt/SiO_2 for CO PROX was also reported, CO conversion and selectivity were enhanced by 2 times and 5 times, respectively.[301] The improved activities were related to the activation of O_2 by promoters.[300,302] As adsorption of O_2 on noble metals is suppressed by adsorbed CO, metal oxides attached on noble metal surfaces may benefit the adsorption and dissociation of O_2.[302] An alternative theory was proposed by Tanaka *et al.*[303,304] They suggest the existence of promoters, such as FeO_x and CoO_x, which change the CO oxidation path. The new CO oxidation path involves splitting of H_2O (from H_2 oxidation) over metal oxides and formation of an adsorbed $HCOO^-$ species as an intermediate. The promoting effect of metal oxides was attributed to the potentially low activation barrier of the new CO oxidation path.[304] However, they did not calculate the activation energy of CO oxidation over the modified catalyst and compare it with that of unmodified catalyst. It seems there are little mechanistic studies to illustrate the promoting effects of metal oxides on the selectivity of CO oxidation. A plausible explanation could be the enhanced adsorption of water on catalysts due to the addition of metal oxides, which will be discussed in Section 4.2.4.

4.2.3 Support materials. Like all heterogeneous catalysis, interactions between supports and active sites play a decisive role in determining the catalytic performance of the catalysts used in CO oxidation. By employing a carefully controlled co-precipitation method, isolated single Pt atoms were anchored on the surfaces of FeO_x nanocrystals.[305] These highly dispersed Pt atoms were positively charged and very stable in either an H_2 or O_2 atmosphere. It was postulated that there were strong electrostatic and covalent interactions between Pt atoms and the FeO_x support. Compared to supported Pt nanoclusters, a much higher activity was achieved on Pt/FeO_x with atomic dispersion for both CO oxidation and PROX of CO at 300 K. DFT calculations showed that the CO adsorption energy on these positively charged Pt atoms was much lower than that on metallic Pt clusters, which could minimize the poisoning of CO. Additionally, the presence of individual Pt atoms improved the reducibility of FeO_x, promoting the formation of V_O. The influence of intrinsic surface properties of silica (MCM-41) on the activity of Pt nanoparticles for PROX of CO was reported by Fukuoka *et al.*[306] Under the same reaction conditions, 100% conversion of CO was achieved on Pt nanoparticles supported on MCM-41 containing a high density of surface silanol groups (Si-OH), whereas, only 10% conversion was obtained when MCM-41 enriched with superficial siloxane groups (Si–O–Si) was used as a support. Based on intensive studies using an isotope labelling technique, it was proposed that silanol groups in vicinity of Pt nanoparticles may oxidize adsorbed CO on Pt, leaving vacant sites. Subsequently, the active silanol groups were regenerated by combining with oxygen and hydrogen atoms dissociated on Pt surfaces.

Because of the inert property of Au, selection of a proper support for an Au based catalyst is crucial to achieve a high activity for CO oxidation. It has been repeatedly proven that the

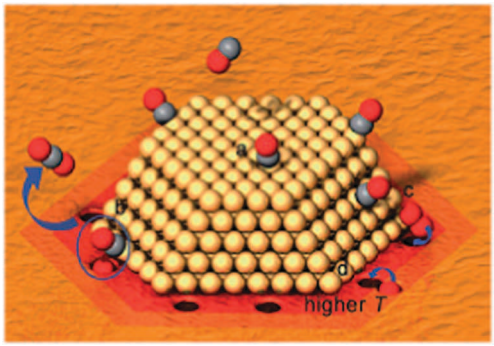

Fig. 28 Description of the pathway for CO oxidation on Au/TiO_2 at temperatures $\leq$353 K, involving (a) CO adsorption on Au nanoparticles; (b) CO reaction with O(s-t) at the perimeter of the Au–TiO_2 interface; (c) replenishment of O(s-t) by dissociative adsorption of O_2 at the perimeter sites; at higher temperatures above 353 K, (d) migration of surface lattice oxygen and to the perimeter sites of Au nanoparticle.[246] Reprinted from ref. 246, with the permission of the John Wiley and Sons.

interface between Au and TiO_2 plays a critical role in CO oxidation. At 300 K, CO oxidation can take place smoothly on Au nanoparticles supported by TiO_2(110) or TiO_2 decorated Au(111), whereas, both TiO_2(110) and Au(111) were inactive under the same conditions.[240] The oxygen storage capacity of Au/TiO_2 was measured by TAP technique.[246] The presence of Au nanoparticles is indispensable for the adsorption and activation of O_2, because pure TiO_2 showed zero oxygen storage capacity even at 673 K. It was proposed that the dissociation of O_2 and storage of active oxygen atoms may occur at the periphery of Au nanoparticles (as shown in Fig. 28). This activation of O_2 can be expressed as:

$$O_2 \rightarrow O_2(ad) \rightarrow 2O(s\text{-}t) \quad (57)$$

Au also played a role in activating adjacent surface O(latt), *i.e.*, O(s-t) of TiO_2 for CO oxidation. Based on the number of O(s-t) at the perimeter of Au nanoparticles, the coverage of stored oxygen at the boundary between Au and TiO_2 was estimated to be 0.89 at 353 K and 3.65 at 673 K. The high value (>1) of oxygen coverage at 673 K implied the migration of surface oxygen, which was driven by elevated temperature (see Fig. 28). The surface reconstruction of TiO_2(110) as a support was observed by STM during the CO oxidation over Au/TiO_2(110).[307] The interaction between Au nanoparticles and oxygen from the support (ceria) was also reported by Corma *et al.*[271] EXAFS spectra revealed that Au interacted with the surface oxygen of ceria in two ways: a covalent bonding of Au and oxygen; a weak nonbonding interaction. It was found that the activity of Au/CeO_2 was proportional to the amount of surface oxygen that weakly interacts with Au. The dynamic fluctuation of the Au nanoparticle morphology was observed directly using *in situ* environmental TEM in O_2-rich conditions when CeO_2 was used as a support,[236] while no morphological change was detected for Au nanoparticles supported by an inert supporting material—TiC. These observations suggested the CeO_2-assisted dissociation of O_2.

Au nanoclusters on an MgO(100) surface with high density of V_O showed catalytic activity for CO oxidation, whereas Au nanoclusters on defect-free MgO(100) were inactive.[229] These observations were explained by the partial electron transfer from V_O to Au, resulting in the back-donation of electrons from Au to CO(ad). The electron transfer from MgO(100) to Au was further verified by STM techniques.[308] Simulation results showed that the transferred charge was mainly localized at the kinks of Au nanoclusters. The preferential adsorption of CO at the fringe of Au clusters was directly observed by STM.

One of the advantages of using NTM oxides as catalysts for CO oxidation is the non-competitive adsorption between CO and O_2, whereas the poisoning effect of CO is well-known for noble metals. To reduce the CO poisoning effect, Ir was loaded on Fe$(OH)_x$, which was also active for CO oxidation.[220,309] *In situ* diffuse-reflectance infrared absorption spectroscopy (DRIFTS) measurements revealed that O_2 was mainly adsorbed on the surface of Fe$(OH)_x$, while Ir nanoparticles were covered by CO. Therefore, it was suggested that CO oxidation on Ir/Fe$(OH)_x$ followed the non-competitive L–H mechanism. It was also demonstrated that Fe$(OH)_x$ was an excellent support for all other Pt-group metals, such as Pt and Rh. NTM oxides could serve as oxygen reservoirs by providing lattice oxygen to noble metals. A perovskite oxide ($BaCeO_3$) was doped with Pd and used for CO oxidation.[310] Under high O_2 partial pressure, CO and O_2 competed for the same adsorption sites (most probably Pd(II)), showing the L–H mechanism; whereas, with the decrease of O_2 partial pressure, the apparent reaction order with respect to CO was increased from -1 to 0.41, implying a contribution of oxygen from $BaCeO_3$.

"Hot" electrons generated by CO oxidation could cause sintering of supported Au nanoparticles.[307] TiO_2 was modified by various metal oxides (Al_2O_3, CaO, ZnO, Pr_2O_3 *etc.*), which act as spacers, before the deposition of Au to minimize the growth of Au nanoparticles during CO oxidation.[311,312] Small Au clusters (*ca.* 3 nm) trapped inside silicate matrix also showed a high tolerance for sintering as well as high activity for CO oxidation.[313] Although silica is usually considered as an inert support, the activity of Au nanoparticles confined in silica is comparable to Au/TiO_2 and much higher than that of Au/Fe_2O_3.

Various types of materials have been utilized to support active metals for CO PROX, such as SiO_2,[301] Al_2O_3,[261] TiO_2[294] and CeO_2[283] *etc.* Among them, CeO_2 and doped CeO_2 have been frequently employed as the supports of both noble metals and NTM oxides for CO PROX.[283,294,295,314,315] The distinct redox properties of CeO_2 (Ce^{4+}/Ce^{3+}) allow transient oxygen storage and promote oxidation under oxygen-poor conditions.[283,315] Participation of oxygen from CeO_2 has been validated by oxygen-exchange measurements between $C^{16}O$ and ^{18}O-predosed Pt/CeO_2.[316] On the other hand, both adsorbed CO and H on Pt can migrate to CeO_2 *via* a "spillover" process, leading to reduction of Ce^{4+} to Ce^{3+}, *i.e.*, an oxygen vacancy.[283,287] Water, produced from the oxidation of hydrogen, can be stabilized on these oxygen vacancies, preventing further oxidation of hydrogen, and thus improving selectivity of CO oxidation.[287] The interface between noble metal and CeO_2 plays a very important role in CO PROX process. The interfacial Pt–O–Ce sites are responsible for the M–v K type redox pathway when CO coverage on Pt is high.[265] This assumption is supported by the fact that the density of active redox sites per interfacial length (the periphery of Pt nanoparticles) is

nearly constant for Pt/CeO_2 catalysts with different Pt dispersions.[265] Both linear and bridged adsorptions of CO on the Pt–Ce interface sites were detected by *in situ* DRIFTS under PROX conditions.[283] Linearly adsorbed CO contributes to the selectivity of CO oxidation *via* the low temperature water gas shift (LTWGS) reaction, whereas the bridged CO at the interface may dissociate, leading to the formation of methylidyne or hydrogenated graphitic species surrounding Pt nanoparticles, and thus the deactivation of catalysts. The redox properties of CeO_2 can be modified by doping other metals in its structure, for example Zr.[315] For Au/CeO_2, introduction of Zr^{4+} ions increases the reducibility of Ce and stabilizes Ce^{3+} species, resulting in a significant increasing in activity but a decrease in selectivity.[315] A similar improvement in activity was found on $Co_3O_4/CeZrO_x$, whereas selectivity was less affected by doping of Zr in CeO_2,[317] probably because of the high activation energy for H_2 oxidation over NTM oxides.[264] Coprecipitation of Cu and Ce led to the formation of CuO supported by $CeCuO_x$ in the form of a solid solution.[263] The strong interaction between CuO and CeO_2 facilitates the reducibility of Cu^{2+} under PROX conditions, promoting the formation of Cu^+–CO species evidenced by *in situ* DRIFTS. It is found that the specific CO oxidation rate increases with the intensity of this Cu^+–CO band.

4.2.4 Moisture effect. Catalytic CO oxidation is very sensitive to reaction parameters. Here, only the effects of moisture on catalytic performance are discussed. It has been found that the activities of Au based catalysts are improved in the presence of a trace amount of water moisture. By varying the water content from 0.1 to 6000 ppm, a general increase in activity of Au based catalysts was observed, regardless of the type of supports and the mean particle size of Au.[318] Acceleration of CO oxidation over $Au/TiO_2(110)$ was observed at 300 K and a low content of water ($<1.3 \times 10^{-4}$ bar).[240] It was proposed that O_2 might react with water at the periphery of Au nanoparticles, forming hydroperoxide species. The hydroperoxides can oxidize adsorbed CO on Au to produce CO_2. Based on theoretical calculations, dissociation of water on V_O of supports promotes the formation of hydroxyl groups, which can stabilize the adsorbed O_2.[229] The promoting effect of water was also found on support-free nanoporous Au.[275] It was confirmed that water was not consumed during CO oxidation, implying that water may act as a co-catalyst. However, high humidity deteriorates the activity of Au/TiO_2, because a significant amount of carbonates are formed on the surface of TiO_2 then migrate to the Au surface, which blocks the adsorption of CO on Au.[319]

Different from Au, the presence of water reduces the activity of NTM oxides. The light-off temperature T_{50} (temperature at 50% conversion) for CO oxidation over Co_3O_4 was increased from *ca.* 219 K to 323 K by introducing 3 ppm of water to an exclusively dry system.[320] At low temperature (303 K), the deactivation of Co_3O_4 nanosheets was ascribed to the accumulation of water on the catalyst.[321] The deactivation was mitigated by increasing the temperature to 373 K. Pretreatment of Co_3O_4 with steam led to a drastic increase of the reaction order of CO whereas the order of O_2 remained unchanged. This observation suggests that water may be preferentially adsorbed on Co(III), blocking the adsorption of CO.[322] The negative effect of water on CO PROX over NTM oxide based catalysts was also reported.[323]

The distinct effects of water on noble metals and NTM oxides catalyzed CO oxidation was investigated using first principles calculations.[324] For water adsorbed on metallic surfaces of noble metals, an alternative reaction channel rather than the classical reaction path ($CO(ad) + O(ad) \rightarrow CO_2$) was proposed:

$$H_2O + * \rightarrow H_2O(ad) \quad (58)$$

$$O(ad) + H_2O(ad) \rightarrow 2OH(ad) \quad (59)$$

$$CO(ad) + OH(ad) \rightarrow COOH(ad) + * \quad (60)$$

$$COOH(ad) + OH(ad) \rightarrow CO_2 + H_2O(ad) + * \quad (61)$$

The energy barriers for all reaction steps are much lower than that of combination of CO(ad) and O(ad), therefore the role played by $H_2O(ad)$ is similar to a molecular catalyst on the surface of a metallic catalyst. In contrast, the adsorption and dissociation of water on a metal oxide such as Co_3O_4 leads to the transformation of lattice O on the surface to hydroxyl groups. These surface hydroxyl groups are more inert for CO oxidation compared to the superficial lattice oxygen ($O_{s\text{-}t}$). Also, water can induce the formation of bicarbonate species (HCO_3^-) from CO_2 adsorption. It was expected that adsorption of these bicarbonates could result in serious deactivation due to their high stability. The dramatic difference between barriers for the reaction of CO(ad) and surface OH on metals or metal oxides is derived from the distinct potential energy surfaces of OH groups. Namely, OH groups on metallic surfaces are more flexible and active than those on the surface of metal oxides.

For CO PROX catalyzed by Pt-based catalysts, the presence of H_2 in the reaction mixture leads to an increase in catalytic activity in comparison to CO oxidation without H_2.[283,289,303] One reason could be the formation of oxygen vacancies on reducible supports, which are responsible for the activation of oxygen.[291] Another possible explanation that has been repeatedly proved is the formation of water from the oxidation of H_2.[283,289,291,303] Indeed, conversion and selectivity of CO increased when water vapour was directly added to the CO PROX system.[289,303] Studies on the Pt/CeO_2 catalyzed CO PROX suggested that water accumulated on the CeO_2 *via* oxidation of hydrogen spilled from Pt.[283] Pozdnyakova and co-workers proposed that the water adsorbed on CeO_2 could have three positive effects on the selective oxidation of CO.[283] Firstly, water molecules gathered on CeO_2 minimize the further oxidation of hydrogen migrating from Pt, while CO oxidation still occurs, because coverage of CO on Pt is high and oxygen transfer from CeO_2 to Pt may not be hindered by water; secondly, water locating at the periphery of Pt could promote the LTWGS reaction, leading to consumption of CO and producing CO_2 and H_2; thirdly, CO adsorbed at the interface between Pt and CeO_2 in a bridged manner could disproportionate, giving rise to formation of hydrogenated graphitic species and deactivating the catalysts. Adsorption of water on the unsaturated $Ce^{\delta+}$ sites could inhibit the formation of this type of adsorbed CO. The promoting effect of a low concentration of H_2O (<6000 ppm) on Au catalyzed CO oxidation

has been reported by Daté *et al.*[318] Adsorbed O_2 would react with adsorbed H_2O at the periphery of Au, leading to the formation of hydroxyl groups and active oxygen.[318] Enhanced CO oxidation was found on Au/ZrO_2 when hydrogen was introduced in the stream of CO and O_2, which was related to the formation of water.[325] However, addition of a high concentration of water may have little effect on the catalytic performance of Au based catalysts,[293] or even suppress the activity of Au, which was attributed to the adsorption of an excess amount of water on the catalytic active site.[326]

5. New methodology on catalyst design/optimization for selective oxidation

Once a catalytic system is established, it is necessary to optimize influential factors that determine the catalytic performance. Usually, the critical reaction parameters involve the content of active metal, the ratio of active metal to promoter, concentration of substrates, temperature, pressure and flow rate of oxygen *etc.* The common ''trial-and-error'' method is to adjust each factor in turn while keeping others constant in order to study how the response varies with respect to that particular factor. However, this approach ignores interactions between factors and typically results in a sub-optimal process performance.[327] The ''trial-and-error'' approach is unable to achieve a comprehensive understanding of the synergistic effects between factors. In addition, extensive data have to be collected as the number of factors increase, which can make the approach impractical. By using a proper design of experiments (DoE), a comprehensive understanding of the effect of individual factors and their interactions can be derived with a small number of experiments.

To optimize the production of formaldehyde from partial oxidation of methane over vanadium based catalysts, a statistical model was built using DoE approach with 32 experimental runs.[327] The application of statistical multivariate analysis, prediction through a multi-regression model and optimization of the processing parameters in the complex reaction process were demonstrated. The statistical modelling in this work showed good prediction ability in terms of conversion, selectivity and space time yield. The synergistic effects between reaction parameters were revealed. This statistical approach also enabled a comprehensive understanding of the whole production process over variation of all reaction parameters, which could facilitate the generation of new ideas for commercialization process.

Followed by the development of K promoted Mn/AC catalysts, Tang *et al.* built a statistical model to investigate the Mn catalyzed oxidation of benzyl alcohol using the Response Surface Design (RSD).[328] RSD is capable of identifying an optimal response within the factor range and predicting a response with a given factor setting. Five factors, such as temperature, oxygen pressure and K : Mn ratio, were assessed for the conversion and TOF of benzyl alcohol. It was found that, among the examined factors, temperature has the most significant impact on the activity of the catalyst (indicated by TOF). The synergistic effects between these five factors were also revealed, as the responses were influenced by the interaction variables. Based on 38 experimental results, a regression model, in the form of quadratic polynomial equations, was constructed. This model can accurately predict the conversion and TOF of benzyl alcohol oxidation. For the oxidation of benzyl alcohol over Pd supported by modified TUD-1, a similar modelling approach was employed to illustrate the correlation between the properties of a Pd based catalyst and its catalytic performance.[189] The experimental results indicated that surface basicity and Pd nanoparticle size were two vital factors controlling both the catalytic activity and selectivity. Furthermore, the surface basicity could also affect the particle size of Pd, *i.e.*, there was a clear interaction between these two factors. As such, it is unreasonable to isolate the effect of an individual factor, in this case, the statistical modelling provided a more rigorous interpreting methodology.

In our group, the model-oriented methodology was also applied for the development of efficient catalysts for CO oxidation.[329] The screening of metal-promoter/support combinations was facilitated by the application of Hammersley sequence sampling, a space-filling DoE method that has been shown to provide better coverage of design space than traditional DoE methods. By testing the statistically designed combinations of 4 noble metals (Au, Pt, Pd, Ru) as active sites, 4 metal oxides as promoters and 4 metal oxides as supports, it turned out that $Au–ZnO/Al_2O_3$ showed the best catalytic performance. To optimize the loadings of Au and ZnO, a Gaussian process regression model was developed from experimental data. By using this approach, a high-performance catalyst was identified as 4.9%Au–5.0%ZnO/Al_2O_3. Considering the high cost of Au, loading of Au was reduced with the aid of a Gaussian process regression model, which halved the Au content (2.3%), with marginal deterioration of activity (5% decrease in conversion of CO). Compared to other model-aided methods, such as quantitative property–activity relationships and artificial neural networks, one advantage of our approach was that large amounts of experimental data from high-throughput experimentation was not necessary, the overall development process was achieved within 21 experiments.

6. Concluding remarks

Heterogeneous catalytic oxidation processes are paramount important in the production of commodity chemicals, synthesis of fine compounds and environmental cleanup. Recent advances in three catalytic oxidation reactions are summarized and discussed in this review: selective oxidation of CH_4, selective oxidation of alcohols and oxidation of CO. Tremendous efforts have been devoted to the development of ''green'' pathways for these processes, such as the selective oxidation of CH_4 with O_2, aerobic selective oxidation of alcohol in water or under solvent-free conditions, preferential oxidation of CO in H_2-rich stream for fuel cells. Based on this survey, we would like to summarize important factors that determining the performance of each catalytic system, regarding the active site, active structure and advanced strategies for the design of efficient catalysts.

Moreover, by re-examining these three catalytic systems, deeper connections among them are also highlighted here.

The catalytic capability of a catalyst can be related directly to the nature of its active site. The activation of methane, in particular under mild conditions, is regarded as one of major challenges in contemporary catalysis, due to its thermodynamically strong and kinetically stable C–H bond. Nevertheless, the strong C–H bond of methane can be broken down by the electrophilic attack of Pt(II) or Pd(II) under super-acidic solution, giving rise to H^+ and methyl anion coordination with Pt(II).[330] Supported Au–Pd alloy was applied in oxidation of methane to methanol with H_2O_2 as oxidant.[59] However, the role of Au–Pd is to generate active oxygen species which is directly responsible for the cleavage of the C–H bond. The presence of active oxygen species on the surface of heterogeneous catalysts could be indispensable for the oxidative activation of methane. Typical examples are Fe-ZSM-5 or $FePO_4$ with N_2O or H_2–O_2 and Cu-ZSM-5 with O_2, in which hydrogen of CH_4 was abstracted by Fe(III)–$O^{\bullet-}$ and Cu(II)–$O^{\bullet-}$–Cu(II) species, respectively.[32,33] Selective oxidation of alcohols also involves the activation of the C–H bond, although they contain the OH functional group. Pd is probably the best candidate for the oxidation of alcohols by O_2, compared to other noble metals, with regard to its high activity and selectivity.[187] Formation of surface noble metal oxides hampers the activities of noble metals for alcohol oxidation. Initial reaction rates increased after the pre-reduction of air-stored Pt based catalysts,[162] probably because Pt oxide hinders the cleavage of O–H bonds of alcohols, which involves insertion of metallic atoms. NTM oxides, such as MnO_x[200] and V_2O_5,[204] could serve as an economic choice, in respect to their high selectivity to aldehydes, although their activities are usually 1000 times lower than those of noble metals. Preferential oxidation of CO has been achieved on Pt based catalysts, due to the preferential adsorption of CO on the Pt surface, which largely inhibits the oxidation of H_2.[287] Accordingly, poor selectivity is observed when the CO concentration decreases to ppm level, because the competitive adsorption and oxidation of H_2 becomes dominant.[283] Pd is very active for CO oxidation but it is a poor catalyst for CO PROX, due to its strong affinity to hydrogen, leading to the formation of Pd–H hydride.[284] Interestingly, this phenomenon provides a good proof for the high activity of Pd for alcohol oxidation, in which abstraction of H from alcohols and formation of Pd–H hydrides are very important for the activation of alcohols. Different to alcohol oxidation, partially oxidized Pt and Pd are much more active than their metallic form during CO oxidation, as oxygens of the superficial noble metal oxides can be readily reduced by adsorbed CO.[233] Small Au nanoparticles show excellent low temperature activity for CO oxidation, and Au-based catalysts have been applied to CO PROX.[286] High selectivity (up to 100%) can be obtained on NTM oxides, which is explained by the lower activation barrier of CO oxidation compared to that of H_2 oxidation.[264] A concentration of CO (ranging from several ppms to several percentages) barely affects the high selectivity of NTM oxides.[283] However, a relatively high temperature (>400 K) is required for the NTM oxide-catalyzed CO PROX.

The nature of an active site determines how it interacts with reactants, which, in turn, plays a critical role in all types of catalytic systems. For the oxidation of methane, partially reduced Fe or Cu (Fe(II) or Cu(I)) favors the reductive activation of O_2, forming radical-like oxygen species, which are active enough to break C–H bond.[32,33] The catalytic behavior of noble metals for both CO and alcohol oxidation supports the principle of adsorbate–surface interaction proposed by Nørskov *et al.*[331] Based on this theory, the bonding energy of reactants on the surface of catalysts cannot be too weak or too strong, to achieve a reasonable catalytic activity. Take the activation of O_2 as an example. If the metal–oxygen (M–O) bond is too weak, O_2 can hardly dissociate on the surface of metallic catalysts, whereas, if the M–O bond is too strong, surface oxygen species could be not active enough to oxidize the substrates. As discussed in Section 4.2.1, the heat of O_2 dissociative chemisorption on different noble metals follows an order of: Ru $>$ Rh $>$ Pt $>$ Pd $\gg$ Au. Accordingly, Pt and Pd are efficient metal catalysts for both CO and alcohol oxidations, while Ru and Au exhibit relatively poor catalytic capabilities. When NTM oxides are used as catalysts, both alcohols and O_2 dissociate over V_O sites, implying a competitive adsorption of reactants.[182] In contrast, CO is preferentially adsorbed on metal cations, while V_O sites are responsible for the adsorption and activation of O_2.[251]

Besides the intrinsic properties of active sites, the catalytic performance of a catalyst could also change with the arrangement of active components at atomic level, namely the active structure of an active site. Isolated NTM oxide sites are important for the selective oxidation of methane, because larger oxide clusters catalyze the complete oxidation of CH_4 to CO_2.[92,106–109] For the oxidation of alcohols, the best activity was obtained on noble metal nanoparticles with a balanced number of atoms locating at terraces, edges or corners,[190] whereas, noble metal nanoparticles containing a high density of cus atoms are preferred for CO oxidation.[230] This difference may originate from the additional interactions between functional groups of the alcohol (*e.g.*, phenyl and C=C) and noble metal nanoparticles. For NTM oxide-based catalytic systems, the pivotal role of coupled bi-valent metal cations has been evidenced in all these three catalytic oxidation systems. Fe(III)/Fe(II) and Cu(II)/Cu(I) redox pairs have been found to play key roles during the activation of oxidant for the selective oxidation of CH_4 over Fe-ZSM-5, $FePO_4$, Cu-ZSM-5 and CuO_x/SBA-15.[67,69,85,108] The high activities of MnO_x for alcohol oxidation and $CuCeO_x$ for CO oxidation are attributed to the existence of Mn(II)/Mn(III)[213] and Ce(III)/Cu(II),[257] respectively. These bi-valent metal cations can facilitate the oxygen transfer during oxidation reactions. The importance of oxygen mobility inside NTM oxides is further confirmed by studying the activity of MnO_2 with different crystal structures. α-MnO_2 always outperforms β-MnO_2 for oxidation of both benzyl alcohol and CO,[201,248] which can be explained by the weaker Mn–O bond of α-MnO_2 than that of β-MnO_2. Based on the analysis using a TPA reactor, the bulk lattice oxygen of NTM oxides could also participate in the oxidation of CH_4,[29] therefore oxygen mobility may also affect this catalytic reaction.

Active sites with unique structures are found at the interface between noble metals and metal oxides. The influences of these interfacial sites could be decisive. The high activities of Au/CeO_2 for both alcohol and CO oxidation have been correlated with the existence of positively charged Au as a result of the interaction of Au and the oxygen of CeO_2.[215,271] Deposition of FeO_x on the surface of supported Pt nanoparticles promotes the activation of O_2 at the periphery of FeO_x nanoislands, leading to high activities for oxidation of benzyl alcohol[209] and CO.[223] The PROX of CO achieved on Pt/CeO_2 under high concentration of CO (>1%) has been ascribed to the CO oxidation at the interfacial Pt–O–Ce sites following the M–v K type reaction.[265]

Based on mechanistic understanding, interesting strategies for design of efficient catalytic systems has been developed. Regarding the distinct features of noble metals and NTM metal oxides, an intuitively practical approach to develop new catalysts is the combination of noble metals and NTM oxides with specific functions. Successful cases can be found in all three catalytic systems. Methyl acetate was directly synthesized from the gas mixture of CH_4, CO and N_2O by using Rh doped iron phosphate as a catalyst.[126] In this reaction, Rh(I) favors the adsorption of CO, while Fe(II) is responsible for the activation of CH_4. Either alcohols or CO compete with O_2 to adsorb on the surfaces of noble metals. This competitive adsorption can be mitigated by coupling noble metals with redox NTM oxides, in which substrates adsorb on noble metals, while O_2 adsorption and dissociation take place on the surfaces of NTM oxides. Practical examples include the alcohol oxidation over $Pd/Mn_xCe_yO_z$[188] and CO oxidation over Au/TiO_2[246] and $Ir/Fe(OH)_x$.[309] As the lattice oxygen of NTM oxides could participate in the oxidation reactions, NTM oxides also act as an oxygen reservoir by providing active oxygen species to react with substrates on noble metals.[187,310]

In addition to direct modification of catalysts, catalytic results can also be significantly improved by modification of other factors of a catalytic system, such as the oxidant. As shown in Section 2.2.1, in Pt complex-catalyzed oxidation of CH_4, H_2SO_4 is reduced by CH_4 to produce SO_2, which is oxidized back to H_2SO_4 by O_2. Here, H_2SO_4 acts as a redox shuttle. A similar strategy has been applied to the CH_4 oxidation with S_2, as shown in Section 2.3. In this case, the low oxidation property of S_2 minimizes the excess oxidation of CH_4. Instead of gas phase CO PROX with O_2 as the oxidant, Kim *et al.* demonstrated liquid phase PROX CO process by using a polyoxometalate (POM) compound (*e.g.*, $H_3PMo_{12}O_{40}$) as an oxidant.[332] The reduced POM by CO can be regenerated by passing electrons to a carbon anode. The special oxidation capability of POM enables 100% selective oxidation of CO in H_2-rich stream. Another effective method to achieve high activity and selectivity is the addition of additives or intermediate reactants. Indirect oxidation of CH_4 by introducing halogens could serve as a good example. Bases are frequently used as additives for the Au-catalyzed oxidation of alcohols, to assist the extraction of H from alcohols.[195] Water vapor has been introduced in the CO PROX to promote both activity and selectivity of CO oxidation. The promoting effect of water is interpreted by its interaction with active sites or WGS reaction.[284]

It has been demonstrated that statistic methodology can serve as a powerful tool to achieve the rational design of a given catalytic system with low cost and high time efficiency. Examples can be found in all three types of oxidation reactions reviewed in this context. In all cases, optimized parameters can be obtained with limited number of experiments. Additionally, statistic modelling allows a comprehensive understanding of the effect of individual factor and their interactions. These futures could be valuable for development of catalytic processes in real industry.

In spite of the significant progress in these three catalytic oxidation systems, there are still some challenges that need to be overcome. It is not easy to break the C–H bond of methane, and it is even more difficult to control the selectivity of methane oxidation, mainly because of the formation of active radical species during the reaction. These radicals could be present in the gas phase and on the surfaces of catalysts. The surface radicals benefit the selectivity of methane oxidation. Nevertheless, very decent selectivity to methanol (>90%) has been achieved in super-acid solution with Pt complex as a catalyst. The high selective can be attributed to the formation of $Pt–CH_3$ species as intermediates which stabilized the active methyl anion. Therefore, to stabilize active CH_3 species on a solid surface could be a possible solution to improve the selectivity of methane oxidation. A straightforward idea is immobilization of an active Pt complex on a solid support. Alternatively, positively charged noble metal cations stabilized by intimately contacted redox NTM oxide may also be suitable for the selective oxidation of methane. For example, positively charged Au has been found on Au/CeO_2 and applied to oxidation of alcohols and CO.[215,271]

Compared to the extensive understanding of the catalytic CO oxidation process, the mechanistic studies on catalytic oxidation of alcohols in three phases remain at the primary stage. Benchmarked with the details of the CO oxidation process, one may raise several questions about the catalytic cycle of alcohol oxidation: (a) Do solvents compete with alcohols, O_2 and hydride to adsorb on the same active sites on either noble metal or NTM oxide? (b) Does oscillation of reaction rates occur during the oxidation of alcohols? (c) What is the active surface oxygen species (*e.g.*, O_2^-, O_2^{2-} or O^-) for the NTM oxides to catalyze alcohol oxidation? The mechanistic details become more complex, when mixed-oxides or metal-oxides supported noble metals are used as catalysts. Advanced experimental techniques and extensive kinetic studies may give the answers to these questions.

Conventionally, addition of bases (*e.g.*, K_2CO_3) is indispensable for Au-catalyzed alcohol oxidation, it is believed that the base assists Au to abstract hydrogen from alcohol. However, under a relatively high temperature (433 K) and a high pressure of O_2 (10 bar), TOF of 4800 h^{-1} has been reported for the oxidation of benzyl alcohol over Au/TiO_2.[196] Therefore, it could be necessary to revisit the mechanism of Au-catalyzed alcohol oxidation.

Pt has a higher oxidizing ability than Pd. However, just because of the high oxidizing capability of Pt, it can be easily over oxidized by O_2 and may promote the further oxidation of aldehydes to carboxylic acids. It would be interesting to

fine-tune the catalytic property of Pt, using modifiers or additives. Recent work on the oxidation of benzyl alcohol over Fe modified Pt/CNT may provide some clues, such as the effect of Pt–Fe alloys and FeO_x nanoislands on the surface of Pt.[209]

Catalytic oxidation of primary aliphatic alcohols to aldehydes remains a big challenge, due to the low stability of primary aldehydes which can be readily oxidized to carboxylic acids. Ru based catalysts showed good selectivity towards aldehydes, but their activities were low.[173] A similar problem was also observed on $Pd/MnO_x/CNT$[187] and the mixed oxides – $Mo_xV_yO_z$.[205] More extensive studies should be carried out to address this issue.

The high activity of Au nanoparticles under low temperatures has long since been discovered, nevertheless, the debate on the active sites of Au-based catalysts continues. Although it has been generally accepted that the size of active Au nanoparticles should be less than 5 nm, CO oxidation over nanoporous Au (ligament size 30–40 nm, doped with Ag) and "big" Au particles (10 nm) enclosed by a TiO_2 shell suggest that active sites may be located on the corner and edges of Au surfaces or the interface between Au and a foreign component.[333] According to a recent review by Bond, the activity of Au based catalysts may be mainly contributed by small Au nanoclusters (<2.5 nm) that can hardly be detected and only account for small portion of all the Au nanoparticles.[268] In this case, true active sites may only site on the surfaces of very small Au nanoparticles. Conventionally, it is believed that O_2 cannot dissociate on Au, as theoretical calculation and experimental measurements indicate that dissociation heat of O_2 on Au is negative.[220] Nevertheless, under 1 bar of O_2, the dynamic fluctuation of facets of Au nanoparticles was directly observed by *in situ* environmental TEM at room temperature.[236] As such, the interaction between O_2 and Au becomes controversial. Advanced characterization methods (such as *in situ* TEM, *in situ* XPS and *in situ* XAS) coupled with theoretical calculations could be helpful to solve this puzzle.

In addition to the detailed mechanistic study and sophisticated catalyst design, desired catalytic results can be achieved by an elaborate reactor design. Chemical looping technology may serve as a potential candidate for all of these three catalytic oxidation reactions discussed above. As shown in Fig. 29, the chemical looping process splits the M–v K type catalytic oxidation into a pair of reactors: oxidizer and reducer. In the reducer, the oxidized oxygen carriers or catalysts (MO) in form of solid particles transfer oxygen to the feedstock, giving rise to the oxidized products and reduced counterparts (M) of oxygen carriers. Subsequently, MO is regenerated in the oxidizer by oxidization of M with oxidants. Chemical looping technology has been applied to combustion and gasification of fossil fuels[334] and recently the direct transformation of methane to syngas.[335] The unique design of the chemical looping process avoids direct contact of the oxidant and feedstock, which affords several advantages of this technology. For example, when air is employed for the combustion of fossil fuel, MO supplies the stoichiometric oxygen needed for CO_2 and water formation, leading to a N_2 free mixture. As a result, the energy requirement of CO_2 separation from N_2, a major cost for CO_2

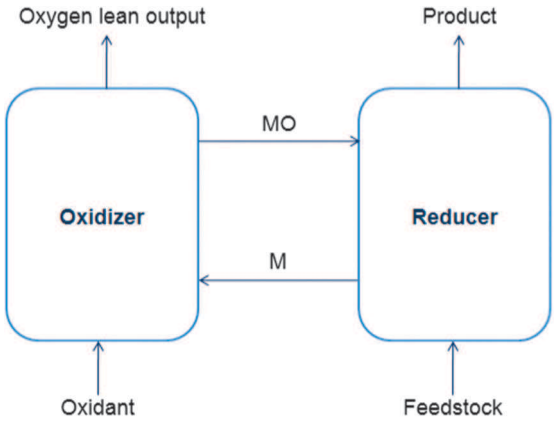

Fig. 29 Scheme of chemical looping process. MO: oxidized catalysts; M: reduced catalysts; MO is reduced in the reactor denoted as reducer, leading to formation of M which is oxidized in the oxidizer. Feedstock could be CH_4, alcohols or CO in an H_2-rich stream.

capture, is circumvented. In fact, the concept of chemical looping technology has been successfully applied in methane oxidation[90] and CO PROX,[332] although the authors did not highlight this point. In the first case, O_2 and CH_4 were purged sequentially through Cu-mordenite. Prior to the next oxidation cycle a H_2O/He stream was introduced to liberate the adsorbed methanol (or methoxy species). For the second case, POM was employed as the oxygen carrier and an electrode served as the oxidizer. On the basis of these works, the high flexibility of chemical looping may enable its more extensive application in catalytic oxidation systems. Some possible points include: (1) production of methanol with 98% selectivity has been achieved by passing methane through preoxidized Cu–zeolite,[82] but methanol can only be obtained by solvent extraction or hydration.[82,90] Application of chemical looping in this "semi-catalytic" system may open the possibility of operation in a real catalytic cycle. (2) Stoichiometric oxidation of substrates (methane or alcohols) with MO may prevent the further oxidation of desired products (oxygenates to CO_x, aldehydes to carboxylic compounds); (3) in a conventional reactor, it is difficult to control the oxidation status of metal oxides in the presence of other compounds, such as methane, CO_x and HCHO. Nonetheless, it is possible to fine-tune the oxidation status of MO by carefully controlling the oxidation parameters in the oxidizer, in order to enhance selectivity. As shown in Fig. 9, the lattice oxygen of CuO_x oxidizes CH_4 to CO_x, while the unique Cu^{m+}–O* species contributes to the selective oxidation of methane to HCHO. (4) For aerobic oxidation of alcohols, one drawback of NTM oxides is its significantly lower activity compared to noble metals. In a chemical looping process, NTM oxides can be efficiently oxidized in the oxidizer, which may lead to an increase in catalytic performance. The adjustable ratio of oxidant/NTM oxides may also help to saving the consumption of oxidant. (5) In the NTM-oxides-catalyzed CO PROX systems, low temperatures are required to obtain high selectivity, due to the accelerated H_2 oxidation at high temperatures. However, low temperatures result in a low oxygen transfer rate from O_2 to NTM oxides. This problem can be overcome by

decoupling the different desired temperatures for oxidation and reduction in a chemical looping reactor, as oxidation of NTM oxides can be performed in the oxidizer at high temperature, while oxidation of CO is conducted in the reducer at low temperature. Moreover, air can be used as the oxidant without concerning the dilution of the H_2-rich stream by N_2.

Acknowledgements

Q. Z. and Y. W. gratefully acknowledge financial support from the National Basic Research Program of China (No. 2010CB732303 and CB2013CB933102), the National Natural Science Foundation of China (No. 21373170 and 21033006), and the Program for Innovation Research Team in Chinese Universities (No. IRT1036).

Notes and references

1 A. M. Thayer, *Chem. Eng. News*, 1992, **70**(10), 27–49.
2 P. Mars and D. W. van Krevelen, *Chem. Eng. Sci.*, 1954, **3**, 41–59.
3 J. Haber and W. Turek, *J. Catal.*, 2000, **190**, 320–326.
4 R. K. Grasselli, *Catal. Today*, 1999, **49**, 141–153.
5 R. K. Grasselli, *Top. Catal.*, 2002, **21**, 79–88.
6 R. Schlögl, A. Knop-Gericke, M. Hävecker, U. Wild, D. Frickel, T. Ressler, R. E. Jentoft, J. Wienold, G. Mestl, A. Blume, O. Timpe and Y. Uchida, *Top. Catal.*, 2001, **15**, 219–228.
7 Y. Moro-oka and W. Ueda, *Adv. Catal.*, 1994, **40**, 233–273.
8 P. T. Anastas and J. C. Warner, *Oxford University Press*, Oxford, 1998, p. 30.
9 P. T. Anastas and M. M. Kirchhoff, *Acc. Chem. Res.*, 2002, **35**, 686–694.
10 T. Mallat and A. Baiker, *Chem. Rev.*, 2004, **104**, 3037–3058.
11 K. Kaneda, K. Ebitani, T. Mizugaki and K. Mori, *Bull. Chem. Soc. Jpn.*, 2006, **79**, 981–1016.
12 T. Matsumoto, M. Ueno, N. Wang and S. Kobayashi, *Chem.–Asian J.*, 2008, **3**, 196–214.
13 B. Z. Zhan and A. Thompson, *Tetrahedron*, 2004, **60**, 2917–2935.
14 P. Weiland, *Appl. Microbiol. Biotechnol.*, 2009, **85**, 849–860.
15 H. Schwarz, *Angew. Chem., Int. Ed.*, 2011, **50**, 10096–10115.
16 C. Hammond, S. Conrad and I. Hermans, *ChemSusChem*, 2012, **5**, 1668–1686.
17 V. N. Cavaliere and D. J. Mindiola, *Chem. Sci.*, 2012, **3**, 3356–3365.
18 E. McFarland, *Science*, 2012, **338**, 340–342.
19 B. A. Arndtsen, R. G. Bergman, T. A. Mobley and T. H. Peterson, *Acc. Chem. Res.*, 1995, **28**, 154–162.
20 J. Sauer, M. Bewersdorf, M. Köstner, M. Rinner and D. Wolf, *Handbook of Heterogeneous Catalysis*, Wiley-VCH, Weinheim, 2nd edn, 2008, vol. 5, pp. 2592–2609.
21 M. Y. Sinev, *J. Catal.*, 2003, **216**, 468–476.
22 J. Haber, *J. Catal.*, 2003, **216**, 416–424.
23 A. N. Vedernikov, *Acc. Chem. Res.*, 2012, **45**, 803–813.
24 V. R. Choudhary and V. H. Rane, *J. Catal.*, 1991, **130**, 411–422.
25 R. Burch and M. J. Hayes, *J. Mol. Catal. A: Chem.*, 1995, **100**, 13–33.
26 S. G. Podkolzin, E. E. Stangland, M. E. Jones, E. Peringer and J. A. Lercher, *J. Am. Chem. Soc.*, 2007, **129**, 2569–2576.
27 T. Ito, T. Tashiro, M. Kawasaki, T. Watanabe, K. Toi and H. Kobayashi, *J. Phys. Chem.*, 1991, **95**, 4476–4483.
28 P. F. Nelson, C. A. Lukey and N. W. Cant, *J. Phys. Chem.*, 1988, **92**, 6176–6179.
29 J. H. Lunsford, *Angew. Chem., Int. Ed. Engl.*, 1995, **34**, 970–980.
30 D. J. Driscoll, W. Martir, J. X. Wang and J. H. Lunsford, *J. Am. Chem. Soc.*, 1985, **107**, 58–63.
31 L. Luo, X. Tang, W. Wang, Y. Wang, S. Sun, F. Qi and W. Huang, *Sci. Rep.*, 2013, **3**(1625), 1–7.
32 N. Dietl, M. Schlangen and H. Schwarz, *Angew. Chem., Int. Ed.*, 2012, **51**, 5544–5555.
33 P. Vanelderen, R. G. Hadt, P. J. Smeets, E. I. Solomon, R. A. Schoonheydt and B. F. Sels, *J. Catal.*, 2011, **284**, 157–164.
34 O. V. Buyevskaya, M. Rothaemel, H. W. Zanthoff and M. Baerns, *J. Catal.*, 1994, **146**, 346–357.
35 N. W. Cant, C. A. Lukey, P. F. Nelson and R. J. Tyler, *J. Chem. Soc., Chem. Commun.*, 1988, 766–768.
36 M. Y. Sinev, Z. T. Fattakhova, V. I. Lomonosov and Y. A. Gordienko, *J. Nat. Gas Chem.*, 2009, **18**, 273–287.
37 S. T. Oyama, A. N. Desikan and J. W. Hightower, *Catalytic Selective Oxidation*, American Chemical Society, NW, Washington DC, 1993.
38 F. Arena, N. Giordano and A. Parmaliana, *J. Catal.*, 1997, **167**, 66–76.
39 W. Weng, M. Chen, H. Wan and Y. Liao, *Catal. Lett.*, 1998, **53**, 43–50.
40 M. R. Smith, L. Zhang, S. A. Driscoll and U. S. Ozkan, *Catal. Lett.*, 1993, **19**, 1–15.
41 A. Parmaliana and F. Arena, *J. Catal.*, 1997, **167**, 57–65.
42 R. H. Crabtree, *Chem. Rev.*, 1995, **95**, 987–1007.
43 A. E. Shilov and G. B. Shul'pin, *Chem. Rev.*, 1997, **97**, 2879–2932.
44 J. A. Labinger and J. E. Bercaw, *Nature*, 2002, **417**, 507–514.
45 R. Bergman, *Nature*, 2007, **446**, 391–393.
46 A. Caballero, E. Despagnet-Ayoub, M. M. Díaz-Requejo, A. D. Díaz-Rodríguez, M. E. González-Núñez, R. Mello, B. K. Muñoz, W. S. Ojo, G. Asensio, M. Etienne and P. J. Pérez, *Science*, 2011, **332**, 835–838.
47 A. S. Borovik, *Chem. Soc. Rev.*, 2011, **40**, 1870–1874.
48 J. R. Webb, T. Bolaño and T. B. Gunnoe, *ChemSusChem*, 2011, **4**, 37–49.
49 R. A. Periana, O. Mironov, D. Taube, G. Bhalla and C. J. Jones, *Science*, 2003, **301**, 814–818.
50 M. Ahlquist, R. J. Nielsen, R. A. Periana and W. A. Goddard III, *J. Am. Chem. Soc.*, 2009, **131**, 17110–17115.
51 R. Palkovits, M. Antonietti, P. Kuhn, A. Thomas and F. Schüth, *Angew. Chem., Int. Ed.*, 2009, **48**, 6909–6912.
52 R. Palkovits, C. von Malotki, M. Baumgarten, K. Müllen, C. Baltes, M. Antonietti, P. Kuhn, J. Weber, A. Thomas and F. Schüth, *ChemSusChem*, 2010, **3**, 277–282.
53 Q. Yuan, W. Deng, Q. Zhang and Y. Wang, *Adv. Synth. Catal.*, 2007, **349**, 1199–1209.

54 G. V. Nizova, G. Süss-Fink and G. B. Shul'pin, *Chem. Commun.*, 1997, 397–398.
55 G. B. Shul'pin, G. V. Nizova, Y. N. Kozlov, L. G. Cuervo and G. Süss-Fink, *Adv. Synth. Catal.*, 2004, **346**, 317–332.
56 C. Hammond, M. M. Forde, M. H. A. Rahim, A. Thetford, Q. He, R. L. Jenkins, N. Dimitratos, J. A. Lopez-Sanchez, N. F. Dummer, D. M. Murphy, A. F. Carley, S. H. Taylor, D. J. Willock, E. E. Stangland, J. Kang, H. Hagen, C. J. Kiely and G. J. Hutchings, *Angew. Chem., Int. Ed.*, 2012, **51**, 5129–5133.
57 C. Hammond, R. L. Jenkins, N. Dimitratos, J. A. Lopez-Sanchez, M. H. A. Rahim, M. M. Forde, A. Thetford, D. M. Murphy, H. Hagen, E. E. Stangland, M. Moulijn, J. S. H. Taylor, D. J. Willock and G. J. Hutchings, *Chem.–Eur. J.*, 2012, **18**, 15735–15745.
58 C. Hammond, N. Dimitratos, R. L. Jenkins, J. A. Lopez-Sanchez, S. A. Kondrat, M. H. A. Rahim, M. M. Forde, A. Thetford, S. H. Taylor, H. Hagen, E. E. Stangland, J. H. Kang, J. M. Moulijn, D. J. Willock and G. J. Hutchings, *ACS Catal.*, 2013, **3**, 689–699.
59 M. H. A. Rahim, M. M. Forde, R. L. Jenkins, C. Hammond, Q. He, N. Dimitratos, J. A. Lopez-Sanchez, A. F. Carley, S. H. Taylor, D. J. Willock, D. M. Murphy, C. J. Kiely and G. J. Hutchings, *Angew. Chem., Int. Ed.*, 2013, **52**, 1280–1284.
60 J. K. Edwards and G. J. Hutchings, *Angew. Chem., Int. Ed.*, 2008, **47**, 9192–9198.
61 I. G. Denisov, T. M. Makris, S. G. Sligar and I. Schlichting, *Chem. Rev.*, 2005, **105**, 2253–2277.
62 G. I. Panov, *CATTECH*, 2000, **4**, 18–31.
63 V. I. Sobolev, K. A. Dubkov, O. V. Panna and G. I. Panov, *Catal. Today*, 1995, **24**, 251–252.
64 G. I. Panov, K. A. Dubkov and E. V. Starokon, *Catal. Today*, 2006, **117**, 148–155.
65 B. R. Wood, J. A. Reimer, A. T. Bell, M. T. Janicke and K. C. Ott, *J. Catal.*, 2004, **225**, 300–306.
66 E. V. Starokon, M. V. Parfenov, L. V. Pirutko, S. I. Abornev and G. I. Panov, *J. Phys. Chem. A*, 2011, **115**, 2155–2161.
67 E. V. Starokon, M. V. Parfenov, S. S. Arzumanov, L. V. Pirutko, A. C. Stepanov and G. I. Panov, *J. Catal.*, 2013, **300**, 47–54.
68 Y. Wang and K. Otsuka, *J. Chem. Soc., Faraday Trans.*, 1995, **91**, 3953–3961.
69 X. Wang, Y. Wang, Q. Tang, Q. Guo, Q. Zhang and H. Wan, *J. Catal.*, 2003, **217**, 457–467.
70 Y. Wang, W. Yang, L. Yang, X. Wang and Q. Zhang, *Catal. Today*, 2006, **117**, 156–162.
71 J. R. Anderson and P. Tsai, *J. Chem. Soc., Chem. Commun.*, 1987, 1435–1436.
72 J. L. Que and W. R. Toman, *Angew. Chem., Int. Ed.*, 2002, **41**, 1114–1137.
73 S. Friedle, E. Reisner and S. J. Lippard, *Chem. Soc. Rev.*, 2010, **39**, 2768–2779.
74 A. S. Hakemian and A. C. Rosenzweig, *Annu. Rev. Biochem.*, 2007, **76**, 223–241.
75 R. Balasubramanian and A. C. Rosenzweig, *Acc. Chem. Res.*, 2007, **40**, 573–580.
76 S. I. Chan and S. S. F. Yu, *Acc. Chem. Res.*, 2008, **41**, 969–979.
77 R. A. Himes and K. D. Karlin, *Curr. Opin. Chem. Biol.*, 2009, **13**, 119–131.
78 K. Yoshizawa and Y. Shiota, *J. Am. Chem. Soc.*, 2006, **128**, 9873–9881.
79 S. I. Chan, V. C. C. Wang, J. C. H. Lai, S. S. F. Yu, P. P. Y. Chen, K. H. C. Chen, C. L. Chen and M. K. Chan, *Angew. Chem., Int. Ed.*, 2007, **46**, 1992–1994.
80 P. P. Y. Chen, R. B. G. Yang, J. C. M. Lee and S. I. Chan, *Proc. Natl. Acad. Sci. U. S. A.*, 2007, **104**, 14570–14575.
81 S. I. Chan, Y. J. Lu, P. Nagababu, S. Maji, M. C. Huang, M. M. Lee, I. J. Hsu, P. D. Minh, J. C. H. Lai, K. Y. Ng, S. Ramalingam, S. S. F. Yu and M. K. M. K. Chan, *Angew. Chem., Int. Ed.*, 2013, **52**, 3731–3735.
82 M. H. Groothaert, P. J. Smeets, B. F. Jacobs and R. A. Schoonheydt, *J. Am. Chem. Soc.*, 2005, **127**, 1394–1395.
83 J. S. Woertink, P. J. Smeets, M. H. Groothaert, M. A. Vance, B. F. Sels, R. A. Schoonheydt and E. I. Solomon, *Proc. Natl. Acad. Sci. U. S. A.*, 2009, **106**, 18908–18913.
84 P. J. Smeets, R. G. Hadt, J. S. Woertink, P. Vanelderen, R. A. Schoonheydt, B. F. Sels and E. I. Solomon, *J. Am. Chem. Soc.*, 2010, **132**, 14736–14738.
85 P. Vanelderen, J. Vancauwenbergh, B. F. Sels and R. A. Schoonheydt, *Coord. Chem. Rev.*, 2013, **257**, 483–494.
86 N. V. Beznis, B. M. Weckhuysen and J. H. Bitter, *Catal. Lett.*, 2009, **136**, 52–56.
87 N. V. Beznis, A. N. C. Van Laak, B. M. Weckhuysen and J. H. Bitter, *Microporous Mesoporous Mater.*, 2011, **138**, 176–183.
88 M. C. Kung, S. S. Y. Lin and H. H. Kung, *Top. Catal.*, 2012, **55**, 108–115.
89 J. Xu, A. Zheng, X. Wang, G. Qi, J. Su, J. Du, Z. Gan, J. Wu, W. Wang and F. Deng, *Chem. Sci.*, 2012, **3**, 2932–2940.
90 E. M. Alayon, M. Nachtegaal, M. Ranocchiari and J. A. V. Bokhoven, *Chem. Commun.*, 2012, **48**, 404–406.
91 N. Ohler and A. T. Bell, *J. Phys. Chem. B*, 2006, **110**, 23419–23429.
92 S. Chempath and A. T. Bell, *J. Catal.*, 2007, **247**, 119–126.
93 K. Otsuka and Y. Wang, *Appl. Catal., A*, 2001, **222**, 145–161.
94 K. Tabata, Y. Teng, T. Takemoto, E. Suzuki, A. A. Bañares, M. A. Peña and J. L. G. Fierro, *Catal. Rev. Sci. Eng.*, 2002, **44**, 1–58.
95 A. Arena and A. Parmaliana, *Acc. Chem. Res.*, 2003, **36**, 867–875.
96 A. Holmen, *Catal. Today*, 2009, **142**, 2–8.
97 Y. Wang, D. An and Q. Zhang, *Sci. China: Chem.*, 2010, **53**, 337–350.
98 M. C. Alvarez, N. Mota, M. Ojeda, S. Rojas, R. M. Navarro and J. L. G. Fierro, *Catal. Today*, 2011, **171**, 15–23.
99 G. Fu, X. Xu, X. Lu and H. Wan, *J. Am. Chem. Soc.*, 2005, **127**, 3989–3996.
100 D. A. Ruddy, N. L. Ohler, A. T. Bell and T. D. Tilley, *J. Catal.*, 2006, **238**, 277–285.
101 L. D. Nguyen, S. Loridant, H. Launay, A. Pigamo, J. L. Dubois and J. M. M. Millet, *J. Catal.*, 2006, **237**, 38–48.

102 Y. Li, S. Chen, Q. Zhang and Y. Wang, *Chem. Lett.*, 2006, **35**, 572–573.
103 T. Kobayashi, K. Nakagawa, K. Tabata and M. Haruta, *J. Chem. Soc., Chem. Commun.*, 1994, 1609–1610.
104 F. Arena, G. Gatti, G. Martra, S. Coluccia, L. Stievano, L. Spadaro, P. Faulari and A. Parmaliana, *J. Catal.*, 2005, **231**, 365–380.
105 Q. Zhang, W. Yang, X. Wang, Y. Wang, T. Shihsido and K. Takehira, *Microporous Mesoporous Mater.*, 2005, **77**, 223–234.
106 Q. Zhang, Y. Li, D. An and Y. Wang, *Appl. Catal., A*, 2009, **356**, 103–111.
107 J. He, Y. Li, D. An, Q. Zhang and Y. Wang, *J. Nat. Gas Chem.*, 2009, **18**, 288–294.
108 Y. Li, D. An, Q. Zhang and Y. Wang, *J. Phys. Chem. C*, 2008, **112**, 13700–13708.
109 D. An, Q. Zhang and Y. Wang, *Catal. Today*, 2010, **157**, 143–148.
110 G. Thiabaud, G. Guillemot, I. Schmitz-Afonso, B. Colasson and O. Reinaud, *Angew. Chem., Int. Ed.*, 2009, **48**, 7383–7386.
111 M. Lin and A. Sen, *Nature*, 1994, **368**, 613–615.
112 M. Lin, T. E. Hogan and A. Sen, *J. Am. Chem. Soc.*, 1996, **118**, 4574–4580.
113 C. Jia, T. Kitamura and Y. Fujiwara, *Acc. Chem. Res.*, 2001, **34**, 633–639.
114 P. M. Reis, J. A. L. Silva, A. F. Palavra, J. J. R. F. Da Silva, T. Kitamura, Y. Fujiwara and A. J. L. Pombeiro, *Angew. Chem., Int. Ed.*, 2003, **42**, 821–823.
115 H. Hogeveen, J. Lukas and C. F. Roobeek, *J. Chem. Soc. D*, 1969, 920–921.
116 A. Bagno, J. Bukala and G. A. Olah, *J. Org. Chem.*, 1990, **55**, 4284–4289.
117 A. G. Stepanov, M. V. Luzgin, A. V. Krasnosloslobodtsev, V. P. Shmachkova and N. S. Kotsarenko, *Angew. Chem., Int. Ed.*, 2000, **39**, 3658–3660.
118 M. V. Luzgin, K. Thomas, J. van Gestel, J. P. Gilson and A. G. Stepanov, *J. Catal.*, 2004, **223**, 290–295.
119 M. V. Luzgin, V. A. Rogov, N. S. Kotsarenko, V. P. Shmachkova and A. G. Stepanov, *J. Phys. Chem. C*, 2007, **111**, 10624–10629.
120 J. Macht, M. J. Janik, M. Neurock and E. Iglesia, *Angew. Chem., Int. Ed.*, 2007, **46**, 7864–7868.
121 J. Yang, M. J. Janik, M. Ma, Z. Zhang, M. Zhang, M. Neurock, R. J. Davis, C. Ye and F. Deng, *J. Am. Chem. Soc.*, 2005, **127**, 18274–18280.
122 M. Sun, E. Abou-Hamad, A. J. Rossini, J. Zhang, A. Lesage, H. Zhu, J. Pelletier, L. Emsley, V. Caps and J. M. Basset, *J. Am. Chem. Soc.*, 2013, **135**, 804–810.
123 M. V. Luzgin, A. G. Stepanov, A. sassi and J. Sommer, *Chem.–Eur. J.*, 2000, **6**, 2368–2376.
124 J. F. Wu, W. D. Wang, F. Deng and W. Wang, *Chem.–Eur. J.*, 2010, **16**, 14016–14025.
125 X. Wang, G. Qi, J. Xu, B. Li, C. Wang and F. Deng, *Angew. Chem., Int. Ed.*, 2012, **51**, 3850–3853.
126 Y. Wang, M. Katagiri and K. Otsuka, *Chem. Commun.*, 1997, 1187–1188.
127 Q. Yuan, Q. Zhang and Y. Wang, *J. Catal.*, 2005, **233**, 221–233.
128 Y. Wang, Q. Yuan, Q. Zhang and W. Deng, *J. Phys. Chem. C*, 2007, **111**, 2044–2053.
129 M. O. Adebajo, *Green Chem.*, 2007, **9**, 526–539.
130 J. H. Lunsford, P. Qiu, M. P. Rosynek and Z. Yu, *J. Phys. Chem. B*, 1998, **102**, 167–173.
131 T. Baba, *Catal. Surv. Asia*, 2005, **9**, 147–154.
132 J. S. Lee and S. T. Oyama, *Catal. Rev. Sci. Eng.*, 1988, **30**, 249–280.
133 G. J. Hutchings, M. S. Scurrell and J. R. Woodhouse, *Chem. Soc. Rev.*, 1989, **18**, 251–283.
134 Y. Amenomiya, V. I. Birss, M. Goledzinowski, J. Galuszka and A. R. Sanger, *Catal. Rev. Sci. Eng.*, 1990, **32**, 163–227.
135 Z. Zhang, X. E. Verykios and M. Baerns, *Catal. Rev. Sci. Eng.*, 1994, **36**, 507–556.
136 S. Arndt, G. Laugel, S. Levchenko, R. Hom, M. Baerns, M. Scheffler, R. Schlögl and R. Schomacker, *Catal. Rev. Sci. Eng.*, 2011, **53**, 424–514.
137 U. Zavyalova, M. Holena, R. Shlögl and M. Baerns, *ChemCatChem*, 2011, **3**, 1935–1947.
138 Y. S. Su, J. Y. Ying and W. H. Green, Jr., *J. Catal.*, 2003, **218**, 321–333.
139 H. Liu, Y. Wei, J. Cari and H. Wang, *ChemCatChem*, 2010, **2**, 1539–1542.
140 E. V. Kondratenko and U. Rodemerck, *ChemCatChem*, 2013, **5**, 697–700.
141 D. Noon, A. Seubsai and S. Senkan, *ChemCatChem*, 2013, **5**, 146–149.
142 B. Neumann, T. W. Elkins, W. Dreher, H. Hagelin-Weaver, J. C. Nino and M. Bäumer, *Catal. Sci. Technol.*, 2013, **3**, 89–93.
143 Y. Wang, Y. Takahashi and Y. Ohtsuka, *J. Catal.*, 1999, **186**, 160–168.
144 Y. Wang and Y. Ohtsuka, *J. Catal.*, 2000, **192**, 252–255.
145 Y. Wang and Y. Ohtsuka, *Appl. Catal., A*, 2001, **219**, 183–193.
146 S. Wang and Z. H. Zhu, *Energy Fuels*, 2004, **18**, 1126–1139.
147 Q. Zhu, S. L. Wegener, C. Xie, O. Uche, M. Neurock and T. J. Marks, *Nat. Chem.*, 2012, **5**, 104–109.
148 I. Lorkovic, M. Noy, M. Weiss, J. Sherman, E. McFarland, G. D. Stucky and P. C. Ford, *Chem. Commun.*, 2004, 566–567.
149 M. Weissman and S. W. Benson, *Int. J. Chem. Kinet.*, 1984, **16**, 307–333.
150 G. A. Olah, B. Gupta, M. Farina, J. D. Felberg, W. M. Ip, A. Husain, R. Karpeles, K. Lammertsma, A. K. Melhotra and N. J. Trivedi, *J. Am. Chem. Soc.*, 1985, **107**, 7097–7105.
151 F. Li and G. Yuan, *Angew. Chem., Int. Ed.*, 2006, **45**, 6541–6544.
152 K. X. Wang, H. F. Xu, W. S. Li and X. P. Zhou, *J. Mol. Catal. A: Chem.*, 2005, **225**, 65–69.
153 Z. Liu, L. Huang, W. S. Li, F. Yang, C. T. Au and X. P. Zhou, *J. Mol. Catal. A: Chem.*, 2007, **273**, 14–20.
154 R. Lin, Y. Ding, L. Gong, W. Dong, J. Wang and T. Zhang, *J. Catal.*, 2010, **272**, 65–73.

155 R. Wang, R. Lin, Y. Ding, J. Liu, J. Wang and T. Zhang, *Appl. Catal., A*, 2013, **453**, 235–243.
156 J. He, T. Xu, Z. Wang, Q. Zhang, W. Deng and Y. Wang, *Angew. Chem., Int. Ed.*, 2012, **51**, 2438–2442.
157 E. Peringer, S. G. Podkolzin, M. E. Jones, R. Olindo and J. A. Lercher, *Top. Catal.*, 2006, **38**, 211–220.
158 E. Peringer, M. Salzinger, M. Hutt, A. L. Lemonidou and J. A. Lercher, *Top. Catal.*, 2009, **52**, 1220–1231.
159 M. Nolan, S. Grigoleit, D. C. Sayle, S. C. Parker and G. W. Watson, *Surf. Sci.*, 2005, **576**, 217–229.
160 Y. Chen, L. Bai, C. Zhou, J. M. Lee and Y. Yang, *Chem. Commun.*, 2011, **47**, 6452–6454.
161 Y. Chen, H. Lim, Q. Tang, Y. Gao, T. Sun, Q. Yan and Y. Yang, *Appl. Catal., A*, 2010, **380**, 55–65.
162 T. Mallat and A. Baiker, *Catal. Today*, 1994, **19**, 247–284.
163 J. Muzart, *Tetrahedron*, 2003, **59**, 5789–5816.
164 J. H. J. Kluytmans, A. P. Markusse, B. F. M. Kuster, G. B. Marin and J. C. Schouten, *Catal. Today*, 2000, **57**, 143–155.
165 S. E. Davis, M. S. Ide and R. J. Davis, *Green Chem.*, 2013, **15**, 17–45.
166 P. J. Perez, *Organometallics*, 2001, **20**, 337–345.
167 K. M. Choi, T. Akita, T. Mizugaki, K. Ebitani and K. Kaneda, *New J. Chem.*, 2003, **27**, 324–328.
168 D. o. Stacchiola, L. Burkholder and W. T. Tysoe, *J. Am. Chem. Soc.*, 2002, **124**, 8984–8989.
169 K. Yamaguchi and N. Mizuno, *Angew. Chem., Int. Ed.*, 2002, **41**, 4538–4541.
170 K. Yamaguchi and N. Mizuno, *Chem.–Eur. J.*, 2003, **9**, 4353–4361.
171 D. W. McKee, *Trans. Faraday Soc.*, 1968, **64**, 2200–2212.
172 R. DiCosimo and G. M. Whitesides, *J. Phys. Chem.*, 1989, **93**, 768–775.
173 K. Yamaguchi, K. Mori, T. Mizugaki, K. Ebitani and K. Kaneda, *J. Am. Chem. Soc.*, 2000, **122**, 7144–7145.
174 K. Mori, T. Hara, T. Mizugaki, K. Ebitani and K. Kaneda, *J. Am. Chem. Soc.*, 2004, **126**, 10657–10666.
175 C. Keresszegi, T. Burgi, T. Mallat and A. Baiker, *J. Catal.*, 2002, **211**, 244–251.
176 Y. Schuurman, B. F. M. Kuster, K. v. d. Wiele and G. B. Marin, *Appl. Catal., A*, 1992, **89**, 31–46.
177 I. W. C. E. Arends, R. A. Sheldon, M. Wallau and U. Schuchardt, *Angew. Chem., Int. Ed. Engl.*, 1997, **36**, 1144–1163.
178 T. J. Yang and J. H. Lunsford, *J. Catal.*, 1987, **103**, 55–64.
179 A. M. Khenkin and R. Neumann, *Angew. Chem., Int. Ed.*, 2000, **39**, 4088–4090.
180 V. D. Makwana, Y. C. Son, A. R. Howell and S. L. Suib, *J. Catal.*, 2002, **210**, 46–52.
181 R. P. Groff, *J. Catal.*, 1984, **86**, 215–218.
182 J. S. Chung, R. Miranda and C. O. Bennett, *J. Catal.*, 1988, **114**, 398–410.
183 F. Kooli, C. Martín and V. Rives, *Langmuir*, 1997, **13**, 2303–2306.
184 Z. Dohnálek, I. Lyubinetsky and R. Rousseau, *Prog. Surf. Sci.*, 2010, **85**, 161–205.
185 Q. Tang, C. Wu, R. Qiao, Y. Chen and Y. Yang, *Appl. Catal., A*, 2011, **403**, 136–141.
186 D. I. Enache, J. K. Edwards, P. Landon, B. Solsona-Espriu, A. F. Carley, A. A. Herzing, M. Watanabe, C. J. Kiely, D. W. Knight and G. J. Hutchings, *Science*, 2006, **311**, 362–365.
187 H. T. Tan, Y. Chen, C. Zhou, X. Jia, J. Zhu, J. Chen, X. Rui, Q. Yan and Y. Yang, *Appl. Catal., B*, 2012, **119–120**, 166–174.
188 Y. Chen, H. Zheng, Z. Guo, C. Zhou, C. Wang, A. Borgna and Y. Yang, *J. Catal.*, 2011, **283**, 34–44.
189 Y. Chen, Z. Guo, T. Chen and Y. Yang, *J. Catal.*, 2010, **275**, 11–24.
190 J. Chen, Q. Zhang, Y. Wang and H. Wan, *Adv. Synth. Catal.*, 2008, **350**, 453–464.
191 H. Wu, Q. Zhang and Y. Wang, *Adv. Synth. Catal.*, 2005, **347**, 1356–1360.
192 F. Li, Q. Zhang and Y. Wang, *Appl. Catal., A*, 2008, **334**, 217–226.
193 K. Layek, H. Maheswaran, R. Arundhathi, M. L. Kantam and S. K. Bhargava, *Adv. Synth. Catal.*, 2011, **353**, 606–616.
194 Z. Hou, N. Theyssen, A. Brinkmann and W. Leitner, *Angew. Chem., Int. Ed.*, 2005, **44**, 1346–1349.
195 N. Dimitratos, A. Villa, D. Wang, F. Porta, D. Su and L. Prati, *J. Catal.*, 2006, **244**, 113–121.
196 N. Dimitratos, J. A. Lopez-Sanchez, D. Morgan, A. Carley, L. Prati and G. J. Hutchings, *Catal. Today*, 2007, **122**, 317–324.
197 T. Mitsudome, A. Noujima, T. Mizugaki, K. Jitsukawa and K. Kaneda, *Adv. Synth. Catal.*, 2009, **351**, 1890–1896.
198 H. Miyamura, R. Matsubara, Y. Miyazaki and S. Kobayashi, *Angew. Chem., Int. Ed.*, 2007, **46**, 4151–4154.
199 B. Z. Zhan, M. A. White, T. K. Sham, J. A. Pincock, R. J. Doucet, K. V. R. Rao, K. N. Robertson and T. S. Cameron, *J. Am. Chem. Soc.*, 2003, **125**, 2195–2199.
200 Q. Tang, T. Liu and Y. Yang, *Catal. Commun.*, 2008, **9**, 2570–2573.
201 Q. Tang, X. Huang, C. Wu, P. Zhao, Y. Chen and Y. Yang, *J. Mol. Catal. A: Chem.*, 2009, **306**, 48–53.
202 Q. Tang, X. Gong, P. Zhao, Y. Chen and Y. Yang, *Appl. Catal., A*, 2010, **389**, 101–107.
203 Q. Tang, X. Gong, C. Wu, Y. Chen, A. Borgna and Y. Yang, *Catal. Commun.*, 2009, **10**, 1122–1126.
204 Q. Tang, Y. Chen and Y. Yang, *J. Mol. Catal. A: Chem.*, 2010, **315**, 43–50.
205 F. Wang and W. Ueda, *Appl. Catal.,A*, 2008, **346**, 155–163.
206 Q. Wang, M. Zhang, C. Chen, W. Ma and J. Zhao, *Angew. Chem., Int. Ed.*, 2010, **49**, 7976–7979.
207 Y. M. Yamada, T. Arakawa, H. Hocke and Y. Uozumi, *Angew. Chem., Int. Ed.*, 2007, **46**, 704–706.
208 T. Mallat, A. Baiker and L. Botz, *Appl. Catal., A*, 1992, **86**, 147–163.
209 C. Zhou, Y. Chen, Z. Guo, X. Wang and Y. Yang, *Chem. Commun.*, 2011, **47**, 7473–7475.
210 Y. Chen, H. Wang, C. J. Liu, Z. Zeng, H. Zhang, C. Zhou, X. Jia and Y. Yang, *J. Catal.*, 2012, **289**, 105–117.

211 C. Jiang, S. Ranjit, Z. Duan, Y. L. Zhong, K. P. Loh, C. Zhang and X. Liu, *Nanoscale*, 2009, **1**, 391–394.
212 Y. Chen, W. Chen, Q. Tang, Z. Guo, Y. Yang and F. Su, *Catal. Lett.*, 2010, **141**, 149–157.
213 Q. Tang, X. Huang, Y. Chen, T. Liu and Y. Yang, *J. Mol. Catal. A: Chem.*, 2009, **301**, 24–30.
214 T. Mallat, Z. Bodnar and A. Baiker, *Stud. Surf. Sci. Catal.*, Elsevier, 1993, vol. 78, pp. 377–384.
215 A. Abad, P. Concepción, A. Corma and H. García, *Angew. Chem., Int. Ed.*, 2005, **44**, 4066–4069.
216 M. L. Kantam, U. Pal, B. Sreedhar, S. Bhargava, Y. Iwasawa, M. Tada and B. M. Choudary, *Adv. Synth. Catal.*, 2008, **350**, 1225–1229.
217 C. Donze, P. Korovchenko, P. Gallezot and M. Besson, *Appl. Catal., B*, 2007, **70**, 621–629.
218 K. Ebitani, Y. Fujie and K. Kaneda, *Langmuir*, 1999, **15**, 3557–3562.
219 M. Haruta, T. Kobayashi, H. Sano and N. Yamada, *Chem. Lett.*, 1987, 405–408.
220 S. Royer and D. Duprez, *ChemCatChem*, 2011, **3**, 24–65.
221 C. W. Corti, R. J. Holliday and D. T. Thompson, *Appl. Catal., A*, 2005, **291**, 253–261.
222 H. J. Freund, G. Meijer, M. Scheffler, R. Schlögl and M. Wolf, *Angew. Chem., Int. Ed.*, 2011, **50**, 10064–10094.
223 Q. Fu, W. X. Li, Y. Yao, H. Liu, H. Y. Su, D. Ma, X. K. Gu, L. Chen, Z. Wang, H. Zhang, B. Wang and X. Bao, *Science*, 2010, **328**, 1141–1144.
224 Q. Zhang, X. Liu, W. Fan and Y. Wang, *Appl. Catal., B*, 2011, **102**, 207–214.
225 M. Ehsasi, M. Berdau, A. Karpowicz, K. Christmann and J. H. Block, *Stud. Surf. Sci. Catal.*, 1993, **75**, 321–332.
226 S. Y. Yamamoto, C. M. Surko, M. B. Maple and R. K. Pina, *J. Chem. Phys.*, 1995, **102**, 8614–8625.
227 H. Over and M. Muhler, *Prog. Surf. Sci.*, 2003, **72**, 3–17.
228 D.-J. Liu and J. W. Evans, *Surf. Sci.*, 2009, **603**, 1706–1716.
229 B. K. Min and C. M. Friend, *Chem. Rev.*, 2007, **107**, 2709–2724.
230 H. Falsig, B. Hvolbaek, I. S. Kristensen, T. Jiang, T. Bligaard, C. H. Christensen and J. K. Nørskov, *Angew. Chem., Int. Ed.*, 2008, **47**, 4835–4839.
231 R. Imbihl and G. Ertl, *Chem. Rev.*, 1995, **95**, 697–733.
232 B. Hendriksen, S. Bobaru and J. Frenken, *Catal. Today*, 2005, **105**, 234–243.
233 B. L. M. Hendriksen, M. D. Ackermann, R. v. Rijin, D. Stoltz, L. Popa, O. Balmes, A. Rests, D. Wermeille, R. Felici, S. Ferrer and J. W. M. Frenken, *Nat. Chem.*, 2010, **2**, 730–743.
234 K. Reuter and M. Scheffler, *Phys. Rev. B: Condens. Matter Mater. Phys.*, 2006, **73**, 045433.
235 B. L. M. Hendriksen, S. C. Bobaru and J. W. M. Frenken, *Top. Catal.*, 2005, **36**, 43–54.
236 T. Uchiyama, H. Yoshida, Y. Kuwauchi, S. Ichikawa, S. Shimada, M. Haruta and S. Takeda, *Angew. Chem., Int. Ed.*, 2011, **50**, 10157–10160.
237 H. Yoshida, Y. Kuwauchi, J. R. Jinschek, K. Sun, S. Tanaka, M. Kohyama, S. Shimada, M. Haruta and S. Takeda, *Science*, 2012, **335**, 317–319.
238 J. Singh, E. M. Alayon, M. Tromp, O. V. Safonova, P. Glatzel, M. Nachtegaal, R. Frahm and J. A. van Bokhoven, *Angew. Chem., Int. Ed.*, 2008, **47**, 9260–9264.
239 P. Nolte, A. Stierle, N. Y. Jin-Phillipp, N. Kasper, T. U. Schulli and H. Dosch, *Science*, 2008, **321**, 1654–1658.
240 T. Fujitani and I. Nakamura, *Angew. Chem., Int. Ed.*, 2011, **50**, 10144–10147.
241 L. Yang, S. Shan, R. Loukrakpam, V. Petkov, Y. Ren, B. N. Wanjala, M. H. Engelhard, J. Luo, J. Yin, Y. Chen and C. J. Zhong, *J. Am. Chem. Soc.*, 2012, **134**, 15048–15060.
242 J. Singh, M. Nachtegaal, E. M. C. Alayon, J. Stötzel and J. A. van Bokhoven, *ChemCatChem*, 2010, **2**, 653–657.
243 B. V. L'vov and A. K. Galwey, *J. Therm. Anal. Calorim.*, 2012, **111**, 145–154.
244 V. P. Zhdanov, *J. Chem. Phys.*, 2007, **126**(7), 074706.
245 V. K. Noussiou and A. Provata, *Chem. Phys.*, 2008, **348**, 11–20.
246 D. Widmann and R. J. Behm, *Angew. Chem., Int. Ed.*, 2011, **50**, 10241–10245.
247 G. G. Jernigan and G. A. Somorjai, *J. Catal.*, 1994, **147**, 567–577.
248 S. Liang, F. Teng, G. Bulgan, R. Zong and Y. Zhu, *J. Phys. Chem. C*, 2008, **112**, 5307–5315.
249 X. Xie, Y. Li, Z. Q. Liu, M. Haruta and W. Shen, *Nature*, 2009, **458**, 746–749.
250 W. Xue, Z. C. Wang, S. G. He, Y. Xie and E. R. Bernstein, *J. Am. Chem. Soc.*, 2008, **130**, 15879–15888.
251 H. F. Wang, R. Kavanagh, Y. L. Guo, Y. Guo, G. Z. Lu and P. Hu, *J. Catal.*, 2012, **296**, 110–119.
252 P. Broqvist, I. Panas and H. Persson, *J. Catal.*, 2002, **210**, 198–206.
253 M. Che and A. J. Tench, *Adv. Catal.*, Academic Press, 1983, vol. 32, pp. 1–148.
254 C. Li, K. Domen, K. Maruya and T. Onishi, *J. Am. Chem. Soc.*, 1989, **111**, 7683–7687.
255 X. L. Xu, E. Yang, J. Q. Li, Y. Li and W. K. Chen, *ChemCatChem*, 2009, **1**, 384–392.
256 H. J. Jung, J. T. Lim, S. H. Lee, Y. R. Kim and J. G. Choi, *J. Phys. Chem.*, 1996, **100**, 10243–10248.
257 G. Sedmak, S. Hočevar and J. Levec, *J. Catal.*, 2004, **222**, 87–99.
258 K. S. Chan, J. Ma, S. Jaenicke, G. K. Chuah and J. Y. Lee, *Appl. Catal., A*, 1994, **107**, 201–227.
259 V. A. Sadykov and S. F. Tikhov, *J. Catal.*, 1997, **165**, 279–283.
260 J. Cortés, E. Valencia and P. Araya, *Catal. Lett.*, 2012, **143**, 176–183.
261 M. J. Kahlich, H. A. Gasteiger and R. J. Behm, *J. Catal.*, 1997, **171**, 93–105.
262 G. Sedmak, S. Hočevar and J. Levec, *J. Catal.*, 2003, **213**, 135–150.
263 A. Martínez-Arias, D. Gamarra, M. Fernández-García, A. Hornés and C. Belver, *Top. Catal.*, 2009, **52**, 1425–1432.
264 P. Gawade, B. Bayram, A.-M. C. Alexander and U. S. Ozkan, *Appl. Catal., B*, 2012, **128**, 21–30.
265 C. S. Polster, R. Zhang, M. T. Cyb, J. T. Miller and C. D. Baertsch, *J. Catal.*, 2010, **273**, 50–58.

266 T. Jiang, D. J. Mowbray, S. Dobrin, H. Falsig, B. Hvolbæk, T. Bligaard and J. K. Nørskov, *J. Phys. Chem. C*, 2009, **113**, 10548–10553.
267 T. Froschl, U. Hormann, P. Kubiak, G. Kucerova, M. Pfanzelt, C. K. Weiss, R. J. Behm, N. Husing, U. Kaiser, K. Landfester and M. Wohlfahrt-Mehrens, *Chem. Soc. Rev.*, 2012, **41**, 5313–5360.
268 G. C. Bond, *Faraday Discuss.*, 2011, **152**, 277–291.
269 E. Kadossov, S. Cabrini and U. Burghaus, *J. Mol. Catal. A: Chem.*, 2010, **321**, 101–109.
270 A. W. Castleman, *Catal. Lett.*, 2011, **141**, 1243–1253.
271 J. Guzman, S. Carrettin, J. C. Fierro-Gonzalez, Y. Hao, B. C. Gates and A. Corma, *Angew. Chem., Int. Ed.*, 2005, **44**, 4778–4781.
272 J. Guzman and B. C. Gates, *J. Am. Chem. Soc.*, 2004, **126**, 2672–2673.
273 G. M. Veith, A. R. Lupini, S. J. Pennycook and N. J. Dudney, *ChemCatChem*, 2010, **2**, 281–286.
274 A. Wittstock, A. Wichmann, J. Biener and M. Bäumer, *Faraday Discuss.*, 2011, **152**, 87–98.
275 A. Wittstock, J. Biener and M. Baumer, *Phys. Chem. Chem. Phys.*, 2010, **12**, 12919–12930.
276 D. Rosenthal, *Phys. Status Solidi A*, 2011, **208**, 1217–1222.
277 M. A. Newton, A. J. Dent, S. Diaz-Moreno, S. G. Fiddy, B. Jyoti and J. Evans, *Chem.–Eur. J.*, 2006, **12**, 1975–1985.
278 M. E. Grass, Y. Zhang, D. R. Butcher, J. Y. Park, Y. Li, H. Bluhm, K. M. Bratlie, T. Zhang and G. A. Somorjai, *Angew. Chem., Int. Ed.*, 2008, **47**, 8893–8896.
279 H. K. Lin, H. C. Chiu, H. C. Tsai, S. H. Chien and C. B. Wang, *Catal. Lett.*, 2003, **88**, 169–174.
280 Y. Xie, F. Dong, S. Heinbuch, J. J. Rocca and E. R. Bernstein, *Phys. Chem. Chem. Phys.*, 2010, **12**, 947–959.
281 M. J. Pollard, B. A. Weinstock, T. E. Bitterwolf, P. R. Griffiths, A. Piers Newbery and J. B. Paine Iii, *J. Catal.*, 2008, **254**, 218–225.
282 O. Z. Didenko, G. R. Kosmambetova and P. E. Strizhak, *J. Mol. Catal. A: Chem.*, 2011, **335**, 14–23.
283 O. Pozdnyakova, D. Teschner, A. Wootsch, J. Krohnert, B. Steinhauer, H. Sauer, L. Toth, F. Jentoft, A. Knopgericke and Z. Paal, *J. Catal.*, 2006, **237**, 1–16.
284 O. Pozdnyakova, D. Teschner, A. Wootsch, J. Krohnert, B. Steinhauer, H. Sauer, L. Toth, F. Jentoft, A. Knopgericke and Z. Paal, *J. Catal.*, 2006, **237**, 17–28.
285 F. Arena, P. Famulari, G. Trunfio, G. Bonura, F. Frusteri and L. Spadaro, *Appl. Catal., B*, 2006, **66**, 81–91.
286 R. J. H. Grisel and B. E. Nieuwenhuys, *J. Catal.*, 2001, **199**, 48–59.
287 D. Teschner, A. Wootsch, O. Pozdnyakovatellinger, J. Krohnert, E. Vass, M. Havecker, S. Zafeiratos, P. Schnorch, P. Jentoft and A. Knopgericke, *J. Catal.*, 2007, **249**, 318–327.
288 E. Y. Ko, E. D. Park, H. C. Lee, D. Lee and S. Kim, *Angew. Chem., Int. Ed.*, 2007, **46**, 734–737.
289 G. Uysal, A. N. Akın, Z. İ. Önsan and R. Yıldırım, *Catal. Lett.*, 2006, **111**, 173–176.
290 J. L. Ayastuy, M. P. González-Marcos and M. A. Gutiérrez-Ortiz, *Catal. Commun.*, 2011, **12**, 895–900.
291 M. Ruszel, B. Grzybowska, M. Łaniecki and M. Wójtowski, *Catal. Commun.*, 2007, **8**, 1284–1286.
292 W.-Y. Yu, C.-P. Yang, J.-N. Lin, C.-N. Kuo and B.-Z. Wan, *Chem. Commun.*, 2005, 354–356.
293 L. Ilieva, G. Pantaleo, I. Ivanov, R. Zanella, J. W. Sobczak, W. Lisowski, A. M. Venezia and D. Andreeva, *Catal. Today*, 2011, **175**, 411–419.
294 E. Moretti, L. Storaro, A. Talon, P. Patrono, F. Pinzari, T. Montanari, G. Ramis and M. Lenarda, *Appl. Catal., A*, 2008, **344**, 165–174.
295 Z. Zhao, X. Lin, R. Jin, Y. Dai and G. Wang, *Catal. Commun.*, 2011, **12**, 1448–1451.
296 J. d. S. L. Fonseca, H. S. Ferreira, N. Bion, L. Pirault-Roy, M. d. C. Rangel, D. Duprez and F. Epron, *Catal. Today*, 2012, **180**, 34–41.
297 A. Tomita, K. i. Shimizu, K. Kato and Y. Tai, *Catal. Commun.*, 2012, **17**, 194–199.
298 H. Xu, Q. Fu, X. Guo and X. Bao, *ChemCatChem*, 2012, **4**, 1645–1652.
299 B. Solsona, M. Conte, Y. Cong, A. Carley and G. Hutchings, *Chem. Commun.*, 2005, 2351–2353.
300 Y. Minemura, S.-i. Ito, T. Miyao, S. Naito, K. Tomishige and K. Kunimori, *Chem. Commun.*, 2005, 1429–1431.
301 H. P. Bideberripe, J. M. Ramallo-López, S. J. A. Figueroa, M. A. Jaworski, M. L. Casella and G. J. Siri, *Catal. Commun.*, 2011, **12**, 1280–1285.
302 Y. Ishida, T. Ebashi, S. Ito, T. Kubota, K. Kunimori and K. Tomishige, *Chem. Commun.*, 2009, 5308–5310.
303 K.-I. Tanaka, M. Shou, H. He and X. Shi, *Catal. Lett.*, 2006, **110**, 185–190.
304 K.-i. Tanaka, M. Shou and Y. Yuan, *J. Phys. Chem. C*, 2010, **114**, 16917–16923.
305 B. Qiao, A. Wang, X. Yang, L. F. Allard, Z. Jiang, Y. Cui, J. Liu, J. Li and T. Zhang, *Nat. Chem.*, 2011, **3**, 634–641.
306 S. Huang, K. Hara and A. Fukuoka, *Chem.–Eur. J.*, 2012, **18**, 4738–4747.
307 F. Yang, M. S. Chen and D. W. Goodman, *J. Phys. Chem. C*, 2009, **113**, 254–260.
308 X. Lin, B. Yang, H. M. Benia, P. Myrach, M. Yulikov, A. Aumer, M. A. Brown, M. Sterrer, O. Bondarchuk, E. Kieseritzky, J. Rocker, T. Risse, H. J. Gao, N. Nilius and H. J. Freund, *J. Am. Chem. Soc.*, 2010, **132**, 7745–7749.
309 J. Lin, B. Qiao, J. Liu, Y. Huang, A. Wang, L. Li, W. Zhang, L. F. Allard, X. Wang and T. Zhang, *Angew. Chem., Int. Ed.*, 2012, **51**, 2920–2924.
310 U. G. Singh, J. Li, J. W. Bennett, A. M. Rappe, R. Seshadri and S. L. Scott, *J. Catal.*, 2007, **249**, 349–358.
311 W. Yan, S. M. Mahurin, Z. Pan, S. H. Overbury and S. Dai, *J. Am. Chem. Soc.*, 2005, **127**, 10480–10481.
312 Z. Ma, S. H. Overbury and S. Dai, *J. Mol. Catal. A: Chem.*, 2007, **273**, 186–197.
313 G. Budroni and A. Corma, *Angew. Chem., Int. Ed.*, 2006, **45**, 3328–3331.
314 L. Ilieva, G. Pantaleo, I. Ivanov, A. Maximova, R. Zanella, Z. Kaszkur, A. M. Venezia and D. Andreeva, *Catal. Today*, 2010, **158**, 44–55.

315 O. H. Laguna, F. Romero Sarria, M. A. Centeno and J. A. Odriozola, *J. Catal.*, 2010, **276**, 360–370.
316 R. Taha, D. Martin, S. Kacimi and D. Duprez, *Catal. Today*, 1996, **29**, 89–92.
317 Z. Zhao, X. Lin, R. Jin, Y. Dai and G. Wang, *Catal. Sci. Technol.*, 2012, **2**, 554–563.
318 M. Daté, M. Okumura, S. Tsubota and M. Haruta, *Angew. Chem., Int. Ed.*, 2004, **43**, 2129–2132.
319 F. Gao, T. E. Wood and D. W. Goodman, *Catal. Lett.*, 2009, **134**, 9–12.
320 D. A. H. Cunningham, T. Kobayashi, N. Kamijo and M. Haruta, *Catal. Lett.*, 1994, **25**, 257–264.
321 C. Xu, Y. Liu, C. Zhou, L. Wang, H. Geng and Y. Ding, *ChemCatChem*, 2011, **3**, 399–407.
322 Y. Yu, T. Takei, H. Ohashi, H. He, X. Zhang and M. Haruta, *J. Catal.*, 2009, **267**, 121–128.
323 J. L. Ayastuy, N. K. Gamboa, M. P. González-Marcos and M. A. Gutiérrez-Ortiz, *Chem. Eng. J.*, 2011, **171**, 224–231.
324 H. F. Wang, R. Kavanagh, Y. L. Guo, Y. Guo, G. Z. Lu and P. Hu, *Angew. Chem., Int. Ed.*, 2012, **51**, 6657–6661.
325 M. Lomello-Tafin, A. A. Chaou, F. Morfin, V. Caps and J. L. Rousset, *Chem. Commun.*, 2005, 388–390.
326 M. Daté and M. Haruta, *J. Catal.*, 2001, **201**, 221–224.
327 G. Du, Y. Yang, W. Qiu, S. Lim, L. Pfefferle and G. L. Haller, *Appl. Catal., A*, 2006, **313**, 1–13.
328 Q. Tang, Y. Chen, C. J. Zhou, T. Chen and Y. Yang, *Catal. Lett.*, 2008, **128**, 210–220.
329 W. Yan, Y. Chen, Y. Yang and T. Chen, *Catal. Today*, 2011, **174**, 127–134.
330 M. Ahlquist, R. A. Periana and W. A. Goddard Iii, *Chem. Commun.*, 2009, 2373–2375.
331 J. K. Nørskov, T. Bligaard, A. Logadottir, S. Bahn, L. B. Hansen, M. Bollinger, H. Bengaard, B. Hammer, Z. Sljivancanin, M. Mavrikakis, Y. Xu, S. Dahl and C. J. H. Jacobsen, *J. Catal.*, 2002, **209**, 275–278.
332 W. B. Kim, T. Voitl, G. J. Rodriguez-Rivera, S. T. Evans and J. A. Dumesic, *Angew. Chem., Int. Ed.*, 2005, **44**, 778–782.
333 I. Lee, J. B. Joo, Y. Yin and F. Zaera, *Angew. Chem., Int. Ed.*, 2011, **50**, 10208–10211.
334 L.-S. Fan and F. Li, *Ind. Eng. Chem. Res.*, 2010, **49**, 10200–10211.
335 K. Li, H. Wang and Y. Wei, *J. Chem.*, 2013, 294817.